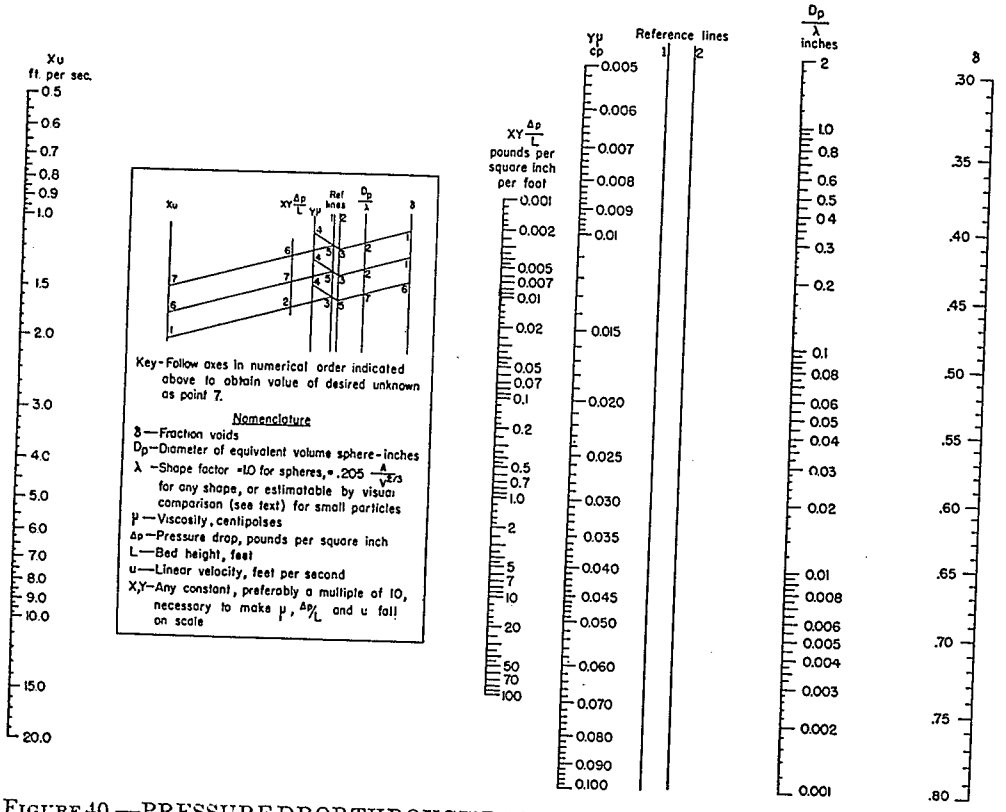

FIGURE 40.—PRESSURE DROP THROUGH PACKED BEDS FOR FLUIDS IN STREAM-LINE FLOW.

ILLUSTRATIVE PROBLEM

It is desired to carry out a given reaction with a magnetite catalyst at a space velocity of 125. The reactor is 6 inches in diameter and 1 foot high. Considerations of the kinetics of the reaction have shown that the smallest possible particle will be the most desirable, but pressure drop across the bed is limited to 1 p.s.i. No change is expected in the density of the flowing gas. Visual comparison of the catalyst with the photographs of figure 67 reveals that the material is identical in shape with that designated as $\lambda=1.73$. The gas viscosity at operating conditions is estimated at 0.018 cp. It is desired to find the smallest particle diameter for which the pressure drop will not exceed 1 p.s.i.

Solution:

$$u=\frac{(125)(1)}{3{,}600}=0.0347 \text{ ft./sec.}$$

$$\frac{\Delta P}{L}=\frac{1}{1}=1.00 \text{ p.s.i./ft.}$$

$$\lambda=1.73$$

$$\mu=0.018 \text{ cp.}$$

$$Xu=3.47 (X=100)$$

$$Y=0.018 (Y=1.0)$$

$$XY=100$$

$$XY\Delta P/L=100.$$

As the desired value sought is D_p, D_p/λ should be the last axis encountered. Therefore, the bottom order given in the key is followed. $Xu=3.47$ is alined with $XY\Delta P/L=100$ to obtain a point on reference 1. This point is connected with $Y\mu=0.018$ to obtain a point on reference 2. Alining this point with an assumed value of $\delta=0.52$ gives a value of $D_p/\lambda=0.0020$ inch, or $D_p=0.00346$ inch. Figure 94 shows that such a small particle would yield a voidage of about 60 percent. Repeating this process for an assumed $\delta=0.60$, $D_p/\lambda=0.0013$ inch and $D_p=0.00225$ inch. A particle of this size should have a voidage of about 61 percent, which is as close to the last assumption of 60 percent as the accuracy of the curves permits.

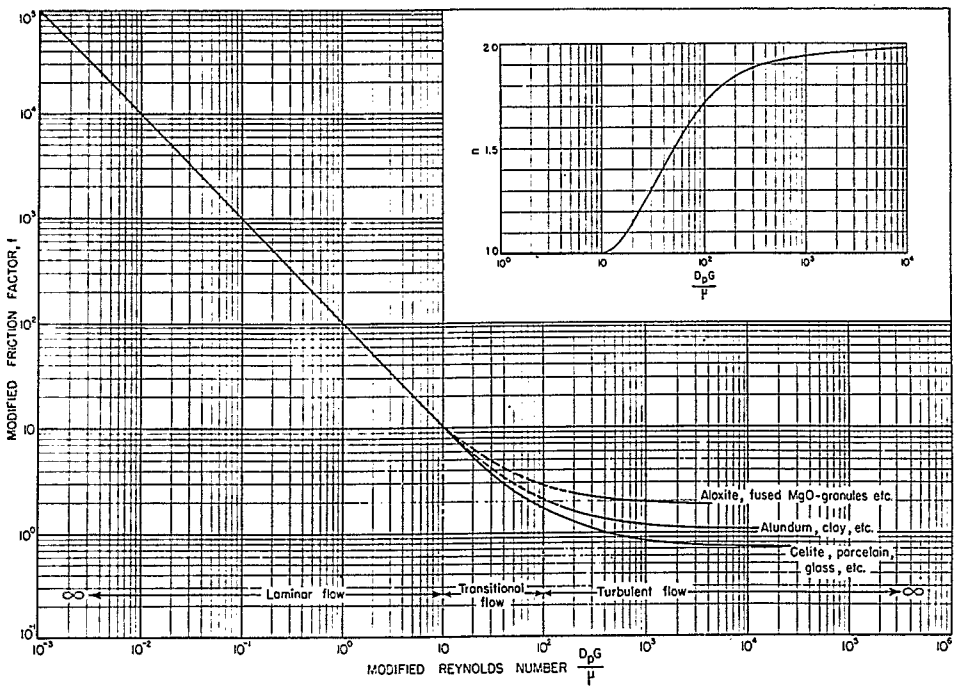

FIGURE 41.—MODIFIED FRICTION FACTORS VS. MODIFIED REYNOLDS NUMBER.

GENERALIZED PRESSURE-DROP EQUATION

TRANSITIONAL RANGE

It has been shown previously that flow through packed beds, like flow through empty pipes, takes place in two distinctly different modes—the laminar and the turbulent. This also can be seen in figure 41. For the transitional region, which, for packed tubes, is described by a range of modified Reynolds numbers 10–100, neither equation (21) nor equation (40) will give accurate results. Equation (5) can be written in the form:

$$\Delta P = \frac{2fG^2L\lambda^{3-n}(1-\delta)^{3-n}}{D_p g_c \rho \delta^3}, \qquad (41)$$

which is the one recommended for use in the intermediate range. Equation (5) shows that n can be evaluated from the slopes of the curves of figure 30. The values thus obtained were used to plot the inset in figure 41.

Values of f were obtained by measuring all other variables in equation (41) and solving. Figure 41 thus permits the evaluation of pressure drop in any range of Reynolds number. The continuity between laminar and turbulent flow which this procedure yields is further verified in figure 42, which shows the pressure drop for two different packings over a flow range covering the laminar, transitional, and turbulent regions. The gradual change in slope from 1 to 1.9 is clearly established in the Reynolds-number range of 10 to 100.

The importance of correct evaluation of the void function $(1-\delta)^{3-n}/\delta^3$ has been stressed previously. As an additional aid in the use of equation 41, figure 43 is presented for the evaluation of the void function.

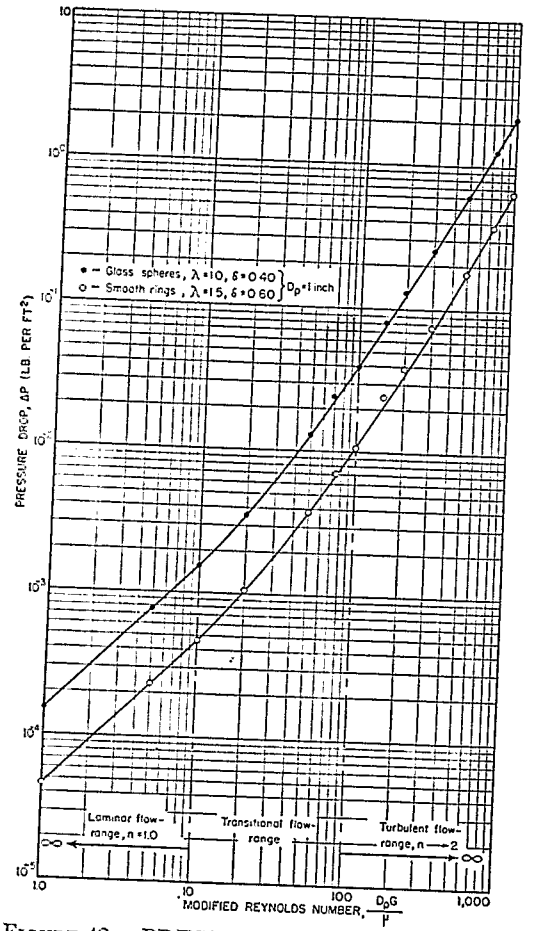

FIGURE 42.—PRESSURE DROP FOR LAMINAR, TRANSITIONAL, AND TURBULENT FLOW OF AIR THROUGH PACKINGS.

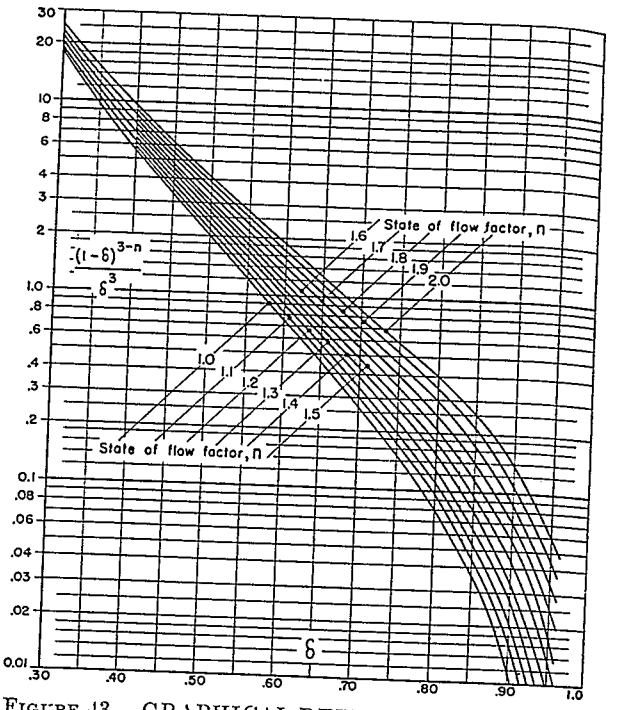

FIGURE 43.—GRAPHICAL REPRESENTATION OF THE VOID FUNCTION.

DIFFERENTIAL EQUATION

The development of equations (41), (21), and (4) is based on isothermal measurements at moderate pressure drops. For the more general case, equation (41) can be considered applicable over a differential length, dL, and used in Bernoulli's energy balance equation for a unit weight of fluid:

$$\bar{v}\,dP+\frac{u\,du}{g_c}+dF=0. \qquad (a)$$

The first term represents the change in pressure head of the fluid, the second term the kinetic-energy change, and the third term the irreversible work. This assumes the usual condition of negligible change in static head.

As the irreversible work is exactly the quantity that was measured in the isothermal, low-pressure-drop experiments, one may write from equation (41)

$$dF=\frac{dP}{\rho}=\left[\frac{2fG^2\lambda^{3-n}}{D_p g_c}\,\frac{(1-\delta)^{3-n}}{\delta^3}\right]\frac{dL}{\rho^2}. \qquad (b)$$

For any given set of flow and equipment conditions, all the factors within the brackets will be constant along the length of the pipe, except for the possible effect of temperature on viscosity (and hence on the Reynolds number), which might produce a small change in f and n. Equation (b) can be written, therefore,

$$dF=C\,\frac{dL}{\rho^2}=C\bar{v}^2dL. \qquad (c)$$

As $u=\bar{v}G$ and $du=Gd\bar{v}$, substitution in (a) yields

$$\bar{v}\,dP+\frac{G^2\bar{v}\,d\bar{v}}{g_c}+C\bar{v}^2dL=0. \qquad (d)$$

From definition of the compressibility factor, Z,

$$\bar{v}=\frac{ZRT}{MP}. \qquad (e)$$

Dividing (d) by $\bar{v}^2$, substituting (e) in the first term of the result, and rearranging gives the generalized differential equation for pressure drop in packed beds:

$$-P\,dP=\frac{ZRG^2}{g_c M}T\,\frac{d\bar{v}}{\bar{v}}+C\,\frac{ZR}{M}\,T\,dL. \qquad (f)$$

For isothermal conditions, (f) integrates to

$$\frac{P_1^2-P_2^2}{2}=\frac{ZRG^2T}{g_c M}\ln\left(\frac{\bar{v}_2}{\bar{v}_1}\right)+C\,\frac{ZR}{M}\,TL,$$

$$P_1^2-P_2^2=\frac{2ZRG^2T}{g_cM}\left[\ln\left(\frac{\bar{v}_2}{\bar{v}_1}\right)+\frac{2f\lambda^{3-n}(1-\delta)^{3-n}}{D_p\delta^3}L\right], \quad (42)$$

which equation may be used when high-pressure drops or large fluid-density changes are to be anticipated.

NOMOGRAPH

Consideration of the preceding section led to the construction of a simple nomograph for the evaluation of a correction factor, which may be applied to results obtained by using the nomograph previously constructed for viscous flow.

If the factor C is defined as the ratio of the pressure drop calculated on the basis of the transitional-flow formula to that calculated from the viscous-flow formula, then

$$C=\frac{2fG^2L\lambda^{3-n}(1-\delta)^{3-n}}{D_pg_c\rho\delta^3}\times\frac{D_pg_c\rho\delta^3}{2f'G^2L\lambda^2(1-\delta)^2}=$$
$$\lambda^{1-n}(1-\delta)^{1-n}f/f',$$

where f' is the friction factor which would be obtained by extrapolation of the viscous-flow section of the f versus Re-number curve to the Reynolds number in question. As n and f/f' are each complex functions of Re, the nomograph of figure 44 could be constructed.

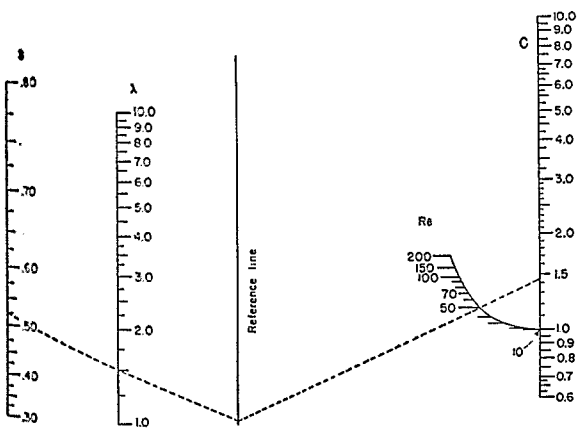

FIGURE 44.—CORRECTION FACTOR FOR TRANSITION RANGE.

Briefly, the procedure for estimating pressure drop in packed beds consists of the determination of the various properties of the system, possibly with the aid of figure 25 or 94 and calculation of the Reynolds number. If the Re is greater than 200, figure 11 is used; if Re is less than 10, figure 40 is used; if Re is between 10 and 200, figure 40 is used along with figure 44 to determine a value of C, by which the pressure drop (determined from figure 40) is to be multiplied to obtain the correct value.

SHAPE-FACTOR ESTIMATIONS

The sands through which flow was investigated are shown in figures 45 to 49, which are presented here to enable others to estimate shape factors for similar material. At present, visual observation seems to be the only practical method (except for experimental determination) of arriving at approximate shape-factor values of fine granular particles. This procedure requires some experience, but careful training should permit the determination of representative values.

Discussion of fluidization will show that shape-factor estimations are sometimes required when dealing with small granular materials. In reactors with co-gravity fluid flow, the particles are usually large enough to permit calculation of the shape factor by direct measurement of the particle dimensions. Small particles of iron Fischer-Tropsch catalyst are shown later to be considerably more irregular than sharp sand granules. In ordinary catalysis with finely divided granular materials, the shape factors most frequently encountered range between 1 and 1.75. Some silica gel cracking catalysts are spherical and approach a shape factor of 1. Most granules have shape factors of about 1.5. As granular catalysts progress in age, shape changes sometimes occur, most materials becoming more round. For design purposes, it is therefore desirable to base the shape factor estimations on the new catalyst.

Frequently, considerable difficulty is involved in the estimation of shape owing to the presence of a large fraction of fine materials. If a standard magnification is applied to such a sample, the shapes of the larger pieces might be easily recognizable, whereas the finer particles might be indistinct. Although no systematic attempts have been made in this work to determine whether the fine particles have the same shape as the coarser particles, the general correlations of friction factor versus modified Reynolds number suggest that shape is independent of particle size. No attempt has been made with shape mixtures to arrive at any rule other than the straight arithmetical one of averaging shape-factor values. It seems that greater refinement was not justified with the present experimental accuracy.

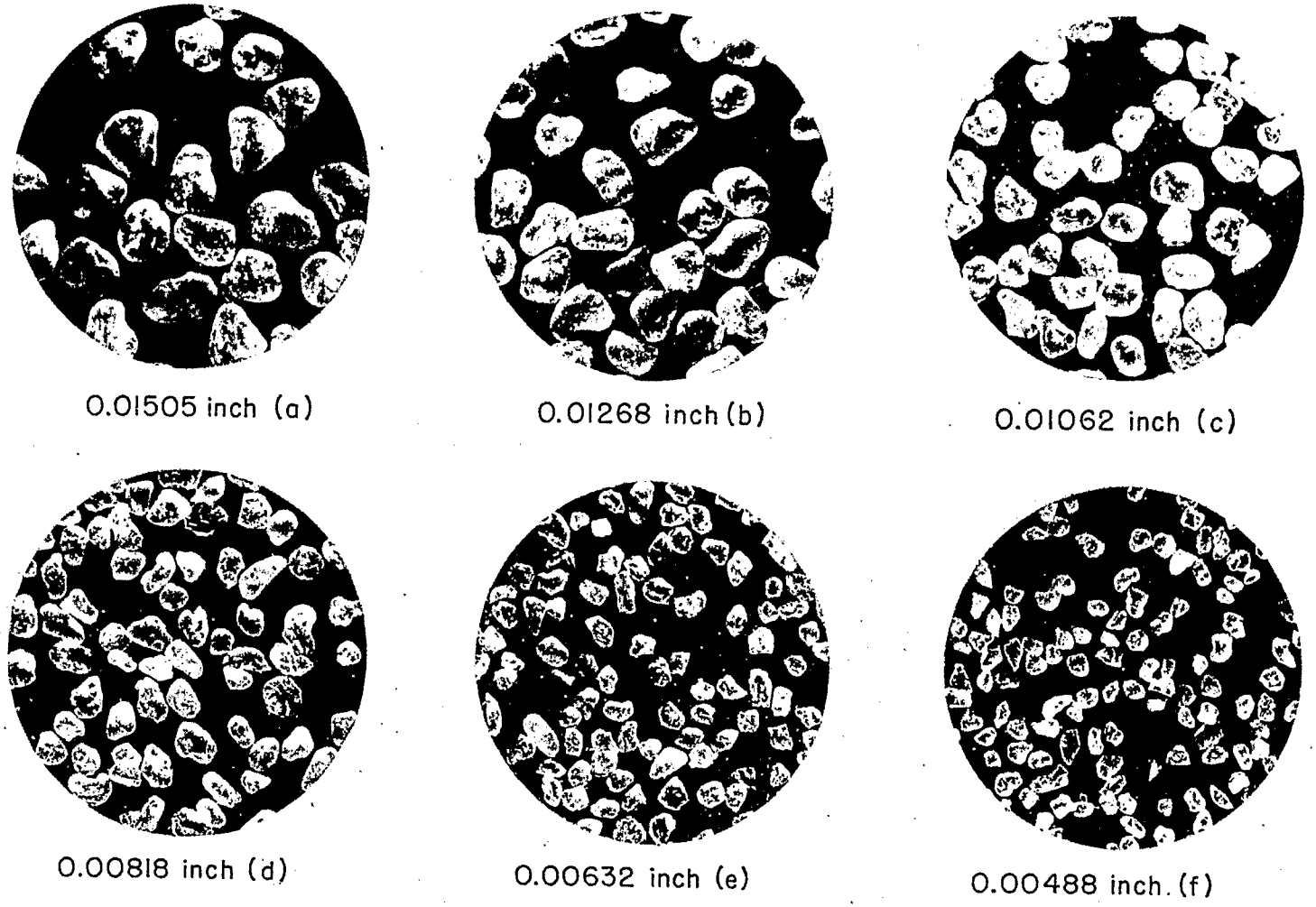

FIGURE 45.—UNIFORM ROUND SANDS. $\lambda = 1.16$.

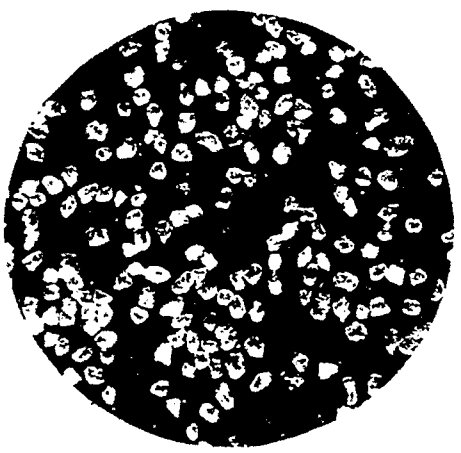

0.00345 inch (g)

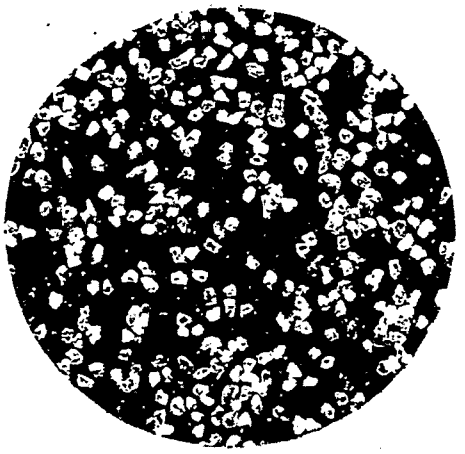

0.00310 inch (h)

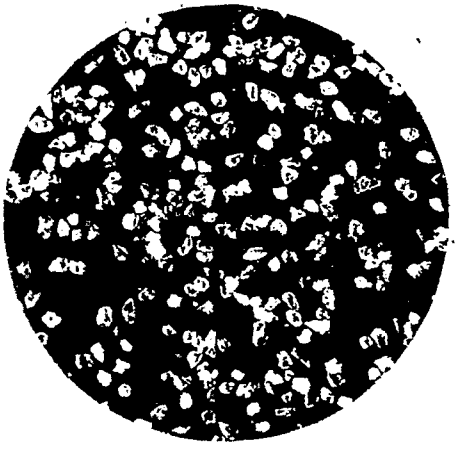

0.00290 inch (i)

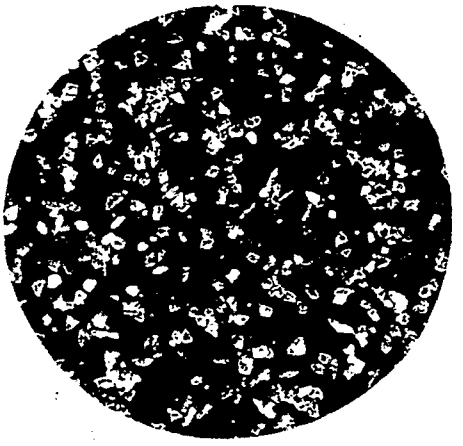

0.00202 inch (j)

0 .0625"

FIGURE 46.—UNIFORM ROUND SANDS. $\lambda = 1.16$.

0 .0625"

FIGURE 45.—UNIFORM ROUND SANDS. $\lambda = 1.16$.

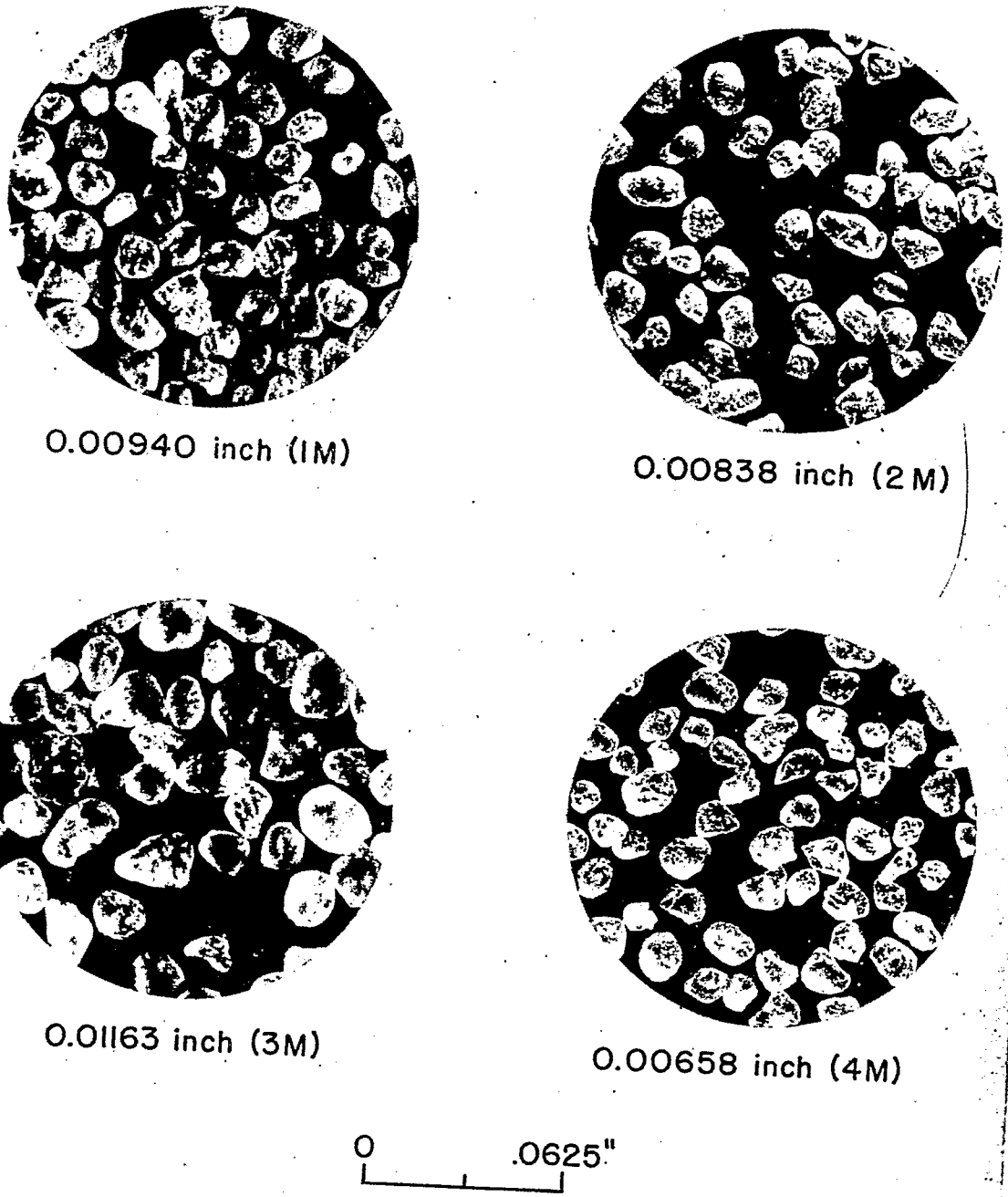

FIGURE 47.—MIXTURES OF ROUND SANDS. $\lambda=1.16$.

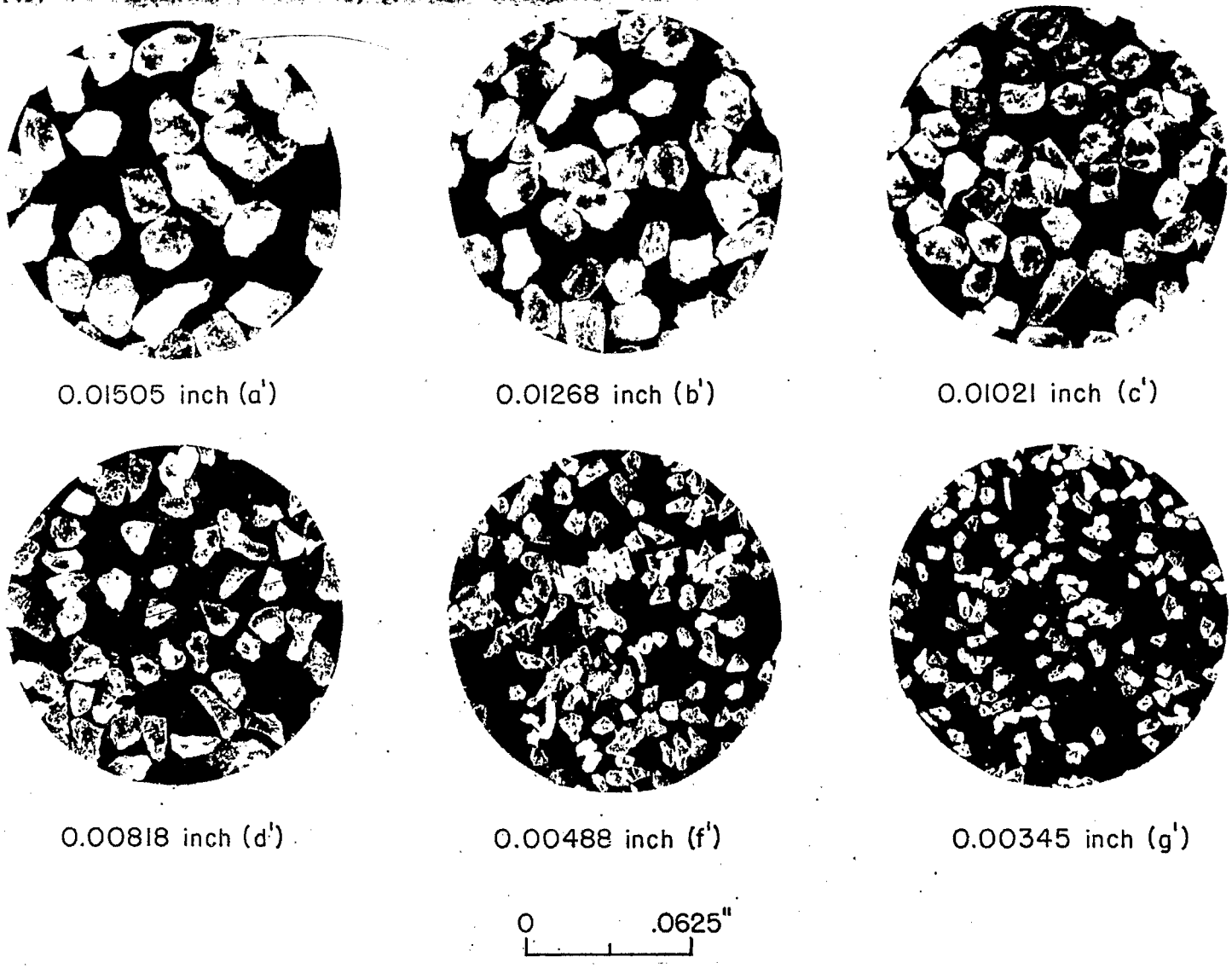

FIGURE 48.—UNIFORM SHARP SANDS. $\lambda = 1.50$.

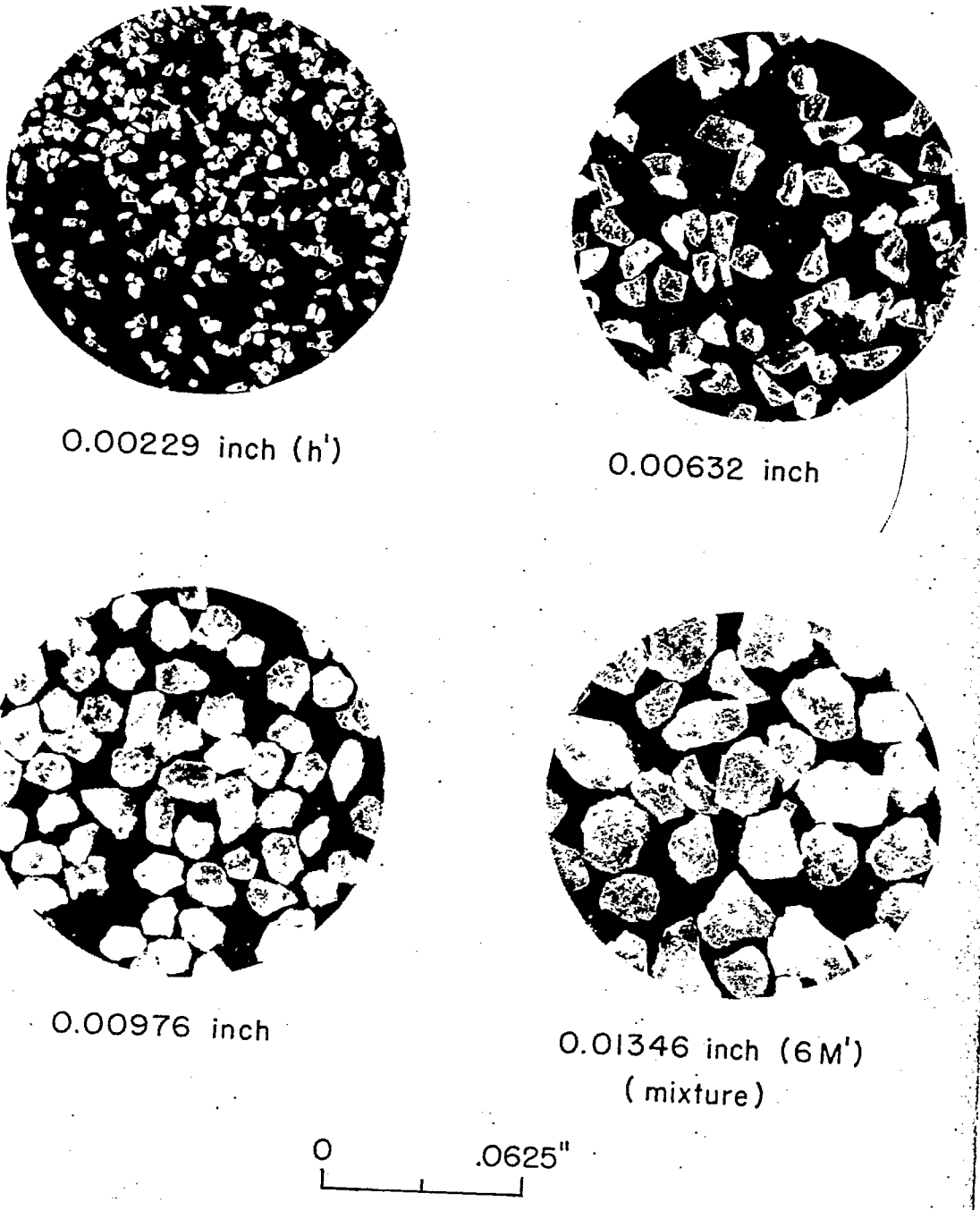

FIGURE 49.—UNIFORM SHARP SANDS. $\lambda=1.50$.

FLUIDIZATION OF SOLIDS

GENERAL

Investigation of fluidization phenomena was undertaken with the aim of developing simple correlations that were primarily intended for use by design engineers and process development men. The present studies are essentially concerned with the mechanics of the operation preliminary to a more complex analysis of heat transfer through such systems. Further attempts were made to arrive at some quantitative means for describing fluidization performance.

VESICULAR AND NONVESICULAR PARTICLES

Fluidization studies showed that for an accurate development of quantitative relationships, knowledge of the fraction of effective voids in a fluidized bed is important. Study of pressure drop through fixed beds has emphasized the importance of the effective-void concept. For fixed beds composed of comparatively large particles, determination of the effective voids by direct measurement is not difficult. For beds composed of small particles such as prevail usually in fluidized units, however, direct measurement of effective voids is possible only with nonvesicular materials. If the conventional water-displacement method is used for the determination of voids in beds of porous (vesicular) materials, a value will be obtained that is too high by an amount depending on the porosity of the particles. In order to preclude these difficulties, investigation of fluidization phenomena was extended first to typical nonporous materials before porous materials were considered.

FLUIDIZATION OF NONPOROUS PARTICLES

DESCRIPTION OF FLUIDIZATION

When a fine granular material is dumped into a vessel, the resulting bed has (as later data confirm) a definite bulk density. This bulk density depends on the size, shape, and density of the individual particles. When the the wall of the vessel is tapped during dumping, the bed packs somewhat more densely than under quiet conditions. Let us assume that illustration (a) in figure 50 represents such a densely packed bed. If a fluid is admitted at a very low rate (G_1) into the bottom of this bed, a small pressure drop will be indicated

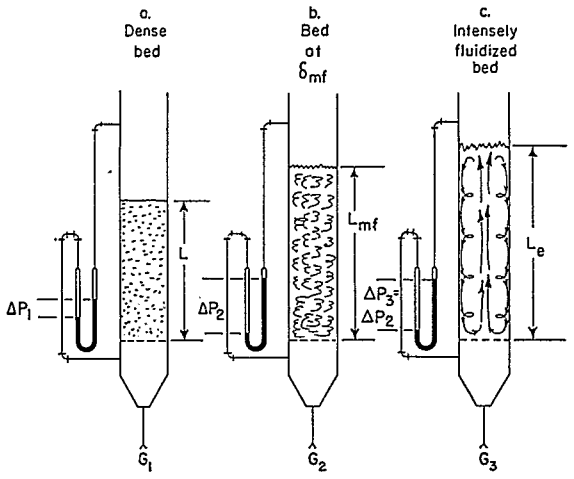

FIGURE 50.—OPERATING STAGES OF FLUIDIZED BEDS.

by the manometer. As the rate of flow is gradually increased, the pressure drop rises to a point of equilibrium at which the weight of the bed in the fluid stream is equal to the fluid pressure drop across the column multiplied by the cross-sectional area of the vessel. Mathematically, this may be expressed by the simple relation:

$$\Delta P = \frac{V_t}{A_t}(1-\delta)(\rho_s-\rho). \qquad (43)$$

As the rate of fluid flow increases still further, the bed begins to expand. This expansion increases the percentage of voids in the bed sufficiently to keep the pressure drop essentially constant despite the accelerated flow rate. At a certain fluid velocity (G_2), the bed will have expanded to such a density that the individual particles have been disengaged from each other sufficiently to permit internal motion of the particles in the bed. This internal motion is induced by the fluid moving through the interstices of the bed and indicates the beginning of fluidization. This condition is illustrated by sketch (b) of figure 50. Just like the bulk density that results from dumping the material into a vessel, this limiting bed density at which fluidization begins depends also on the size and shape of the particles of the bed and has been termed "maximum fluid density." The fractional voids associated with this condition have been called "minimum fluid void-

age." This concept, henceforth referred to as δ_{mf}, is important as far as the onset of fluidization is concerned. It will be discussed in greater detail later.

Additional increase in fluid rate (G_s) expands the bed further and intensifies the motion of the particles. The particle movement, however, is not an entirely random one. It rather appears that particle motion in fluidized beds has definite coordination and resembles a cylindrical vessel filled with liquid, to which heat is added from the bottom. Illustration (c) in figure 50 shows, schematically, these "convection currents," which were usually observed to progress downward on the wall of the vessel. For much higher rates of fluid flow, the state of agitation increases still further, and the position of the top of the bed fluctuates considerably. For very high flow rates, large bubbles usually force their way upward through the bed. In small-diameter fluidization equipment, these bubbles coalesce and form a gas slug, which may also extend over the entire cross section of the unit. This condition is called "slugging" and will be considered later. For conditions (b) and (c) the pressure drop remains essentially constant, with comparatively small fluctuations. For a slugging bed, however, the manometer fluctuates considerably between rather wide limits. These fluctuations of the pressure drop were found to be a fair indication of the slugging behavior of the bed.

Another phenomenon that interferes with smooth fluidization is known as "channeling." Channeling is very important, as it influences heat transfer and space-velocity relations through fluidized reactors very severely.

EXPERIMENTAL DETAILS

It has been observed that pressure drop across an expanded and fluidized bed is readily calculated by means of equation (43). However, the question of particular interest is: What fluid velocity is required to induce bed expansion and incipient fluidization in a given reactor bed? The answer to this is readily obtained by a combination of equation (43) with either pressure-drop equation (40) or (21), depending on whether flow is laminar or turbulent.

Because industrial catalysts intended for fluidization are rarely spherical, the influence of particle shape upon fluidization seemed worthy of investigation. This problem, however, was not difficult, because shape factors had already been assigned to various small-grained materials; the method of correlation and analysis has already been described in connection with the development of equation (40).

The apparatus used for the fluidization study

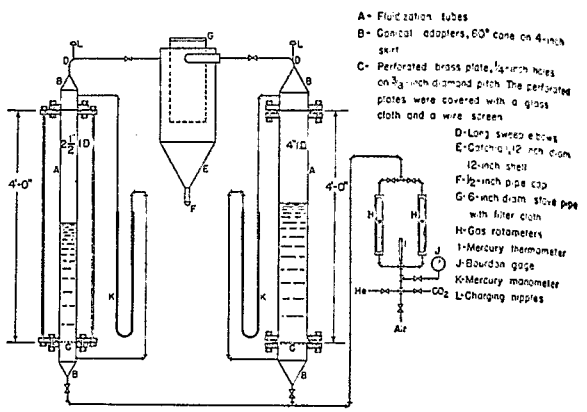

FIGURE 51.—FLUIDIZATION APPARATUS.

is shown in figure 51. The device for leading gas into the fluidization tubes was found satisfactory, and no equalizing material was required. Pressure-drop readings were corrected for screen resistance wherever necessary. Materials investigated were the same round and sharp silica sands that have been described earlier and are shown in figures 45 to 49.

For fluidization runs, known weights of sand were charged into the unit, and a blast of air was admitted for a few seconds. The air was then turned off slowly, and the column height was measured. This measurement served as a basis for calculating the fractional voids in the static bed. Increasing quantities of fluid were then permitted to enter the bottom of the column, and the pressure drop across the column was determined for every flow rate. It was observed that once the bed had been expanded sufficiently further increases in flow imparted motion to the particles. The height of the bed and the pressure drop were carefully recorded for each flow rate. For high flow rates, the top of the bed and the pressure drop fluctuated considerably. At these flow rates, the bed was allowed to operate for several minutes, and the highest and lowest readings were recorded. The maximum and minimum values were then averaged and recorded as the bed height under these flow conditions. In general, the fluctuations of the top of the bed were less pronounced for small-size sands than for large particles. Many of these measurements were examined frequently and found to be satisfactorily reproducible. After the fluidization run was terminated, the dust receiver was opened to recover the material carried over. In no case did the weight of the carry-over amount to more than 1 percent of the total charge in the unit. The error introduced into the measurements owing to loss of sand by elutriation was negligible, therefore.

DATA AND CORRELATIONS

Original and calculated data of the investigation are shown in tables VII to X of the appendix. Figures 52 to 55 present the data

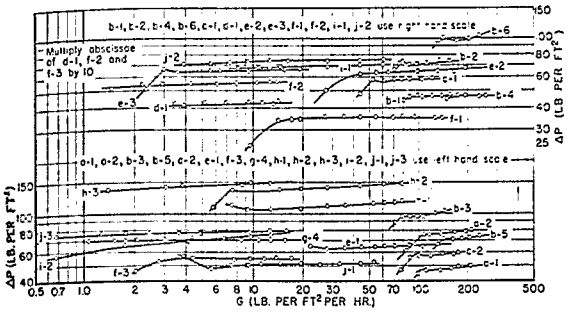

FIGURE 52.—FLUIDIZATION OF ROUND SANDS IN 2½-INCH UNIT.

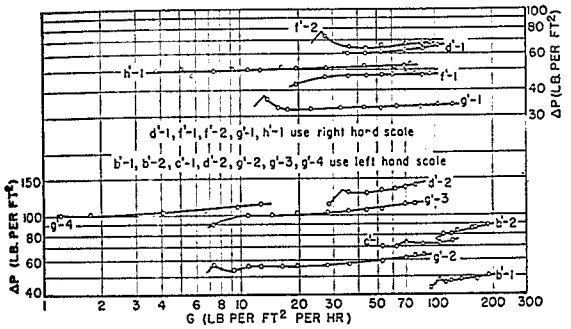

FIGURE 53.—FLUIDIZATION OF SHARP SAND IN 2½-INCH UNIT.

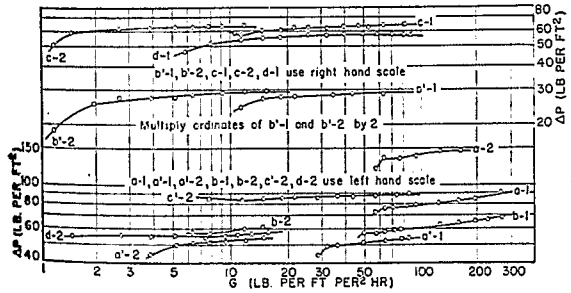

FIGURE 54.—FLUIDIZATION OF SHARP SANDS IN 2½-INCH UNIT.

graphically in a form of log ΔP versus log G. All the runs appear as characteristic flat lines, indicating slight variation of pressure drop with flow rate. For the initial point of bed expansion:

$$\Delta P=\frac{V_t}{A_t}(1-\delta)(\rho_s-\rho); \tag{43}$$

and, if the flow is viscous,

$$\Delta P=\frac{200G\mu L\lambda^2(1-\delta)^2}{D_p^2\rho g_c\delta^3}. \tag{40}$$

943247—51——5

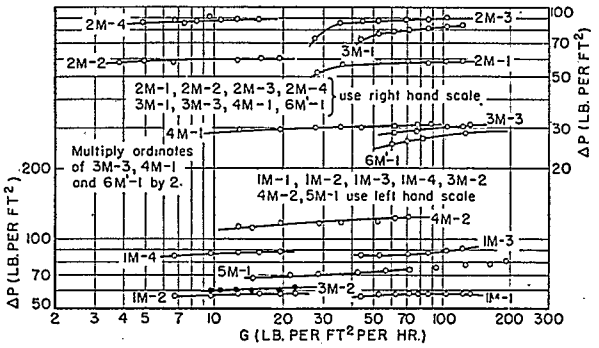

FIGURE 55.—FLUIDIZATION OF MIXTURES OF ROUND AND SHARP SANDS.

Equating the two expressions and solving for G yields:

$$G=\frac{V_t(1-\delta)(\rho_s-\rho)D_p^2\rho g_c\delta^3}{A_t200\mu L\lambda^2(1-\delta)^2}. \tag{44}$$

As

$$\frac{V_t}{A_t}=L,$$

equation (44) becomes:

$$G=0.005\frac{D_p^2g_c\rho(\rho-\rho)\delta^3}{\mu\lambda^2(1-\delta)}. \tag{45}$$

If the bed has a voidage equal to δ_{mf} incipient fluidization prevails and the mass flow rate for this condition is then given by:

$$G_{mf}=\frac{0.005D_p^2g_c\rho(\rho_s-\rho)\delta_{mf}^3}{\mu\lambda^2(1-\delta_{mf})}. \tag{45a}$$

ILLUSTRATIONS

NO. 1

Microscopic examination of a sample of silica sand indicates that its shape is intermediate between "round" and "sharp." For the following operating conditions, find the air velocity which will just expand the sand:

Vessel diameter	4 in.
Weight of sand bed	10 lb.
Bed height	1.25 ft.
Particle size (150- to 200-mesh)	0.00345 in.
Specific gravity of sand	2.65
Inlet air pressure	15.00 p.s.i.a.
Air temperature	70° F.

The voids in the bed are first calculated by the expression:

$$\delta=\frac{(0.0872)(1.25)-\dfrac{10}{(62.4)(2.65)}}{(0.0872)(1.25)}=0.445,$$

$$\frac{(1-\delta)}{\delta^3}=6.30.$$

The density of the air: $\rho=\frac{(29)(492)(15.00)}{(359)(530)(14.7)}=0.0765$ lb./ft.^{3}

Shape factor: $\lambda=\frac{1.16+1.50}{2}=1.33$

Viscosity of air: 0.043 lb. hr.$^{-1}$ ft.$^{-1}$

For solid-gas systems, ρ is small as compared to ρ_s, and equation (45) may be simplified to:

$$G=(0.005)(g_c)\left(\frac{D_p^2\rho\rho_s\delta^3}{\mu\lambda^2(1-\delta)}\right). \qquad (45b)$$

Substituting into (45b),

$$G=(0.005)(4.18)(10^8)\frac{(0.00345)^2(0.0765)(165)(0.445)^3}{(144)(0.043)(1.33)^2(1-0.445)};$$

$$G=4.54$$

$$u=\frac{4.54}{(3600)(0.0765)}=0.0164 \text{ ft./sec.}$$

NO. 2

Water is passed upward through a column of glass spheres. Find the linear water velocity necessary to expand the column, given the following conditions:

$D_p=0.205$ in.

$\rho_s=146.5$ lb./ft.^{3}

$\rho=62.4$ lb./ft.^{3}

$\mu=2.42$ lb. hr.$^{-1}$ ft.$^{-1}$

$\delta=0.382$

$\lambda=1.00$

Because the bed is composed of large particles, turbulent flow is anticipated, and a similar relation may be developed:

$$\Delta P=\frac{2.00fG^2\lambda^{1.1}(1-\delta)L}{D_p\rho g_c\delta^3}. \qquad (14)$$

Equating (14) with (43) and solving for G yields:

$$G=\sqrt{0.5\frac{g_cD_p\rho(\rho_s-\rho)\delta^3}{f\lambda^{1.1}}},$$

where for smooth particles

$$f=1.75\left(\frac{D_pG}{\mu}\right)^{-0.1}.$$

Assuming $f=1$, a first trial for G yields:

$$G=\sqrt{(0.5)(4.18)(10^8)\frac{(0.205)(62.4)(84.1)(0.382)^3}{(12)(1-0.382)(1)}};$$

$$G=41400$$

$$\frac{D_pG}{\mu}=\frac{(41400)(0.205)}{(12)(2.42)}=292.$$

From figure 10, $f=0.95$ for

$$\frac{D_pG}{\mu}=292.$$

Recalculating G on the basis of $f=0.95$ yields $G=42400$ and

$$\frac{D_pG}{\mu}=300.$$

Because a value of 300 for

$$\frac{D_pG}{\mu}$$

is in good agreement with $f=0.95$, the calculation of G is close enough

$$\therefore, \mu=\frac{42400}{(3600)(62.4)}=0.188 \text{ ft/sec.}$$

This value is of the same order of magnitude as 0.136 ft./sec., a value observed by Wilhelm and Kwauk [40] for the conditions specified.

MINIMUM FLUID VOIDAGE

In the previous section of the paper, a correlation has been developed permitting the prediction of bed expansion for counter-gravity flow. Before an ordinary dense bed of particles can exist in a fluidized state, it must pass through this point of expansion. Mere expansion, however, is not necessarily enough to permit fluidization. The experimental data indicated that before fluidization could begin a definite amount of expansion was necessary, depending primarily on the original static bed density. For high initial densities, a comparatively large amount of expansion was needed, whereas, for low initial densities, very little or no expansion was required. In fact, a static bed at its "maximum fluid density," as this necessary condition for incipient fluidization is defined, does not require any expansion at all before the bed is ready for fluidization. Any bed that has the maximum fluid density or is composed of the corresponding "minimum fluid voidage" will begin to fluidize under the influence of very small fluid quantities moving up the column. It is apparent, therefore, that the prediction of the minimum fluid voidage is of fundamental importance if it is desired to estimate reliably the onset of fluidization.

The minimum fluid voidage of a bed of fine particles is easily determined by fluidizing the bed intensely and gradually reducing the fluid

[40] Work cited in footnote 95, p. 7.

to zero. This permits the particles to settle gradually into a position from which they may readily be picked up again and fluidized. For sands, the minimum fluid voidage could be closely approximated by pouring the material into a vessel at a moderate rate. The voidages thus obtained are somewhat smaller than δ_{mf}, although the difference is insignificant. Values of δ reported in tables 14 to 18 were obtained by charging rather than by settling. As charging is more convenient, it is preferred for rapid determinations.

Figure 56 shows a plot of δ_{mf} versus D_p. It appears that δ_{mf} is considerably higher for sharp

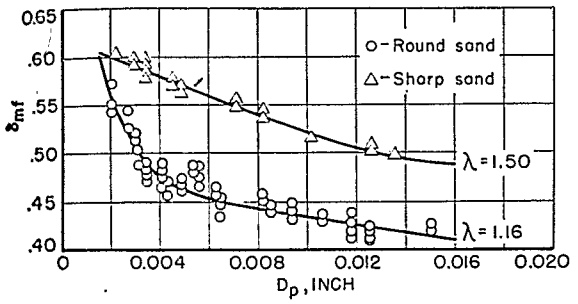

FIGURE 56.—MINIMUM FLUID VOIDAGE, δ_{mf}, FOR ROUND AND SHARP SANDS IN RELATION TO PARTICLE DIAMETER.

sands than for round sands and lowest for mixtures. The differences in δ_{mf} for the various materials may be explained from considerations of the shape of the particles. When sharp sand is poured from a definite height into a vessel, it comes to rest sooner than round sand. (Owing to the sharp corners and uneven surfaces, there is a greater amount of "catching" of particles with sharp particles than with rounder bodies.) These results are similar to the observations made in connection with packing densities of large particles in packed towers, where it was observed that rough, large particles build beds that are less dense than those composed of smooth particles of the same shape, provided loading methods were comparable. Values of δ_{mf} for the round sand are somewhat smaller than 46 percent (the voidage of the loosest arrangement that spheres can have). This may be explained by assuming that the sands (though close cuts) are, nevertheless, mixtures containing a certain proportion of smaller particles. The small bodies tend to fill the spaces between the larger particles and reduce the over-all voidage to below 46 percent.

Figure 56 shows that δ_{mf} increases for decreasing values of D_p. This observation is probably related to the ratio of surface area to volume for the sands in question. The finer the particles, the greater the surface area exhibited by a unit weight of sand. When loaded into a vessel, the sand normally comes to rest when the frictional work between the individual particles, expended in their downward motion into the vessel, is equal to the change in potential energy of the sand between its initial position and final resting position in the tube. Because the frictional work increases with the exposed surface area, a unit weight of small worn or angular sand should come to rest sooner than large sand of the same weight and type. The result should be a higher voidage for the smaller sand. The height of the sand column seemed to have no significant effect upon δ_{mf}.

CORRELATION

Analysis of the fluidization data is based primarily upon the possibility of applying the standard pressure-drop equations to the expanded bed. Because, as indicated by the order of magnitude of the modified Reynolds numbers, the observed data extend over the viscous flow range, application of equation (40)

$$\Delta P=\frac{200G\mu\lambda^2L(1-\delta)^2}{D_p^2g_c\rho\delta^3} \tag{40}$$

is suggested.

Consider a bed of particles of uniform size and of unit height in an unexpanded, static condition. The bed voidage, δ, is determined by the shape characteristics and the mode of packing. Admission of a fluid at an increasing rate increases the pressure drop across the bed until a value of

$$\Delta P=\frac{V_t}{A_t}(1-\delta)(\rho_s-\rho) \tag{43}$$

is reached, after which the pressure drop remains essentially constant despite further increases in rate of flow. Because, for a given material, the particle diameter, D_p, and the shape factor, λ, in equation (40) can be considered constant, equation (40) may be rewritten:

$$\frac{G\mu L}{\rho}\frac{(1-\delta)^2}{\delta^3}=C, \tag{46}$$

where

$$C=\frac{\Delta P\,D_p^2g_c}{200\lambda^2}. \tag{46a}$$

Let the ratio of the height of the expanded bed, L_e, to the height of the static bed, L, be designated by the symbol l_e. If, for convenience, $L=1$, l_e not only represents the instantaneous bed height related to any particular fluid flow rate but also the ratio of expansion

$$\frac{L_e}{L}.$$

Therefore, equation (46) may be rewritten:

$$G\frac{\mu}{\rho}l_e \propto \left[\frac{(1-\delta)^2}{\delta^3}\right]^{-1}. \qquad (47)$$

From equation (47), it follows that, if fluid flow through a fluidized bed conforms with equation (40), a plot of

$$\frac{Gul_e}{\rho}$$

against

$$\frac{(1-\delta)^2}{\delta^3}$$

using logarithmic coordinates should produce a straight line of slope $m=-1$.

All the experimental data have been analyzed in this manner. Figures 57 and 58 show

$$\log G\frac{\mu}{\rho}l_e$$

plotted against

$$\log \frac{(1-\delta)^2}{\delta^3}$$

for large and small round sands. Figure 59 shows a similar correlation for sharp sands. All these data were observed with the 2.5-inch unit. Figure 60 shows a correlation of data obtained with round and sharp sands fluidized in the 4-inch unit. Figure 61 represents data pertaining to mixtures of sands. In the above figures, each line refers to one particular type and size, or mixture of sizes, of sand. The slopes of the various lines differ from each other and deviate markedly from $m=-1$. This suggests immediately that fluid flow through a fluidized bed does not obey equation (40). The apparent irregularity of the numerical values of the slopes indicates greater complexity.

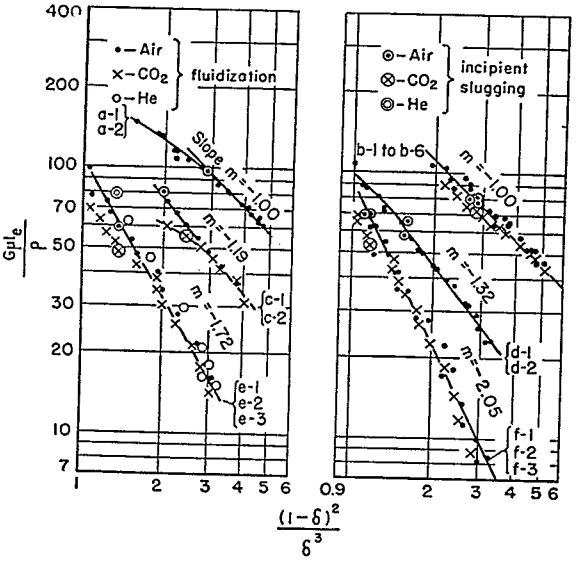

FIGURE 57.—FLUIDIZATION OF LARGE, UNIFORM, ROUND SANDS IN 2½-INCH UNIT.

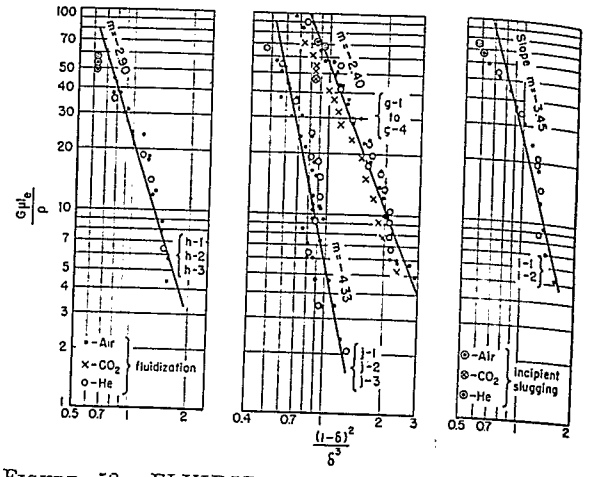

FIGURE 58.—FLUIDIZATION OF SMALL, UNIFORM, ROUND SANDS IN 2½-INCH UNIT.

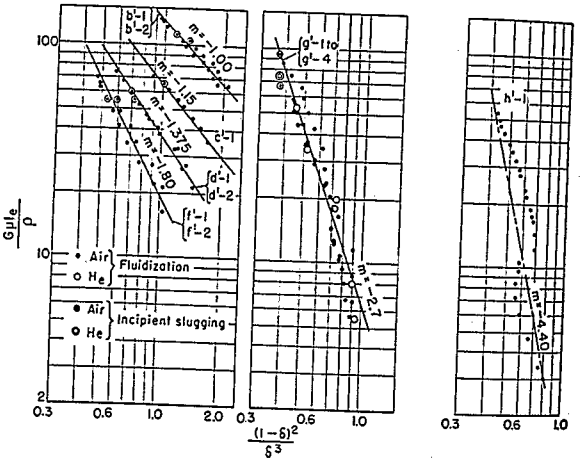

FIGURE 59.—FLUIDIZATION OF UNIFORM SHARP SANDS IN 2½-INCH UNIT.

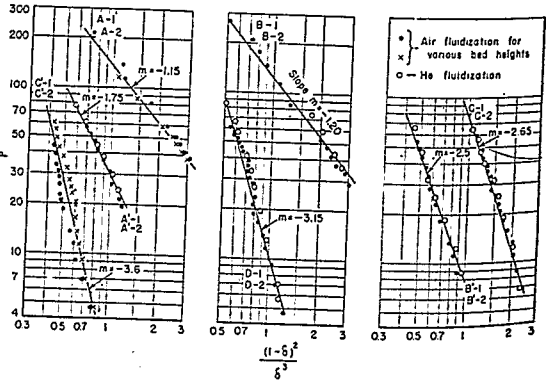

FIGURE 60.—FLUIDIZATION OF UNIFORM ROUND AND SHARP SANDS IN 4-INCH UNIT.

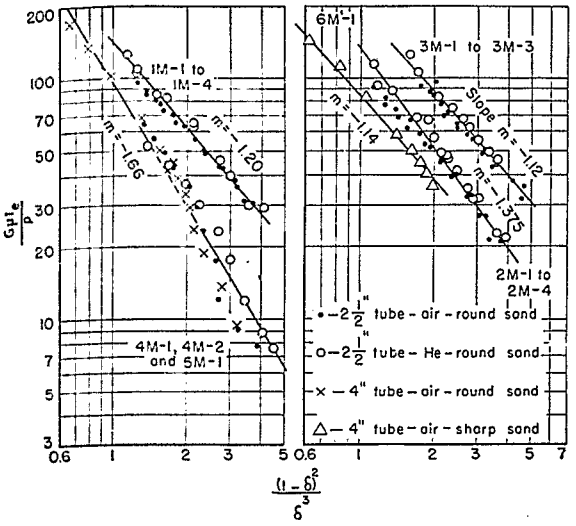

FIGURE 61.—FLUIDIZATION OF MIXTURES OF SANDS IN 2½-INCH AND 4-INCH UNITS.

Figure 62 relates D_p with m, the slopes of the lines represented in figures 57 to 61. In view of the variety of sizes, shapes, and mixtures of sands tested in vessels of different diameters and using fluids of greatly different physical properties, the correlation should be considered significant.

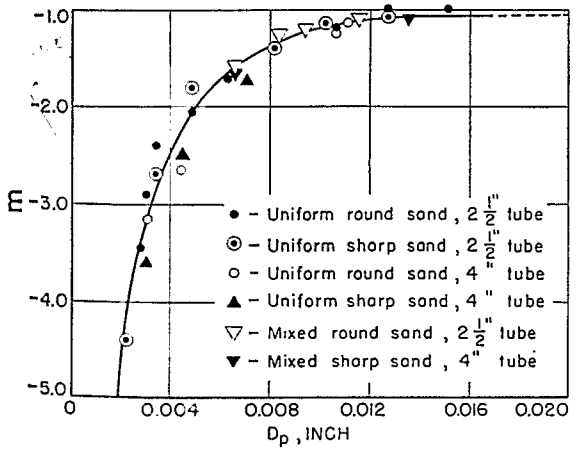

FIGURE 62.—VALUES OF m IN RELATION TO D_p FOR SANDS.

FLUIDIZATION EFFICIENCY

In figure 63, let the straight line $G_{mf}G_f$ be a plot of

$$\log G\frac{\mu}{\rho}l_e$$

against

$$\log \frac{(1-\delta)^2}{\delta^3}.$$

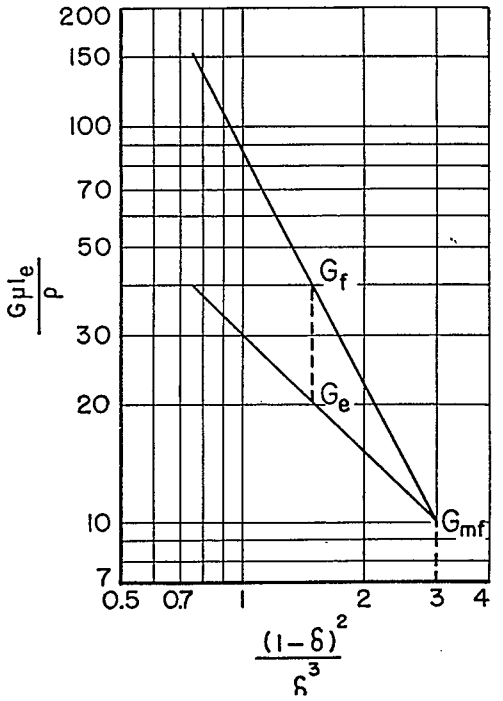

FIGURE 63.—FLUIDIZATION AND EXPANSION LINES OF A TYPICAL SMALL SAND.

For illustration purposes, let the slope of this line, m, equal -2. $G_{mf}G_e$ is another straight line of slope, m, equal -1. If the void factor,

$$\frac{(1-\delta)^2}{\delta^3},$$

corresponding to G_{mf} is the void factor of a bed of minimum fluid voidage, the fluidization line, $G_{mf}G_f$, relates the required mass velocities of the fluid with the respective voidages in the fluidized bed. Because $m=-1$, it is also evident that line $G_{mf}G_e$, the expansion line, relates the required mass velocities of the fluid with the same values of

$$\frac{(1-\delta)^2}{\delta^3},$$

not for a fluidized bed, but merely for an expanded bed. As both the fluidization and the expansion lines are lines of equal and constant pressure drop, the ordinates

$$G\frac{\mu}{\rho}l_e,$$

with reference to the proper line, are proportional to the energy involved in the rate of flow of fluid through the fluidized bed and through the expanded bed, respectively. Furthermore, because the ordinates

$$G\frac{\mu}{\rho}l_e$$

for the same values of

$$\frac{(1-\delta)^2}{\delta^3}$$

are always higher for the fluidization line than for the expansion line, it follows that more energy is expended to pass fluid through a fluidizing bed than would be needed for flow through an expanded bed without fluidization. With this interpretation of the experimental data, it is possible to define fluidization efficiency:

$$E_\phi=\frac{W_\phi}{W_t}=\frac{W_t-W_e}{W_t}=\frac{G_f\frac{\mu}{\rho}l_e-G_e\frac{\mu}{\rho}l_e}{G_f\frac{\mu}{\rho}l_e}, \quad (48a)$$

or simply:

$$E_\phi=\frac{G_f-G_e}{G_f}. \quad (48)$$

EQUATIONS

From equation (48) it appears that for the evaluation of fluidization efficiency it is necessary only to know the mass velocity, G_f, required to fluidize the bed and the mass velocity, G_e, required to expand the bed. As G_e refers to an expanded bed without fluidization, it may be calculated directly from equation (40) provided the necessary data are available. G_f may be calculated from G_e using the relationship developed below.

From figure 63, it appears that for the fluidization line

$$\frac{\log\left(G_f l_f\frac{\mu}{\rho}\right)-\log\left(G_{mf}l_{mf}\frac{\mu}{\rho}\right)}{\log\frac{(1-\delta)^2}{\delta^3}-\log\frac{(1-\delta_{mf})^2}{\delta_{mf}^3}}=m. \quad (49)$$

Cancelling out $\frac{\mu}{\rho}$ and rearranging, equation (49) may be written:

$$\left[\frac{G_f l_f}{G_{mf}l_{mf}}\right]^{1/m}=\frac{(1-\delta)^2\delta_{mf}^3}{(1-\delta_{mf})^2\delta^3}. \quad (49a)$$

Solving equation (49a) for

$$\frac{(1-\delta)^2}{\delta^3},$$

recalling that $l_{mf}=1$, and replacing l_f by

$$l_f=l_e=\frac{V_T(1-\delta_{mf})(A_T)}{A_T V_T(1-\delta)}=\frac{(1-\delta_{mf})}{(1-\delta)} \quad (50)$$

finally yields:

$$\frac{(1-\delta)^{2+1/m}}{\delta^3}=\left(\frac{G_f}{G_{mf}}\right)^{1/m}\frac{(1-\delta_{mf})^{2+1/m}}{\delta_{mf}^3}. \quad (51)$$

A similar analysis is possible for the expansion line. Thus:

$$\left[\frac{G_e l_e\frac{\mu}{\rho}}{G_{mf}l_{mf}\frac{\mu}{\rho}}\right]^{-1}=\frac{(1-\delta)^2\delta_{mf}^3}{(1-\delta_{mf})^2\delta^3}. \quad (52)$$

Substituting (52) into (49a) and cancelling out $\frac{\mu}{\rho}$ yields:

$$\left(\frac{G_f l_f}{G_{mf}l_{mf}}\right)^{1/m}=\frac{G_{mf}l_{mf}}{G_e l_e}. \quad (53)$$

Recalling that $l_{mf}=1$ and $l_e=l_f$, equation (53) becomes:

$$G_f=\frac{G_{mf}}{l_e}\left(\frac{G_{mf}}{G_e l_e}\right)^m. \quad (54a)$$

Since m is inherently negative, equation (54a) may be written in the form:

$$G_f=\frac{G_{mf}}{l_e}\left(\frac{G_e l_e}{G_{mf}}\right)^{[m]}. \quad (54)$$

This is an important equation in connection with fluidization calculations, and its application will be demonstrated in a practical problem.

From equation (52), it also follows that:

$$\frac{(1-\delta)^2}{\delta^3}=\frac{(1-\delta_{mf})^2}{\delta_{mf}^3}\left[\frac{G_{mf}}{G_e l_e}\right]. \quad (51a)$$

Substituting (50) into (51a) yields:

$$\frac{(1-\delta)}{\delta^3}=\frac{(1-\delta_{mf})}{\delta_{mf}^3}\left[\frac{G_{mf}}{G_e}\right]. \quad (55)$$

It is of interest to observe that equation (51) reduces to the form of equation (55) if $m=-1$ and if $G_f=G_e$ is substituted.

Equation (49) permits the calculation of G_f if G_{mf}, G_e, and m are known. For a given size of sand, m may be obtained from figure 60. From figure 54, δ_{mf} can be evaluated and can be used with equation (40) to predict G_{mf}. From the same equation, G_e can be calculated for any expansion ratio, l_e, and then, through application of equations (49) and (51), the necessary mass velocity for fluidization and the efficiency of the operation are easily obtained.

DISCUSSION

The fluidization of round and sharp sands was investigated with air, carbon dioxide, and helium in 2.5-inch- and 4-inch-diameter vessels. Table 25 lists the physical properties of the gases which, according to equation (40), affect flow through nonfluidized beds.

TABLE 25.—*Physical properties of carbon dioxide, air, and helium at 70° F. and 14.7 p.s.i.a.*

	μ	ρ	$\mu/\rho=\eta$	$\eta gas/\eta CO_2$
CO_2	0.0350	0.1140	0.307	1.00
Air	.0435	.0750	.580	1.89
Helium	.0488	.0103	4.350	14.18

The kinematic viscosity, η, of helium is 14.18 times that of carbon dioxide and 7.5 times that of air. The agreement in figures 52 to 56 is therefore significant. For small sizes of sand (especially in the 2.5-inch tube), a peculiar inverted S-shaped trend persists for which no satisfactory explanation could be found. The data indicate that the kinematic viscosity of the fluid affects fluid flow through a fluidized bed just as it affects flow through fixed beds.

Ever since fluidization was considered as a possible operation by which catalysts may be contacted effectively by gases or fluids in general, the phenomenon of slugging has received much attention. The reasons for this consideration were simple, as it was postulated with good evidence that in slugging beds the contact between the solid phase and the fluid is not as effective as would be desirable, primarily because of poor dispersion. There are, of course, other features, primarily mechanical in nature, that render excessive slugging in a fluidized column undesirable.

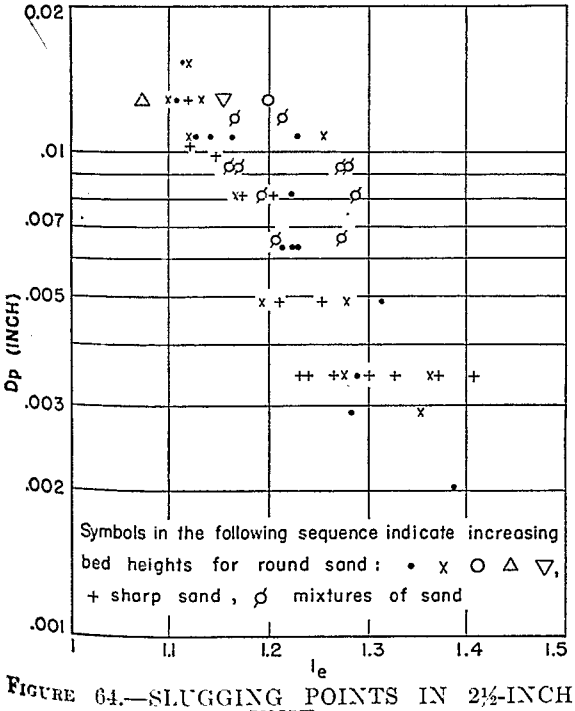

FIGURE 64.—SLUGGING POINTS IN 2½-INCH UNIT.

During many of these simple tests, attempts were made to find the onset of slugging in the various beds. Thus, in the various graphs just discussed, incipient slugging points were indicated, and the results are shown graphically in figure 64. Primarily due to the considerable particle range involved, for the purpose of condensation of scales, the logarithm of the particle diameter was plotted against the expansion ratio of the individual beds. There is a distinct downward trend of the data, indicating that small-diameter particles begin to slug at higher expansion ratios than larger particles. This means simply that with small particles in general the smooth fluidization range, as indicated by mass velocities, is greater than with large materials. The data also seem to indicate that incipient slugging occurs more readily with tall beds than with short beds. This latter fact is to be expected from general observation of the formation of gas slugs. With taller beds, the opportunity for large bubble formation is more favorable, because the travel time of the gases up the column is greater.

In general, the steadiness of the pressure drop was a reliable indication of slugging in the tube. For smooth fluidization—that is, operation with good gas dispersion—the pressure drop fluctuated very little, perhaps 1 to 3 percent. For incipient slugging, however, variations of 5 to 10 percent usually were observed. For severe slugging, the fluctuations of the pressure drop were above 10 percent.

Slugging phenomena have been of considerable interest ever since application of fluidization to process work was considered. Investigation of heat transfer through fluidized beds has shown that slugging apparently does not affect the coefficients as much as one might anticipate. No systematic data on the effect of slugging upon other process variables are available. Besides inefficient gas-solid distribution, another objection to slugging is the increased wear and tear on the equipment.

Figure 65 shows calculated values of fluidization efficiencies for all the materials plotted against the expansion ratio. The graphs follow a regular pattern and indicate that fine materials may be fluidized more efficiently than coarse particles. If, for example, a bed composed of particles of $D_p=0.00632$ inch is compared with a bed of particle size $D_p=0.01100$ inch, then, for an expansion ratio $l_e=1.20$ it appears that the bed composed of small particles utilizes almost 49 percent of the total flow energy for fluidization, whereas the large-particle bed utilizes only about 17 percent of the total energy. The remaining 51 and 83 percent, respectively, of the total energy of the gas are dissipated otherwise. The data analysis reveals here, too, that the mixed particle sizes correlate

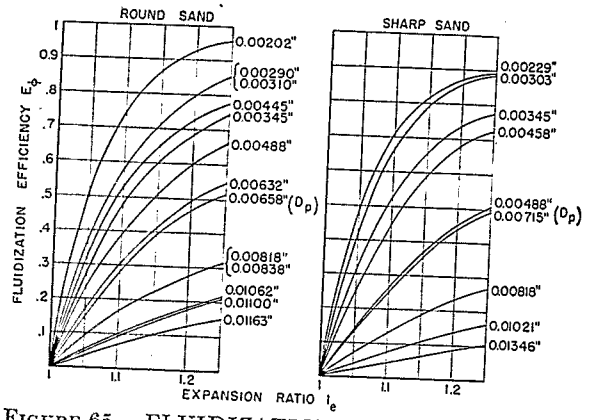

FIGURE 65.—FLUIDIZATION EFFICIENCIES FOR ROUND AND SHARP SANDS.

well when the diameter of the mixture is chosen according to the rule

$$D_p=\sum_{Z=1}^{Z=Z}(Xd_p)_Z. \qquad (20)$$

A comparison of fluidization efficiencies for round and sharp sand is not conclusive at this time. It appears that investigation of many more irregularly shaped particles is necessary before a definite trend can be predicted.

One of the most important variables to be considered in a study of fluidization is the percentage voids in the bed, particularly the minimum fluid voidage. The materials investigated offered little difficulty in evaluating δ_{mf} correctly, because the individual particles were uniformly dense and had well-defined surfaces. A bed of coke or other honeycombed material has a much greater voidage than a sand bed of comparable particle size. However, not all these voids in the coke bed are effective in permitting the fluid to pass through the bed. Any correlation that would apply to flow through a vesicular bed should take into account the fraction of effective voids. This will be discussed in detail in connection with fluidization phenomena of coal particles.

ILLUSTRATION

PROBLEM

A sandy material is poured into a cylindrical vessel, and air is admitted into the base of the vessel through a distributor. The operating conditions are as follows:

Sand:
- Weight — 20 lb.
- Specific gravity — 2.65.
- Size — 100- to 150-mesh.
- Shape factor (estimated) — 1.3.

Air:
- Temperature — 70° F.
- Outlet pressure — 14.7 p.s.i.a.
- Rate (standard conditions) — 40 cu. ft./hr.

Vessel diameter — 4 in.

Determine

1. For the operating conditions stated, will fluidization occur?
2. If fluidization occurs, estimate:
   a. Efficiency of fluidization operation.
   b. Expanded bed height and bulk density at fluidization.
   c. Fluidization energy.

SOLUTION

Effective particle diameter:

$$D_p=\sqrt{(0.0041)(0.0058)}=0.00488 \text{ in.}$$

The estimated shape factor of the sand:

$$\lambda=1.3.$$

From figure 56, $\delta_{mf}=0.50$ (value estimated between round and sharp sand).

Fluidization pressure drop:

$$\Delta P=\frac{20}{(0.785)(0.33)^2}=230 \text{ lb./ft.}^2$$

Static column height:

$$L=\frac{20}{(2.65)(62.4)(0.50)(0.33)^2(0.785)}=2.78 \text{ ft.}$$

G_{mf} may now be calculated from equation (40):

$$230=\frac{(200)(G_{mf})(0.0435)(1.3)^2(2.78)(0.50)^2(144)}{(0.00488)^2(0.0750)(4.18)(10^3)(0.50)^3};$$

from which $G_{mf}=14.6$ lb. hr.$^{-1}$ ft.$^{-2}$.

The mass velocity of the operation:

$$G_f=\frac{(40)(0.0750)}{(0.0850)}=35.2 \text{ lb. hr.}^{-1} \text{ ft.}^{-2}$$

Because $G_f>G_{mf}$ and because, from figure 62, it appears that for this sand $m=-2.05$ the bed will be in a fluidized condition.

Next, it is necessary to calculate the percentage voids in the bed when it fluidized. Since at this point G_f, G_{mf}, δ_{mf}, and m are known, equation (51)

$$\frac{(1-\delta)^{(2+1/m)}}{\delta^3}=\left(\frac{G_f}{G_{mf}}\right)^{1/m}\frac{(1-\delta_{mf})^{(2+1/m)}}{\delta_{mf}^3}$$

may be applied immediately. Thus:

$$\frac{(1-\delta)^{\left(2-\frac{1}{2.05}\right)}}{\delta^3}=\left(\frac{35.2}{14.6}\right)^{-\frac{1}{2.05}}\frac{(1-0.50)^{2-\frac{1}{2.05}}}{(0.5)^3}$$

from which

$$\frac{(1-\delta)^{1.51}}{\delta^3}=1.740.$$

By trial and error, $\delta=0.555$.

Then

$$l_e=\frac{1-\delta_{mf}}{1-\delta}=\frac{1-0.50}{1-0.555}=1.122.$$

Now equation (54) may be applied to find G_e.

$$35.2=\frac{14.6}{1.122}\left[\frac{G_e\ 1.222}{14.6}\right]^{2.05},$$

from which $G_e=21.0$ lb. hr.$^{-1}$ft.$^{-2}$

Efficiency:

$$E_\phi=\frac{35.2-21.0}{35.2}=0.402.$$

Fluidization energy: $W_\phi=(230)(40)(0.402)=3{,}700$ ft.-lb. or 0.112 hp.

The expanded bed height is (2.78) (1.122)= 3.12 ft., and the bulk density at fluidization will be (62.4)(2.65)(1-0.555)=73.5 lb./ft.^{3}

FLUIDIZATION OF AN IRON FISCHER-TROPSCH CATALYST

In the previous section, correlations were developed that apply to the fluidization of nonporous solid particles. The materials used for these studies were round and sharp silica sands. Although the correlations apparently indicate that the density of the particles is not involved, an investigation of materials with densities sufficiently different from that of sand was undertaken to provide a broader basis for application of the correlations. In view of recent interest in synthetic liquid fuel processes and the possible extension of the fluidization technique to these and other operations, it seemed particularly worth while to investigate the fluidization characteristics of a typical iron Fischer-Tropsch (hydrocarbon) catalyst.

MATERIAL AND OPERATION

The chemical composition of the iron Fischer-Tropsch catalyst corresponded closely to the formula Fe_3O_4, magnetite. The pycnometric density was 5.00 g./cc. and in satisfactory agreement with that of Fe_3O_4 (5.18 g./cc.). The material was ferromagnetic of low remanence. Figure 66 shows the weight-size distribution of the various materials investigated. All the beds were composed of mixtures containing 5 to 10 different particle sizes ranging from 28- to 325-mesh. Figure 67 shows photographs of the materials. Comparison with the earlier photographs of samples of round and sharp sands shows the iron-catalyst particles to be considerably more irregular than sharp sand. For this reason, the shape factor of the catalyst particles could not be estimated satisfactorily by comparison with sand particles, and a separate shape-factor determination was necessary.

The apparatus and experimental technique were the same as those described in connection

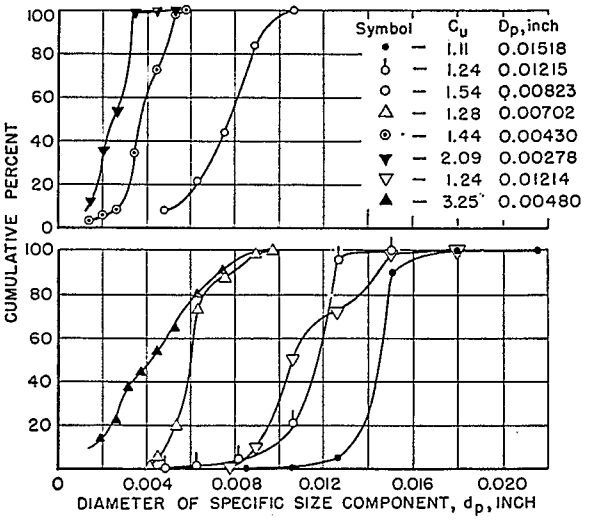

FIGURE 66.—WEIGHT-SIZE DISTRIBUTION OF IRON FISCHER-TROPSCH CATALYST BEDS INVESTIGATED.

with sand fluidization. Known weights of catalyst were charged into a 4-inch-diameter tube, and the static height of the column was recorded. As the catalyst particles were nonvesicular, the percentage voids could be calculated immediately. Air and helium were used as fluidization mediums. When increasing quantities of gas were admitted, the pressure drop increased until the bed began to expand; at this point, a small increase in fluid-flow rate caused a considerable decrease in pressure drop and the formation of channels through the bed. As the gas-flow rate was increased, the pressure drop slowly but steadily recovered, and the channels were destroyed, indicating improved agitation. From the comparatively large bed expansion that preceded internal particle motion (fluidization), it was apparent that the static bed voidage differed appreciably from the minimum fluid voidage, δ_{mf}, for this material. As the formation of channels made the beginning of fluidization rather difficult to observe when gas was admitted into the static bed at increasing flow rates, δ_{mf} had to be determined in another way. It was observed that the cessation of fluidization could be ascertained clearly when the bed was fluidized intensely and when the gas flow was gradually reduced. For the flow rate where fluidization ceased, the column height was recorded, and δ_{mf} was calculated. The apparent deviation between the static bed voidage and δ_{mf} was the chief difference observed between the iron catalyst and light sands. There were also indications that the catalyst exhibited greater slugging tendencies than the sand. Otherwise, a fluidizing catalyst bed closely resembled a similar sand bed.

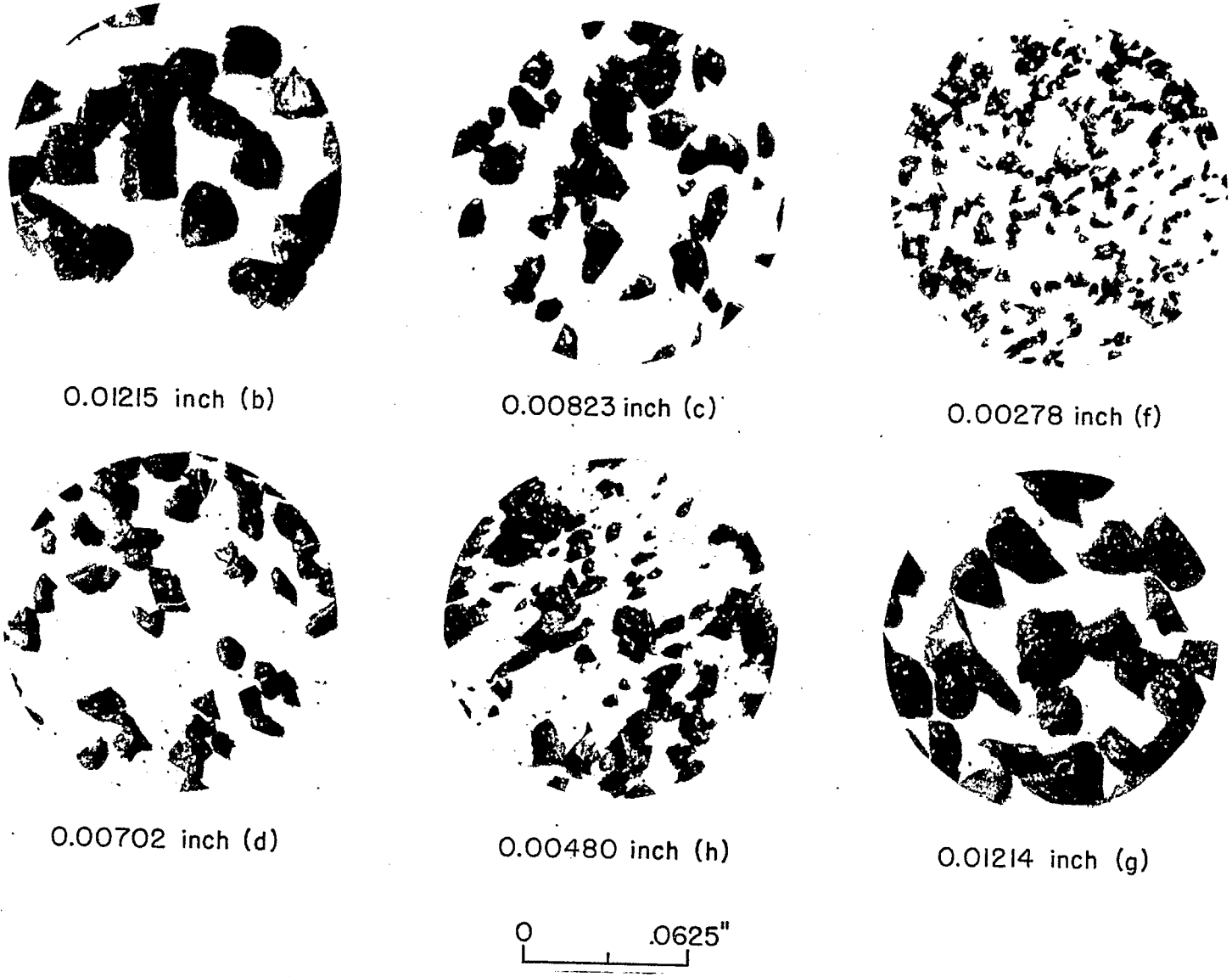

FIGURE 67.—UNIFORM AND MIXED IRON CATALYSTS. $\lambda = 1.73$

DATA AND CORRELATIONS

The original data of this investigation are reported in table XI in the appendix. Table 26 lists pertinent orienting information. The static bed voidage is generally 2 to 5 percent lower than the values of δ_{mf}. In figure 68, δ_{mf} is shown in relation to D_p. For comparison, the curves pertaining to sands also are shown. The data for the iron catalyst lie above those of the sharp sand and agree with the shape requirements.

In figure 69, modified friction factors are shown for the iron catalyst in relation to the modified Reynolds number. The plot permits the evaluation of the catalyst shape factor. Thus, for $R_e=1$, $f=100$ for spheres, and $f=300$ for the catalyst particles. From this:

$$\lambda^2=\frac{300}{100},$$

and

$$\lambda=1.73.^3$$

In figure 70, pressure drop, ΔP, is shown in relation to mass flow rate, G. The fixed-bed portion is characterized by the straight lines of slope +1 (indicating laminar flow) and the fluidization portion by the flat, almost horizontal, section. The data show clearly the existence of a peak where the two branches join, which was considerably more pronounced for iron catalyst than for earlier data on sand. The data from the iron catalyst show the slow, steady recovery of the pressure drop with increasing fluid-flow rates. At high rates of flow,

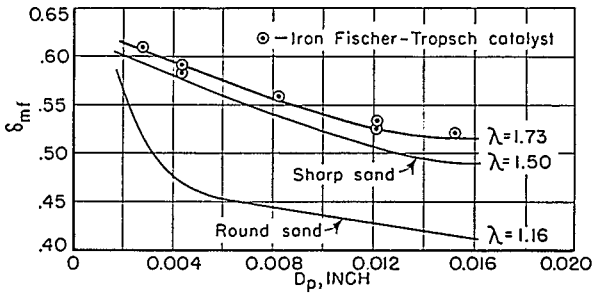

FIGURE 68.—MINIMUM FLUID VOIDAGE δ_{mf} FOR SAND AND IRON FISCHER-TROPSCH CATALYST IN RELATION TO PARTICLE DIAMETER.

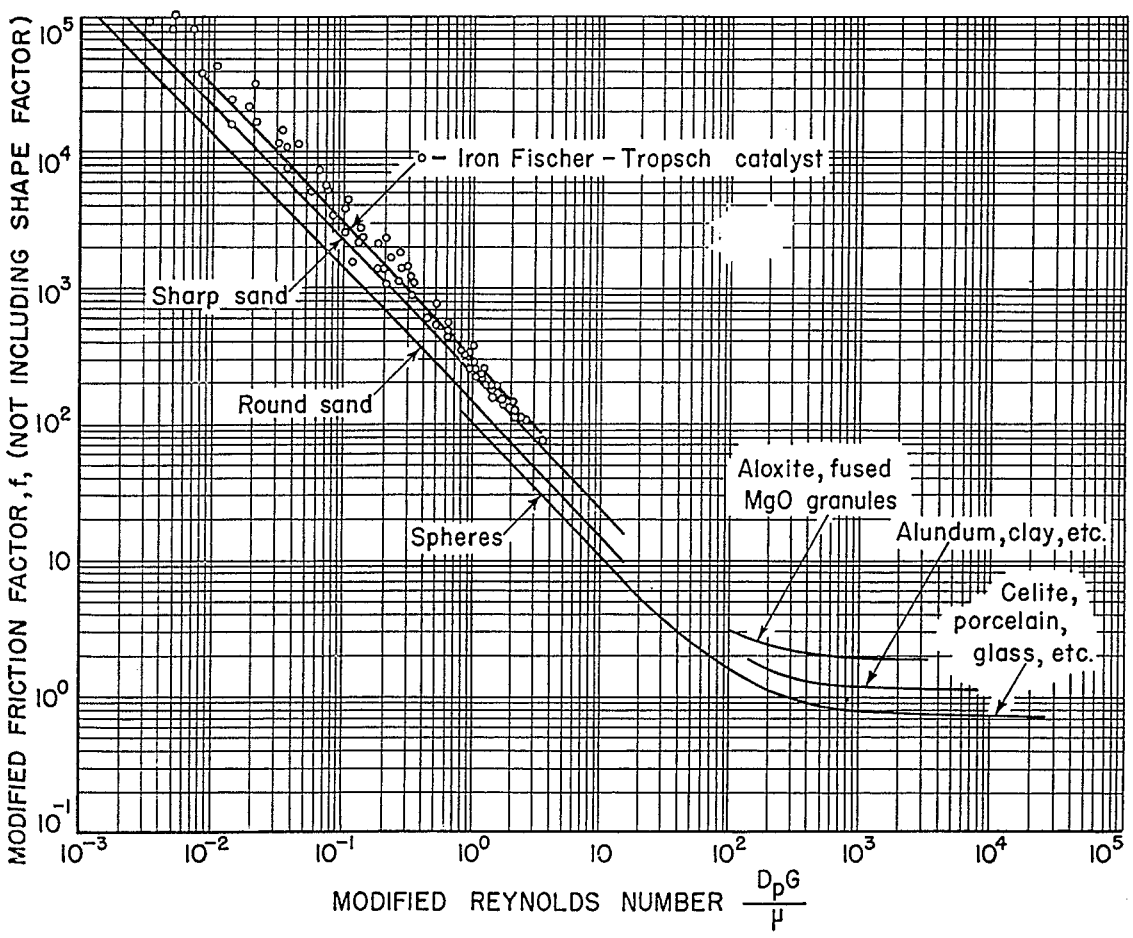

FIGURE 69.—FRICTION-FACTOR PLOT FOR VARIOUS MATERIALS.

the pressure drop across the fluidized bed may be approximated closely by the earlier equation (43).

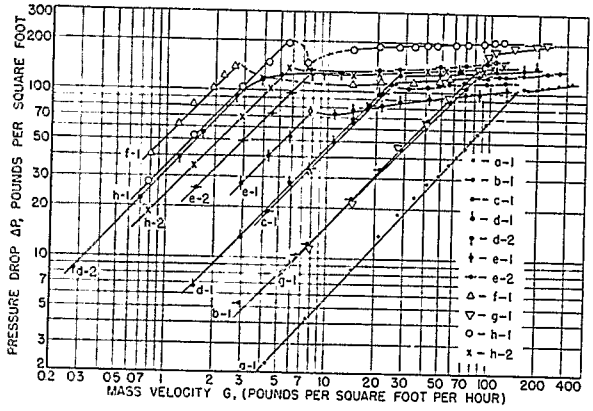

FIGURE 70.—PRESSURE DROP IN RELATION TO MASS VELOCITY FOR FLUIDIZATION OF IRON FISCHER-TROPSCH CATALYST.

Figure 71 shows log

$$\frac{G\mu}{\rho} l_e$$

in relation to log

$$\frac{(1-\delta)^2}{\delta^3}.$$

Runs d-1 and d-2 were made with air and helium, respectively. The satisfactory agreement observed between the two runs when plotted in this manner and a comparison of the plot with figures 47 to 51 indicate that the kinematic viscosity of the fluid affects the fluidization of light and heavy materials alike.

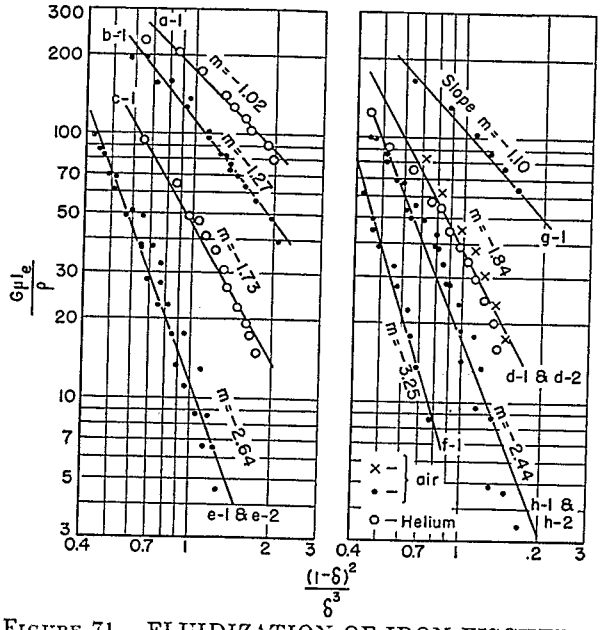

FIGURE 71.—FLUIDIZATION OF IRON FISCHER-TROPSCH CATALYST.

Table 27 reports the slope, m, of various lines of figure 71. Figure 72 shows values of m for the iron catalyst in relation to D_p; lines established earlier pertaining to round and sharp sands are shown also. Although some deviations exist between the new data and the old correlation, no definite trend is indicated.

Figure 73 shows fluidization efficiencies for all the materials at three expansion ratios, $l_e=1.05$, $l_e=1.15$, and $l_e=1.25$. With few exceptions, the agreement is quite satisfactory. It appears, therefore, that general correlations developed on the basis of sand data are applicable to nonvesicular materials of different specific gravities and to shapes more irregular than sand.

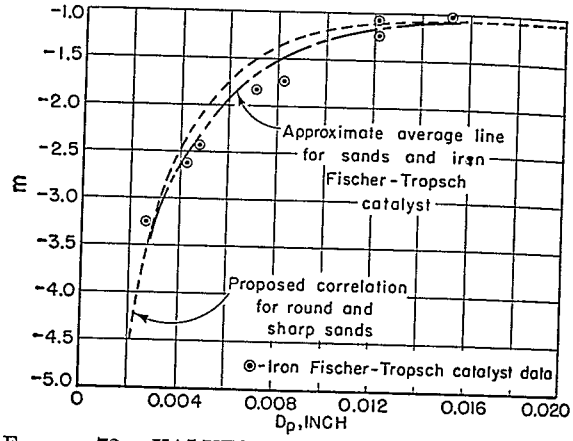

FIGURE 72.—VALUES OF m IN RELATION TO D_p FOR SANDS AND IRON FISCHER-TROPSCH CATALYST.

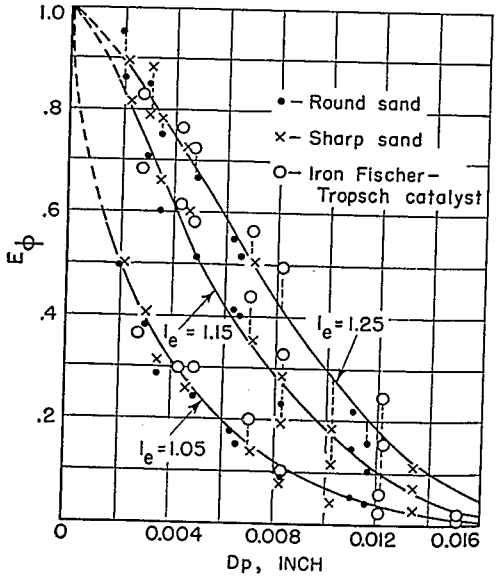

FIGURE 73.—FLUIDIZATION EFFICIENCIES IN RELATION TO PARTICLE DIAMETER CALCULATED FOR BED-EXPANSION RATIOS 1.05, 1.15, AND 1.25.

TABLE 26.—*Fluidization experiments performed with iron Fischer-Tropsch catalyst*

Run	D_p, inch	Weight, gm.	Static height, ft.	Static fractional voids, δ	δ_{mf}	Gas	Fluidization pressure drop, ΔP, lb./ft.² for—		
							Low gas flow	High gas flow	Calculated
a-1	0.01518	4,262	0.685	0.499	0.520	Air	102	110	108
b-1	.01215	5,011	.820	.506	.525	do	118	130	127
c-1	.00823	4,650	.771	.510	.559	do	109	118	118
d-1	.00702	5,229	.915	.636		do	126	140	133
d-2	.00702	5,229	.885	.523		Helium	119	132	133
e-1	.00430	3,986	.724	.555	.576	Air	75	101	101
e-2	.00430	6,019	1.063	.542	.573	do	132	152	152
f-1	.00278	5,580	1.061	.574	.610	do	104	137	141
g-1	.01214	7,234	1.210	.517	.525	do	179	189	182
h-1	.00480	7,863	1.310	.515		do	150	201	199
h-2	.00480	5,637	.945	.517		do	137	143	143

TABLE 27.—*Slopes of experimental runs made with the iron Fischer-Tropsch catalyst as shown in figure 71*

Run	D_p, inch	Tube diameter, inches	m
a-1	0.01518	4	−1.02
b-1	.01215	4	−1.27
c-1	.00823	4	−1.73
d-1 and d-2	.00702	4	−1.84
e-1 and e-2	.00430	4	−2.64
f-1	.00278	4	−3.25
g-1	.01214	4	−1.10
h-1 and h-2	.00480	4	−2.44

APPLICATION TO PROCESS DESIGN

The fluidization correlations developed so far were obtained under nonreaction conditions. The application of the relationships to systems undergoing a chemical reaction requires due consideration of specific process characteristics. The synthetic liquid fuels process is complex in that waxes are formed at low temperatures and carbon is deposited on and throughout the catalyst at high temperatures. Excessive wax formation will have the effect of binding the individual catalyst particles together and, if allowed to proceed uncontrolled, will eventually solidify the catalyst bed. Carbon formation will substantially reduce the density of the bed and might conceivably lead to larger agglomerates. It is apparent, therefore, that excessive formation of waxes and carbon will seriously affect the fluidization operation.

It is currently believed that excessive wax formation can be controlled by operating the reactor above 300° C. If in this temperature range the formation of carbon may be regulated by a proper choice of catalyst, the fluidized reactor seems feasible for carrying out the Fischer-Tropsch reaction. Aside from considerations of temperature and the chemical nature of catalyst, it is necessary to adapt the correct catalyst grain size to a particular mode of operation. The physical properties and linear velocities of the reacting mixture change markedly during the reaction, and such a change large enough to affect significantly the quality of the fluidization operation is conceivable. These studies have revealed that the kinematic viscosity of the fluid,

$$\frac{\mu}{\rho},$$

largely determines the efficiency of fluidization. Let us assume that

$$\frac{\mu}{\rho}$$

of the fluid decreases by 50 percent as the reactants and products pass through the reactor. For a definite fluid flow rate, the use of one particle size may result in fluidization at the inlet to the reactor while essentially a fixed bed exists at the exit. Because of a comparatively poor transfer of heat through a fixed bed, such a condition will result in uncontrollable temperatures, excessive methane and carbon formation, and early deterioration of the catalyst. It is important, therefore, to know how small the catalyst particles must be to assume efficient fluidization throughout the entire unit.

The results of some calculations are presented below, which show how the maximum particle size (for which fluidization still occurs through the entire reactor) depends on the diameter of the reactor and the ratio of fresh gas to recycle gas. The calculations were made for recycle

ratios of 1:0, 1:4, and 1:9. For each operation, 12-inch, 18-inch, and 24-inch diameter reactors were considered. The following conditions served as the basis for the calculations:

Operating temperature, ° C	320
Operating pressure, atm	20
Space velocity (ft.³ fresh gas)/(ft.³ cat.)/hr	300
Synthesis gas composition, percent:	
CO	57
H_2	38
N_2	5
Conversion of synthesis gas, percent	90
Usage ratio, $CO:H_2$	1.5:1
Average molecular weight of hydrocarbon product	C_7H_{14}

All the water is condensed out of the recycle gas, and CO_2 is allowed to accumulate. It was assumed that catalyst activity was not significantly influenced by the particle size, and that no liquid product films existed under the given operating conditions. The calculations that served as the basis for table 29 were made on the assumption that synthesis on the iron catalyst proceeds chiefly according to the following reactions:

$$n(CO+2H_2)=C_nH_{2n}+nH_2O \text{ and } n(2CO+H_2)=C_nH_{2n}+nCO_2.$$

TABLE 28.—*Calculated inlet- and exit-gas compositions for three recycle ratios*

Constituent	Recycle 1:0, mol-percent		Recycle 1:4, mol-percent		Recycle 1:9, mol-percent		Viscosity at 320° C., lb. hr.$^{-1}$ ft.$^{-1}$
	Inlet	Exit	Inlet	Exit	Inlet	Exit	
CO	57. 0	12. 10	22. 8	14. 0	18. 5	14. 1	0. 070
H_2	38. 0	8. 05	15. 8	9. 4	12. 3	9. 4	. 034
N_2	5. 0	10. 60	11. 0	12. 3	11. 8	12. 5	. 068
CO_2		48. 35	45. 0	56. 20	51. 3	56. 5	. 064
H_2O		12. 15		1. 28		. 6	. 050
$(CH_2)_n$		8. 75	5. 4	6. 96	6. 07	6. 9	. 060
Average molecular weight	18. 16	38. 40	35. 18	40. 09	37. 32	39. 44	
Contraction, percent	52.7		12.4		5.5		

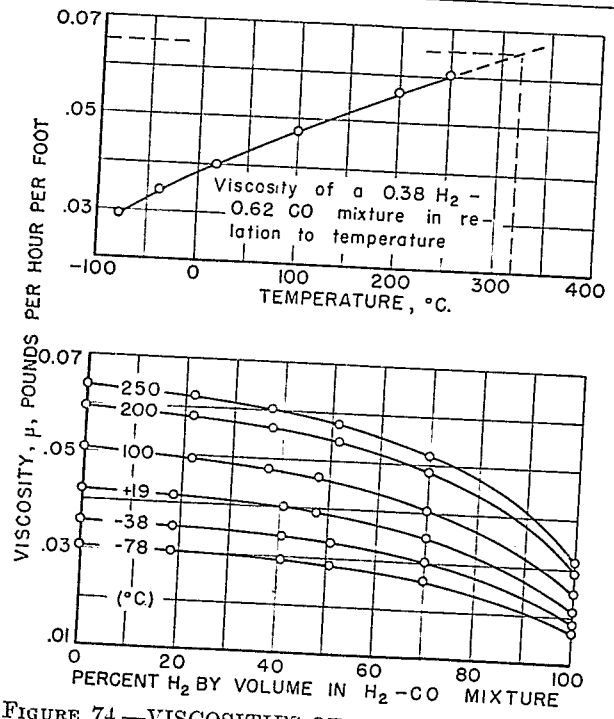

FIGURE 74.—VISCOSITIES OF H_2–CO MIXTURES AT VARIOUS TEMPERATURES.

For a reliable application of fluidization principles to the process, an accurate evaluation of the physical properties, such as viscosity and density, of the fluids becomes necessary. The literature [41] reports various empirical expressions for calculating the viscosity of gas mixtures if values for the individual components are known. Their application is limited, however, to the specific conditions under which these relationships were obtained. An application to higher temperatures, pressures, and different fluid compositions, such as those prevailing in a Fischer-Tropsch reactor, does not seem justified.

Figure 74 shows how the viscosity of H_2–CO mixtures varies with composition and temperature. The data are those of Trautz and Baumann.[42] According to table 29, the fresh gas contains some nitrogen. Trautz and Baumann have shown that the viscosities of H_2–CO mixtures are not greatly different from those of H_2–N_2. For this reason, it is probably permissible to consider the fresh gas as being made up of 0.38 H_2 and 0.62 CO. In figure 74, the viscosity of such a mixture has been

[41] Zipperer, L., and Mueller, G.: Gas und Wasserfach, vol. 75, 1932, pp. 623–7, 641–4, and 660–4.
[42] Trautz, M., and Baumann, P. B.: Ann. Physik, ser. 5, vol. 2, 1929, pp. 733–36.

evaluated for the reaction temperature by extrapolating the data to 320° C. Although the viscosity of the fresh gas could be thus estimated with reasonable accuracy, no information is available for the other gas mixtures for which, because of their complexity, the viscosities cannot be estimated from figure 74.

For a 0.38 H_2–0.62 CO mixture, the viscosity at 320° C. is 0.0655 lb. hr.$^{-1}$ ft.$^{-1}$. If the viscosity is calculated on a mol-fraction additive-rule basis, μ=0.0564 lb. hr.$^{-1}$ ft.$^{-1}$. The resulting error is therefore only 14.8 percent. For lack of a better method, the viscosities of all mixtures will be estimated by this additive rule, and the values thus obtained will be used as a basis for fluidization calculations. The kinematic viscosities estimated in this way are recorded in table 30.

TABLE 29.—*Estimated kinematic viscosities of inlet and exit gases for a Fischer-Tropsch fluid reactor*

Recycle ratio	Viscosity, lb. hr.$^{-1}$ ft.$^{-1}$		Density, lb./ft.^{3}		Average kinematic viscosity η, ft.^{2}/hr.	$\frac{\eta \text{ Exit}}{\eta \text{ Inlet}}$
	Inlet	Exit	Inlet	Exit		
1:0	0. 0562	0. 0607	0. 466	0. 986	0. 091	0. 51
1:4	. 0609	. 0628	. 902	1. 031	. 064	. 90
1:9	. 0616	. 0622	. 957	1. 014	. 063	. 95

The calculations indicate that for low recycle ratios the kinematic viscosity decreases significantly as the reaction mixture proceeds through the unit. For higher recycle ratios, however, the "buffer action" of the diluent gas is more significant, so that, at a ratio of 1:9, the kinematic viscosity varies only little between the inlet and outlet of the unit.

TABLE 30.—*Calculated data pertaining to the operation of a fluid Fischer-Tropsch reactor*

Number	Recycle ratio	D_t, inch	G	u, ft./sec.	D_p max., inch	D_p, inch	l_e	E_ϕ
1a	1:0	9	1054	0. 629	0. 0116	0. 00696	1. 273	0. 387
1b	1:0	12	593	. 353	. 00785	. 00471	1. 219	. 424
1c	1:0	18	264	. 157	. 00475	. 00285	1. 152	. 575
1d	1:0	24	148	. 088	. 00335	. 00201	1. 105	. 632
2a	1:4	21	1873	. 577	. 0162	. 00972	1. 237	. 199
2b	1:4	24	1438	. 443	. 0141	. 00846	1. 182	. 235
2c	1:4	30	920	. 284	. 0105	. 00628	1. 162	. 326
2d	1:4	36	641	. 198	. 00818	. 00491	1. 095	. 384
3a	1:9	30	1950	. 566	. 0165	. 00990	1. 242	. 185
3b	1:9	33	1612	. 469	. 0152	. 00912	1. 187	. 206
3c	1:9	36	1353	. 393	. 0137	. 00822	1. 167	. 238

The data of table 30 were used to calculate the values reported in table 31. As pointed out earlier, the calculations are based on a space velocity of 300 referred to fresh gas. For this rate and the kinematic viscosity at the outlet, the maximum particle diameter for which fluidization will still occur was calculated, and these values are tabulated in column 6. Because the operation of a fluidized bed composed of particles of maximum diameter is critical, values of D_p max. cannot be used in process development work. A practical particle diameter must therefore be smaller than D_p max. Thus, column 7 of table 31 reports values of D_p=0.60 D_p max. D_p values, together with the corresponding fluidization mass flow rates, G, were then used to obtain l_e and E_ϕ. Because of the somewhat involved nature of the calculations, data pertaining to 2b are reproduced as a sample problem at the end of this section.

Figure 75 shows the variation of the particle diameter with the diameter of the vessel for a constant space velocity. For all three recycle ratios, D_p decreases rapidly with increasing D_t. In the limiting case, D_p should approach zero for very large reactors. Furthermore, it appears, as one would expect, that the lowest recycle rates require the smallest particle diameters.

Figure 76 emphasizes the relationship between the bed-expansion ratio, l_e, and the reactor diameter. The expansion ratio is high for beds composed of large particles requiring high rates of flow for fluidization. For high recycle ratios, the expansion ratio is

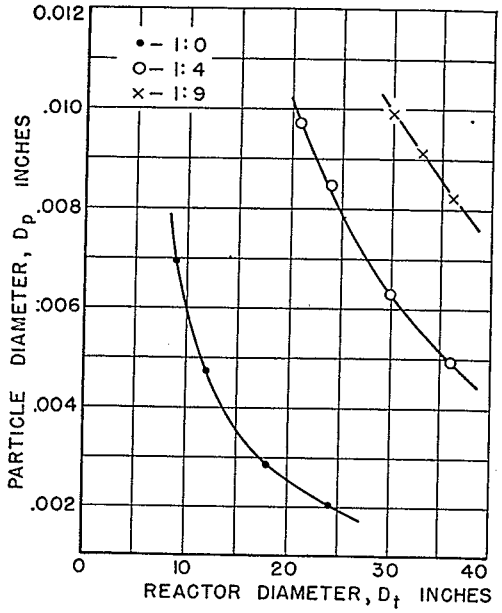

FIGURE 75.—PARTICLE DIAMETER D_p VS. REACTOR DIAMETER D_t FOR A SPACE VELOCITY OF 300 AND VARIOUS RECYCLE RATIOS.

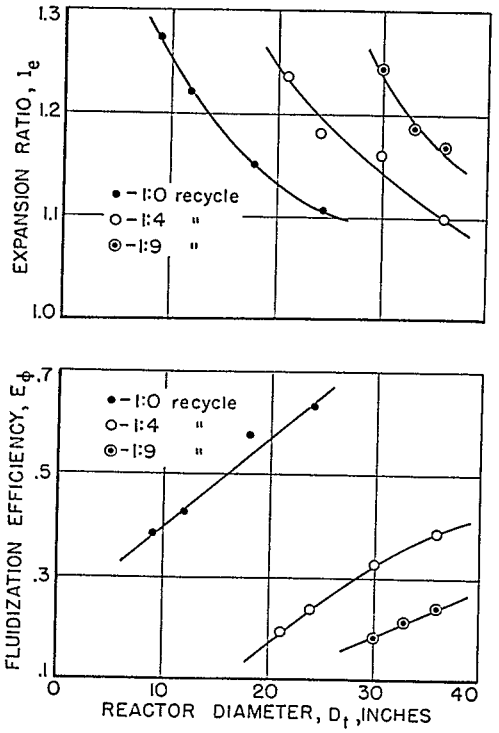

FIGURE 76.—FLUIDIZATION EFFICIENCY, E_ϕ, AND BED-EXPANSION RATIO, l_e, VS. REACTOR DIAMETER, D_t, FOR A SPACE VELOCITY OF 300 AND VARIOUS RECYCLE RATIOS.

greater than for low ratios. In the lower section of the figure, the variation of fluidization efficiency with reactor diameter is shown. It is surprising that E_ϕ increases with increasing reactor diameter. For large values of D_t, E_ϕ asymptotically approaches a value, the magnitude of which seems to depend on the recycle ratio. For very small diameter reactors, E_ϕ approaches zero.

Table 31 lists the inlet velocities of the gas into the reactor. The highest velocity recorded is 0.629 ft./sec. Industrial developments have shown the desirability of working with higher velocities ranging from 0.5 to 2.0 ft./sec. As the particle diameters reported in table 31 are well in accord with those employed in industrial practice, it would appear that industrial units could operate with considerably larger particle diameters without approaching the limits of fluidizability of the bed. Expansion ratios in excess of those calculated in this paper have been reported in industrial equipment, an indication that the particle diameters used in industrial units are small in comparison with the relatively high flow rates.

At the fluidization velocities recorded in column 5, the rate of carry-over from the fluid beds was negligible. Work aimed at finding a relation between the rate of carry-over and the gas velocity has shown that the rate of elutriation from fluidized beds increases unusually quickly with the linear fluid velocity, once a certain flow rate has been surpassed. This observation is in agreement with industrial experience where significant catalyst losses are reported for the comparatively high operating velocities at which larger units are working.

Finally, the rate of attrition in the bed should be of interest. At low flow rates and nonchemical reaction conditions, attrition rates are negligible; it is believed, however, that with higher flow rates and in the presence of chemical reactions, which are accompanied by intense heat effects, attrition can become important. Furthermore, if the bed is composed initially of particles that are too fine, it is difficult to see how formation and loss of fines can be prevented.

One of the chief difficulties encountered in the operation of fluidized beds in Fischer-Tropsch reactors is the formation of carbon on and throughout the catalyst. In an evaluation of the effects that carbon formation will have on fluidization, it is necessary to consider carefully the manner in which the carbon is deposited in the bed. If the carbon appears suddenly, owing to rapid cracking of waxy substances (a condition not likely to occur at the conventional operating temperatures), large agglomerates of

particles will result that may immobilize the bed entirely. A catalyst bed that has experienced such a change must be discharged from the reactor. If the carbon forms more slowly on the surface of the catalyst, the individual particles will be enlarged; however, no substantial aggregation should occur. This change in the bed should not interfere seriously with fluidization unless the particles have enlarged beyond the maximum size that can still be fluidized. A third formation mechanism may be encountered in which the carbon deposits in the interior of the catalyst particle. It has been observed that this type of formation is always associated with size disintegration. At the same time, the bulk density of the bed is reduced greatly. This change has very pronounced effects on fluidization. Owing to the reduced bulk density, such a disintegrated bed will expand considerably beyond the limits of the original bed, and fluidization will become more violent. As a consequence, the rate of carryover will increase. As the carbon is dispersed uniformly through such a bed, separation of carbon by blowing over parts of the bed periodically is not possible.

SAMPLE CALCULATIONS AND COMMENTS

PROBLEM

For a 1:4 recycle ratio, 300 space velocity (on the basis of fresh gas), and 3.33 ft.^{3} of dumped catalyst, the mass velocity, G, equals 1,438 lb. hr.$^{-1}$ ft.$^{-2}$ if flow through a 24-inch diameter reactor is considered. Additional operating data are as follows:

Catalyst:
- Particle density, (ρ_s): 5.00 gm./cc.=312 lb./ft.^{3}
- Shape factor, λ: 1.73.

Synthesis gas:
- Inlet viscosity, μ: 0.0609 lb. hr.$^{-1}$ ft.$^{-1}$
- Inlet density, ρ: 0.902 lb./ft.^{3}
- Exit viscosity, μ: 0.0628 lb. hr.$^{-1}$ ft.$^{-1}$
- Exit density, ρ: 1.031 lb./ft.^{3}

For the above operating conditions, determine:
1. Maximum particle diameter, $D_{p\ max.}$, at minimum fluidization.
2. Using $D_p=0.60\ D_{p\ max.}$, find the expansion ratio, l_e, and the fluidization efficiency, E_ϕ.

SOLUTION

For minimum fluidization:

$$\Delta P = L_e(\rho_s-\rho)(1-\delta_{mf}) = \frac{200G\mu L_e\lambda^2(1-\delta_{mf})^2}{D_p{}^2 g_c\rho\delta^3}, \quad \text{(a)}$$

where D_p is the maximum particle diameter, $D_{p\ max.}$ From this equation,

$$\frac{D_p{}^2\delta_{mf}{}^3}{1-\delta_{mf}} = \frac{200G\mu\lambda^2}{g_c\rho(\rho_s-\rho)}. \quad \text{(b)}$$

As all the quantities in the right-hand expression are known, it follows that:

$$\frac{D_p{}^2\delta_{mf}{}^3}{1-\delta_{mf}} = \frac{(200)(1438)(0.0628)(1.73)^2(144)}{(4.18)(10)^8(1.031)(312-1.031)} =$$

$$58.2\times10^{-6}\ \text{in.}^2$$

In figure 77, values of

$$\frac{D_p{}^2\delta_{mf}{}^3}{1-\delta_{mf}}$$

have been plotted against D_p. The curve pertains to the Fischer-Tropsch iron catalyst and was constructed from the curve shown in figure 68. From figure 77, it follows that for

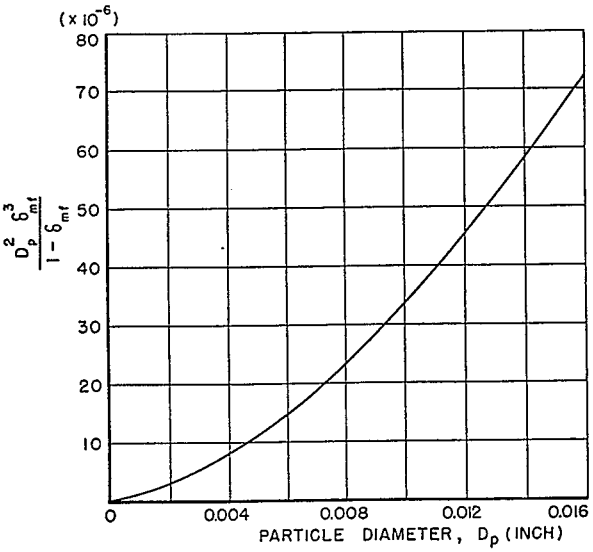

FIGURE 77.— $\frac{D_p{}^2\delta_{mf}{}^3}{1-\delta_{mf}}$ VS. D_p FOR THE IRON FISCHER-TROPSCH CATALYST. (SHAPE FACTOR λ=1.73).

$$\frac{Dp^2\delta_{mf}{}^3}{1-\delta_{mf}} = 58.2\times10^{-6},\ D_{p\ max.} = 0.0141\ \text{in.}$$

Working particle diameter, D_p: (0.75) (0.0141)=0.00846 in.

From figure 68, the minimum fluid voidage for D_p=0.00846 in.: δ_{mf}=0.548.

From figure 72, m=—1.46.

Next, it is necessary to find the minimum fluid mass flow, G_{mf}, for D_p=0.00846 in. This may be calculated from:

$$\Delta P = L_e(\rho_s-\rho)(1-\delta_{mf}) = \frac{200\,G_{mf}\mu L_e\lambda^2(1-\delta_{mf})^2}{D_p{}^2 g_c\rho\delta_{mf}{}^3},$$

943247°—51——6

whence

$$G_{mf}=\frac{(312-0.967)(0.967)(4.18)(10)^3(0.00846)^2(0.548)^3}{(144)(200)(0.0619)(1.73)^2(1-0.548)}=$$
614 lb. hr.$^{-1}$ ft.$^{-2}$.

For obtaining values of G_e, l_e, and E_ϕ, a simple graphical method may be used. Because, at fluidization,

$$\Delta P=L(1-\delta)(\rho_s-\rho)=\frac{200\,G_\mu\lambda^2L(1-\delta)^2}{D_p^2g_c\rho\delta^3},$$

a plot of log G versus

$$\log\frac{(1-\delta)}{\delta^3}$$

should be helpful for the determination of the expansion ratio and efficiency.

As

$$\delta_{mf}=0.548,\ \frac{(1-\delta_{mf})}{\delta_{mf}}=2.73.$$

In figure 78, the point of minimum fluidization

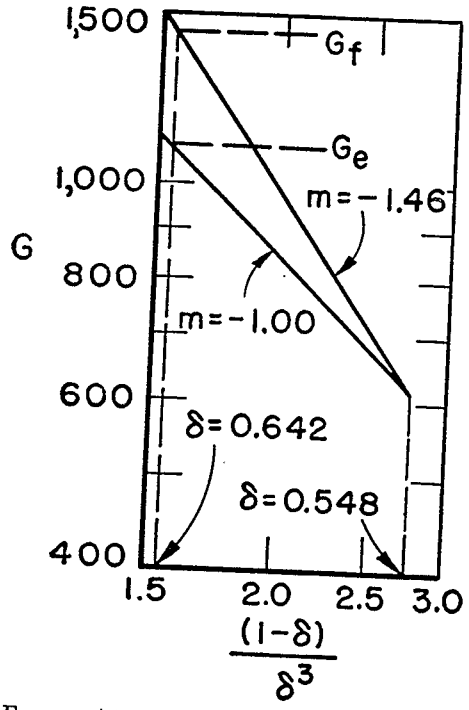

FIGURE 78.—GRAPHICAL SOLUTION FOR EXPANSION OF IRON FISCHER-TROPSCH CATALYST BED.

is readily located by plotting log G_{mf} against

$$\log\frac{(1-\delta)}{\delta^3}.$$

Through this point two straight lines are laid. The slope, m, of the fluidization line is −1.46 and, for the expansion line, −1.00. Operating fluid mass velocity was 1,438 lb. hr.$^{-1}$ ft.$^{-2}$ and by coming down from this point to the expansion line, G_e=1,100 lb. hr.$^{-1}$ ft.$^{-2}$. For the expanded bed,

$$\frac{(1-\delta)}{\delta^3}=1.57,$$

and, from figure 43, δ=0.642. Finally,

$$l_e=\frac{1-\delta}{1-\delta_{mf}}=\frac{1-0.548}{1-0.642}=1.262,$$

and

$$E\phi=\frac{G_f-G_e}{G_f}=\frac{1,438-1,100}{1,438}=0.235.$$

The difficulties of evaluating kinematic viscosities of reaction mixtures have been stressed previously. It is fortunate that the particle diameter is proportional to the square root of the kinematic viscosity as shown by equation (b) of the illustration. Furthermore, the particle diameter is also proportional to the square root of the mass flow rate. As mass flow can be calculated with precision, the calculated particle diameter $D_{p\ max.}$ should be fairly accurate, even though considerable uncertainty exists as far as the true viscosities of the fluids through the reactor are concerned.

The calculations made in this paper are general and may be used for any process that involves the flow of gaseous fluids through fine granular beds. From equation (b) it appears that the maximum particle diameter is directly proportional to the shape factor of the particles. At present the only practical approach to evaluating the shape factor of particles is to compare them with particles for which the shape factor is known. It is hoped that figures 45 to 49 and 67 may be used for this purpose. Once the shape factor has been established, values of δ_{mf} may be estimated from figures 68 or 94 providing the clue for further calculations.

ABRIDGED EQUATIONS FOR ESTIMATING ONSET OF FLUIDIZATION

Inspection of figure 68 shows that with increasing values of λ, both δ_{mf} as well as

$$\frac{\delta_{mf}^3}{(1-\delta_{mf})}$$

increase. Analysis has shown that for a considerable range of particle diameter and shape, the value of

$$\frac{\delta_{mf}^3}{(1-\delta_{mf})\lambda^2}$$

remains sufficiently constant to permit equation (45a) to be written in the following abridged form:

$$G_{mf}=CD_p^2g_c(\rho_s-\rho)\frac{\rho}{\mu}, \qquad (56)$$

where C is a function of D_p as shown in figure 79. If the fluid density may be neglected when compared to the solids density, the equation may be simplified further to read:

$$G_{mf}=C\,D_p^2g_c\rho_s\frac{\rho}{\mu}. \qquad (57)$$

The equation is only applicable to solid-gas systems for modified Reynolds numbers that are smaller than 10.

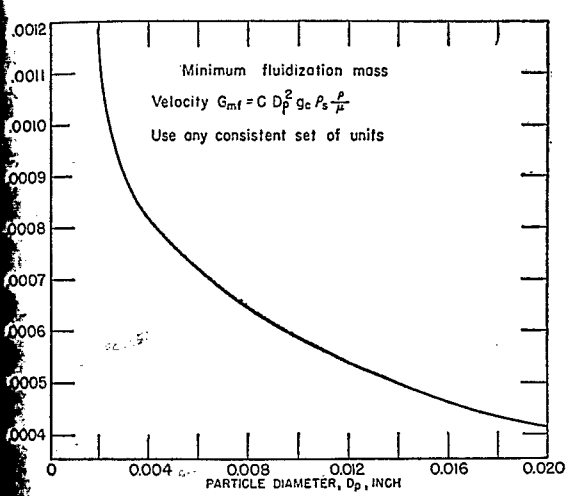

FIGURE 79.—CONSTANT C IN RELATION TO PARTICLE DIAMETER D_p.

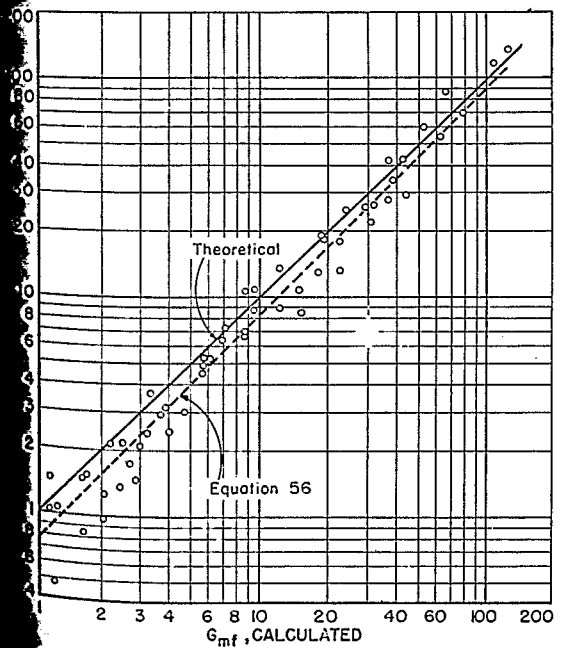

FIGURE 80.—MINIMUM FLUIDIZATION MASS VELOCITIES OBSERVED AND CALCULATED BY LOGWINUK AND COMPARED WITH EQUATION 56.

Equation (57) has been tested by the use of the extensive data Logwinuk [43] obtained with silicon carbides, silicon dioxide, silica gel, and aluminum oxide. The results are shown in figure 80. It appears that the relation gives values that are somewhat high. The following expression suggested by Logwinuk,

$$G_{mf}=\frac{0.0045\,D_p^{2.19}(\rho_s-\rho)^{0.89}\rho^{1.09}g_c^{0.98}}{\mu^{1.21}},$$

fits the data somewhat better than equation (57); owing to the various fractional exponents, the Logwinuk equation is not too convenient for rapid use, however.

CORRELATION OF WILHELM AND KWAUK [44]

In their excellent study, fluidization characteristics of comparatively large particles were investigated. Diameters ranged from 0.0113 to 0.205 inch. The materials were glass beads, Socony catalyst beads, sea sands, lead shot, and crushed rock. Air and water were used as fluids in columns of 3 and 6 inches diameter.

A distinction was made between what the authors termed aggregative and particulate fluidization. Aggregative fluidization usually referred to solid-gas systems, being characterized by the coexistence of comparatively large bubbles in the interior of the bed, whereas particulate fluidization was chiefly observed with solid-liquid systems, in which the particles were individually and uniformly dispersed.

In their correlation, Wilhelm and Kwauk [44] substantiated the validity of equation (43) for all the materials. For their generalized correlation, they show values of $K_{\Delta P}$ or $K_{\Delta\rho}$ in relation to

$$\frac{D_pG}{\mu}.$$

By definition

$$K_{\Delta P}=\frac{D_p^3\rho g_c\,\Delta P}{2\mu^2L_o},$$

which is the product of the Chilton and Colburn modified friction factor [45] multiplied by the square of the modified Reynolds number,

$$K_{\Delta\rho}=\frac{D_p^3\rho g_c(\rho_s-\rho)}{2\mu^2},$$

which constitutes the product of the drag coefficient of particle settling under the influence of gravity and the square of the modified Reynolds number.

It will be observed that the two equations transform into each other by either using

[43] Work cited in footnote 98, p. 7.
[44] Work cited in footnote 95, p. 7
[45] Work cited in footnote 19, p. 4.

$$\frac{\Delta P}{L_o} \text{ or } (\rho_s - \rho)$$

as the pressure gradient.

According to Wilhelm and Kwauk,[46] the onset of fluidization is estimated by evaluation of either $K_{\Delta P}$ or $K_{\Delta \rho}$. These values are then used in combination with plotted data to establish the Reynolds number at which the material begins to fluidize. The expanded bed height for any particular flow is then estimated by proceeding along the particular curve to the desired Reynolds number. Intersection with the corresponding percent void curve gives then the density of the bed in the expanded state.

Wilhelm and Kawuk's correlation for calculating the onset of fluidization is based on the assumption that all solid materials have a more or less constant minimum fluid voidage at $\delta \approx 0.40$. Although this is true for comparatively large and spherical particles, it may be in error for small particles, especially if the shapes deviate considerably from that of a sphere.

In table 31, calculated fluidization data pertaining to both small and large particles are compared with values actually observed, and the comparison emphasizes that more accurate results will be obtained if individual values of δ_{mf} are chosen for the particles in question.

TABLE 31.—*Voidage and flow for start of fluidization from experimental results and as calculated by various correlations*

Experiment	D_p	δ_{mf}	Experimental Re	Long form		Short form		Wilhelm and Kwauk's correlation Re
				G_{mf}	Re	G_{mf}	Re	
2M–1	0. 00838	0. 417	0. 50	26. 7	0. 431	35. 1	0. 567	1. 10
B′–2	. 00458	. 560	. 017	1. 96	. 017	1. 78	. 016	. 011
D–1	. 00310	. 492	. 046	6. 91	. 045	7. 48	. 049	. 15
j–3	. 00202	. 543	. 0014	. 569	. 0021	. 490	. 0018	. 01
j–1	. 00202	. 543	. 014	4. 41	. 0172	3. 82	. 0149	. 09
5M–1	. 00658	. 423	. 125	17. 3	. 220	24. 3	. 309	. 40
13 [1]	. 0201	----------	3. 84	141	5. 43	139	5. 36	8. 0
14 [1]	. 0201	----------	3. 53	141	5. 43	139	5. 36	8. 0
15 [1]	. 0201	----------	4. 16	141	5. 43	139	5. 36	8. 0
24 [1]	. 0113	----------	0. 924	44. 8	0. 97	53. 4	1. 15	2
17 [1]	. 205	----------	520	1656	652	----------	----------	650
18 [1]	. 125	----------	149	638	153	----------	----------	110

[1] Table numbers in accord with work of Wilhelm and Kwauk (see footnote 95, p. 7).

For runs characterized by Reynolds numbers larger than 10, the following general form (obtained by combining equations (41) and (43)) for calculating G_{mf} was used:

$$G_{mf}^2 = \frac{D_p g_c \rho \delta_{mf}^3}{2f\lambda^{3-n}(1-\delta_{mf})^{2-n}}. \qquad (45c)$$

FLUIDIZATION OF MIXED MATERIALS

During the course of catalytic reactions, catalysts frequently undergo significant physical changes. Discussion of application of fluidization principles to the Fischer-Tropsch synthesis has disclosed that in this particular case the density of the bed decreased significantly as a result of carbon formation. Thus, aside from catalyst losses, the bed becomes heterogeneous as far as material density is concerned. An investigation of the behavior of beds containing more than one solid component, therefore, was of interest. The systems chosen for investigation consisted of various mixtures of iron Fischer-Tropsch catalyst and sharp sand. As a fluid, air was used, and the experiments were performed in the 4-inch-diameter column. Table 32 describes experimental details; the original data are given in table XII of the appendix.

STRATIFICATION

During the experimental procedures, which were identical with those described earlier, it was observed that stratification of the materials occasionally occurred. Although no detailed separation studies were made, it appeared that fluid flow rates intermediate between G_{mf} values for sand and iron catalysts caused eventual separation. When flow rates with G_{mf} values larger than those for iron catalysts were used, stratification did not take place. Slight vibrations of the equipment were helpful in promoting the rate of material separation. Before the sand particles moved to the surface of the bed, the formation of tiny channels through the bed could be observed.

[46] Work cited in footnote 95, p. 7.

and these served as passageways for the sand grains. If separation was permitted to proceed, the light-colored sand collected on the top of the bed and fluidized very smoothly, whereas the catalyst fraction below remained essentially a fixed bed. The tendency toward stratification seemed to depend somewhat on the composition of the bed; stratification became more difficult as the percentage of the low-density component increased.

TABLE 32.—*Orientation of experimental work and characteristics of system*

Sample	Weight percent		Sand, volume percent	Specific gravity	δ_{mf}
	Iron catalyst	Sand			
[illegible]	----------	100	100	2.65	0.526
[illegible]	8.2	91.8	95.4	2.76	----------
[illegible]	15.2	84.8	91.3	2.85	----------
[illegible]	26.3	73.7	84.1	3.02	----------
[illegible]	41.7	58.3	72.6	3.30	.543
[illegible]	68.7	31.3	39.2	4.43	.585
[illegible]	77.3	22.7	29.3	4.57	----------
[illegible]	100	----------	----------	5.00	.567
[illegible]	96.7	3.3	6.1	4.86	.561
[illegible]	89.9	10.1	17.3	4.60	.558
[illegible]	85.1	14.9	24.8	4.43	.543
[illegible]	79.5	20.5	32.5	4.23	.558

CORRELATION

At flow rates with G_{mf} values greater than those for iron catalysts, the bed behaved like any other system composed of one type of material. The point of minimum fluidization was easily observed as that point at which all the particles were in motion. Values of δ_{mf} for some mixtures are listed in table 32. Comparison with figure 68 indicates that most values are in good agreement with the data for iron catalyst and sharp sand.

Several two-component systems of D_p= 0.0135 inch and 0.00633 inch were examined, and values of

$$\log \frac{G\mu l_e}{\rho}$$

have been plotted against

$$\log \frac{(1-\delta)^2}{\delta^3}$$

in figures 81 and 82. Because the slopes of the various lines are not influenced by the composition of the beds, it may be concluded that expansion characteristics and fluidization-efficiency characteristics of mixed beds are not essentially different from systems comprised of one type of material.

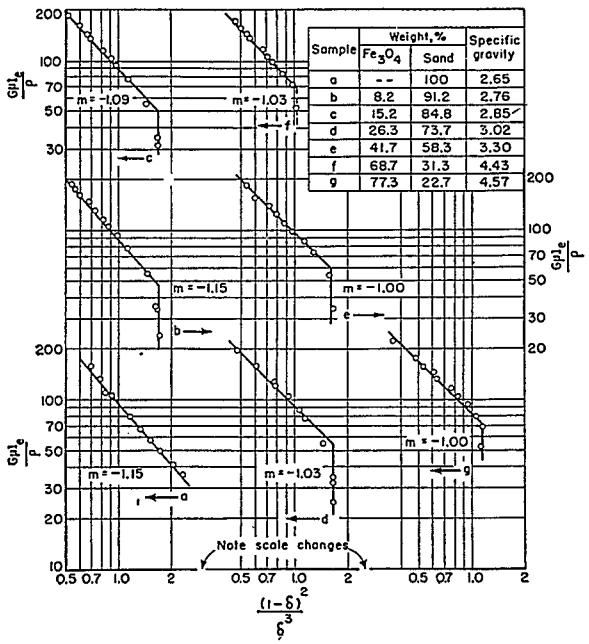

FIGURE 81.—FLUIDIZATION OF MIXED BEDS.

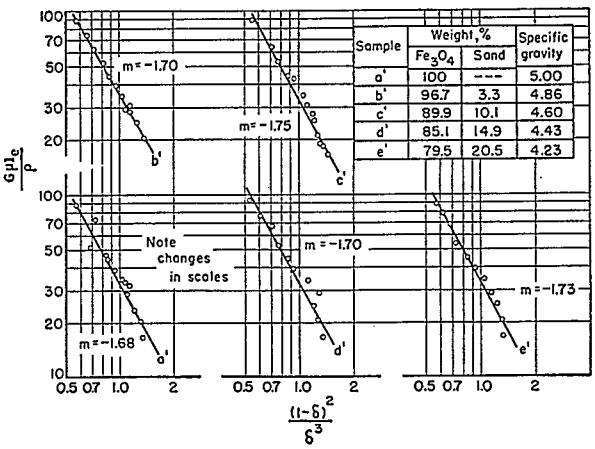

FIGURE 82.—FLUIDIZATION OF MIXED BEDS.

SOLID-LIQUID SYSTEMS

EXPERIMENTAL

The relationships developed so far have been shown to apply to the flow of gases through beds of solid particles. In many industrial processes, however, liquids also are passed up through beds of solid particles such as in the

washing of coal, backwashing of rapid sand filters, and leaching of solids.

Original data observed during the fluidization of sands and iron catalyst particles in water and in oil are reported in tables XIII and XIV in the appendix. A glass tube 1.32 inches in diameter was employed, and a glass cloth was used as a false bottom. Weighed quantities of sand or iron catalyst were introduced into the column, and definite rates of water or oil were passed upward. The height of the expanded bed was measured for the individual rates, but pressure-drop measurements were omitted. The data have been correlated in figure 83 in the usual manner;

$$\log \frac{G\mu l_e}{\rho}$$

was plotted in relation to

$$\log \frac{(1-\delta)^2}{\delta^3}.$$

In figure 84, data of other investigators are shown in the same manner.

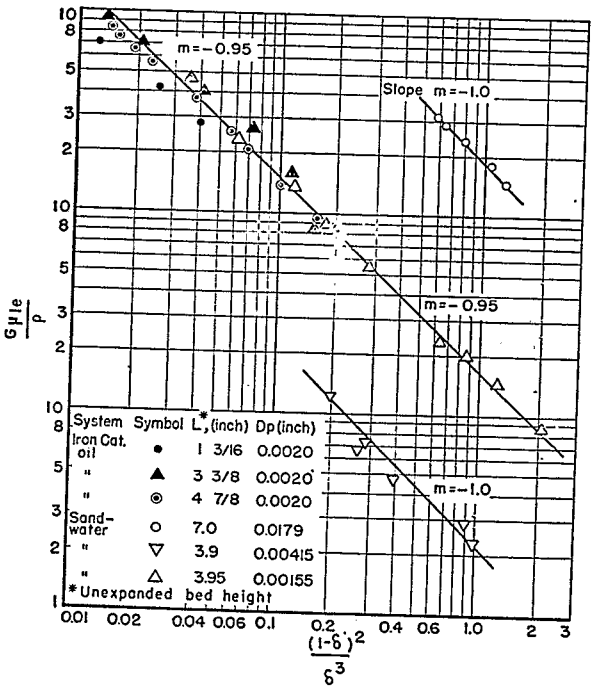

FIGURE 83.—EXPANSION IN LIQUID MEDIUMS.

CONCLUSIONS

Consideration of the slopes, m, of the individual plots of solid-liquid systems shows remarkable deviation from the behavior of solid-gas systems observed thus far. Although for solid-gas systems the slopes for runs using particles of $D_p > 0.01$ inch were essentially equal to (-1.00) and became progressively more negative with decreasing values of D_p, the solid-liquid data exhibit a slope of (-1.00) over the entire range. There is reason to believe that the variation of m with D_p is related to the rate of turnover of the solids in the bed.

The intensity of agitation of a fluidized bed should not be related to fluidization efficiency, but rather to fluidization energy. This becomes apparent from consideration of the fluidization of large-diameter particles. According to the data shown in figure 72, fluidization efficiency approaches zero for particles of $D_p > 0.01$ inch. Visual observation, however, has indicated that the degree of mixing in such beds is not essentially different from that experienced in beds of smaller particles. In figure 85, fluidization efficiencies and fluidization energies are shown in relation to D_p for flows of $G_f = 5G_{mf}$ and $G_f = 2.5G_{mf}$. Although efficiencies decrease consistently with increasing D_p, the fluidization energy increases at first, reaches a maximum near $D_p = 0.09$ inch, and slowly decreases beyond this point. The reason for this maximum is not known.

DATA INTERPRETATION ON THE BASIS OF THE FLOCCULATION THEORY

In an attempt to explain the deviations observed between pressure-drop data and fluidization data (as shown by figure 72, where m is plotted in relation to D_p), Morse[47] calculated modified friction factors according to equation (40) for the data recorded in tables VII to X of the appendix. When the modified friction factors were plotted against the modified Reynolds numbers, severe deviations from the fixed-bed correlation seemed to exist. For the largest sands considered, the friction factors proceeded parallel to the f vs. Re curve. As the particles decreased in size, the slopes of the calculated f values became increasingly more negative. All the data were "anchored" at the f line at the point of minimum fluidization.

[47] Work cited in footnote 96, p. 7.

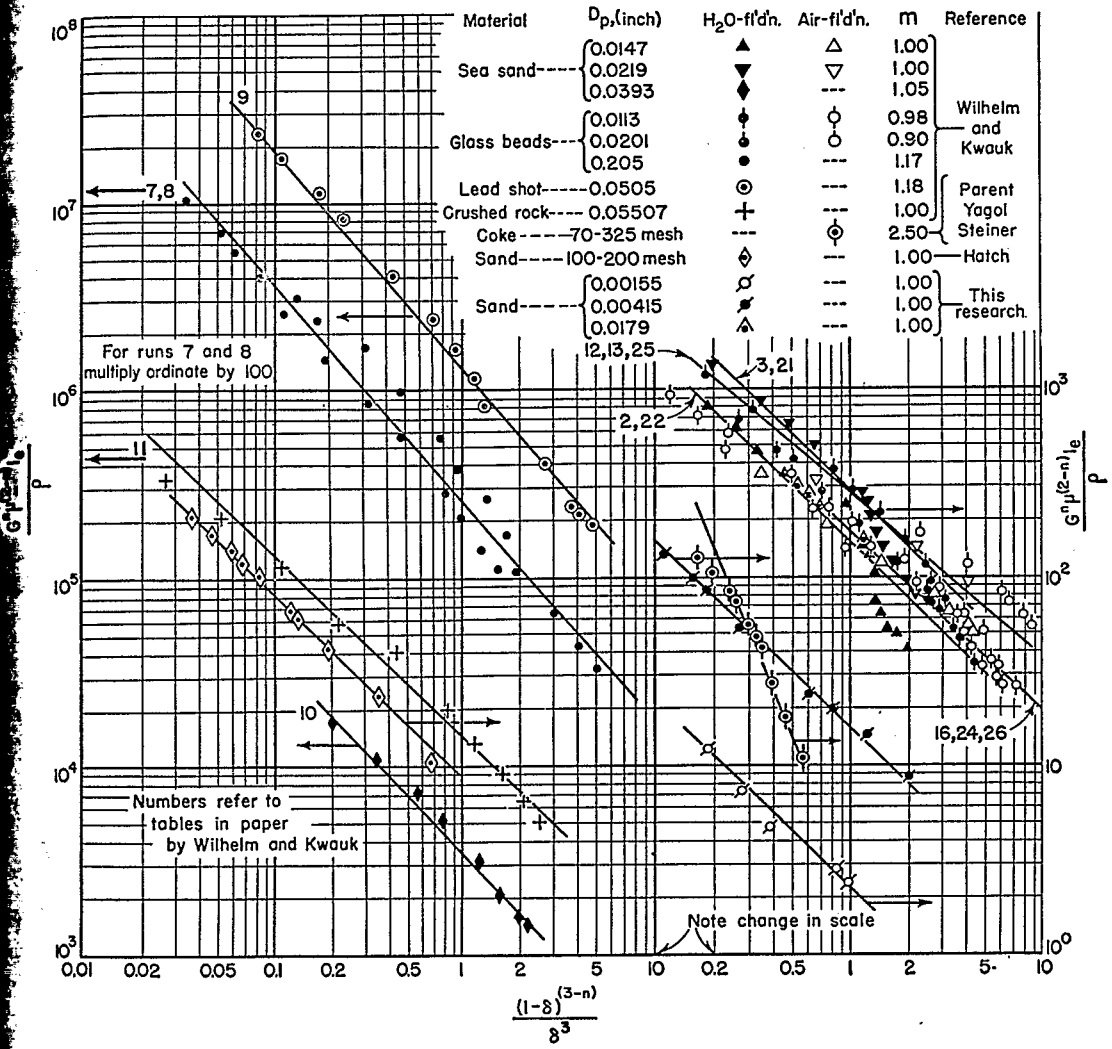

FIGURE 84.—CORRELATION OF LITERATURE DATA.

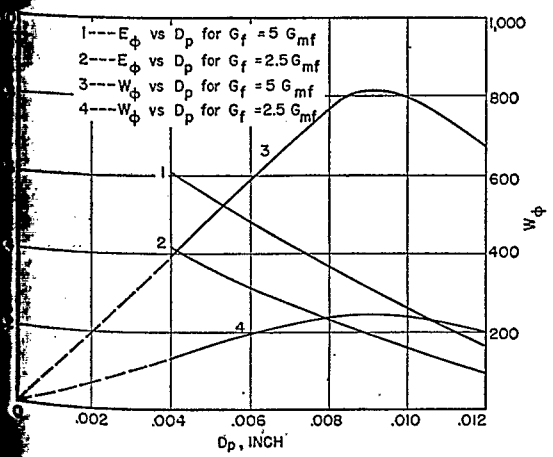

URE 85.—CALCULATED FLUIDIZATION EFFI-IENCIES AND FLUIDIZATION WORK FOR ARIOUS MASS VELOCITIES.

Morse observed that the calculated friction factors could be brought into agreement with the *f* vs. *Re* line if, for the specific sizes, it was assumed that the effective particle diameter increased with increasing flows. It was suggested, therefore, that immediately beyond the minimum-fluidization point (in the fluidized range) particle flocculation occurred (that is, a certain number of particles joined into a definite complex). As the flow increased, the complexes thus formed expanded (swelled) gradually but remained inherently intact as a unit. As a result of this swelling, the effective particle diameter was believed to increase sufficiently to cause the negative deviation. Although this theory explains the negative deviations, there are some serious objections:

1. No complexes were observed during fluidization with sand or any other of the materials tested.

2. It is hard to visualize that such complexes should remain stable under the influence of the increasing internal motion of the particles caused by the increasing fluid rates.

3. One would certainly expect that the tendency to form complexes will depend on the nature of the particles such as shape, density, roughness, and size distribution. From figure 72 as well as figure 93, it is evident that not only sands but also iron Fischer-Tropsch catalyst particles and coke showed similarly large deviations.

The following observations were made on the data of Wilhelm and Kwauk.

For a friction-factor plot of the unexpanded pressure-drop data, the runs using air were observed to give somewhat higher friction factors than the runs using water. The data for water fluidization lay considerably below the friction-factor curve, though parallel to it. The air-fluidization data, on the other hand, were considerably above this curve. A friction-factor plot for the high-Reynolds-number data (large and heavy particles) was several hundred percent above the recommended line for comparable fixed beds. Moreover, the data showed a complete lack of correlation.

Morse does not offer an explanation for the apparent separation of data for flows of air and water through unexpanded beds. It was suggested, however, that the deviation between fluidization data for liquids and gases is interrelated with the nature of fluidization as proposed by Wilhelm and Kwauk—that is, particulate for the water runs and aggregative for the air. The severe deviations observed for the high-Reynolds-number range were believed to be a result of the inherent instability of fluidized beds of large particles. A strong tendency of the solids and the fluid to segregate was given as the chief cause for the deviation of the calculated friction factors from those of comparable fixed beds.

To provide a more rigorous examination of the data, friction factors for the data of Hatch and of Wilhelm and Kwauk were recalculated. Because many of the data fall into the transition and low turbulence range, equation (40), as used by Morse, is not adequate, because it applies only to the laminar-flow range where $Re < 10$. Using the general friction-factor expression,

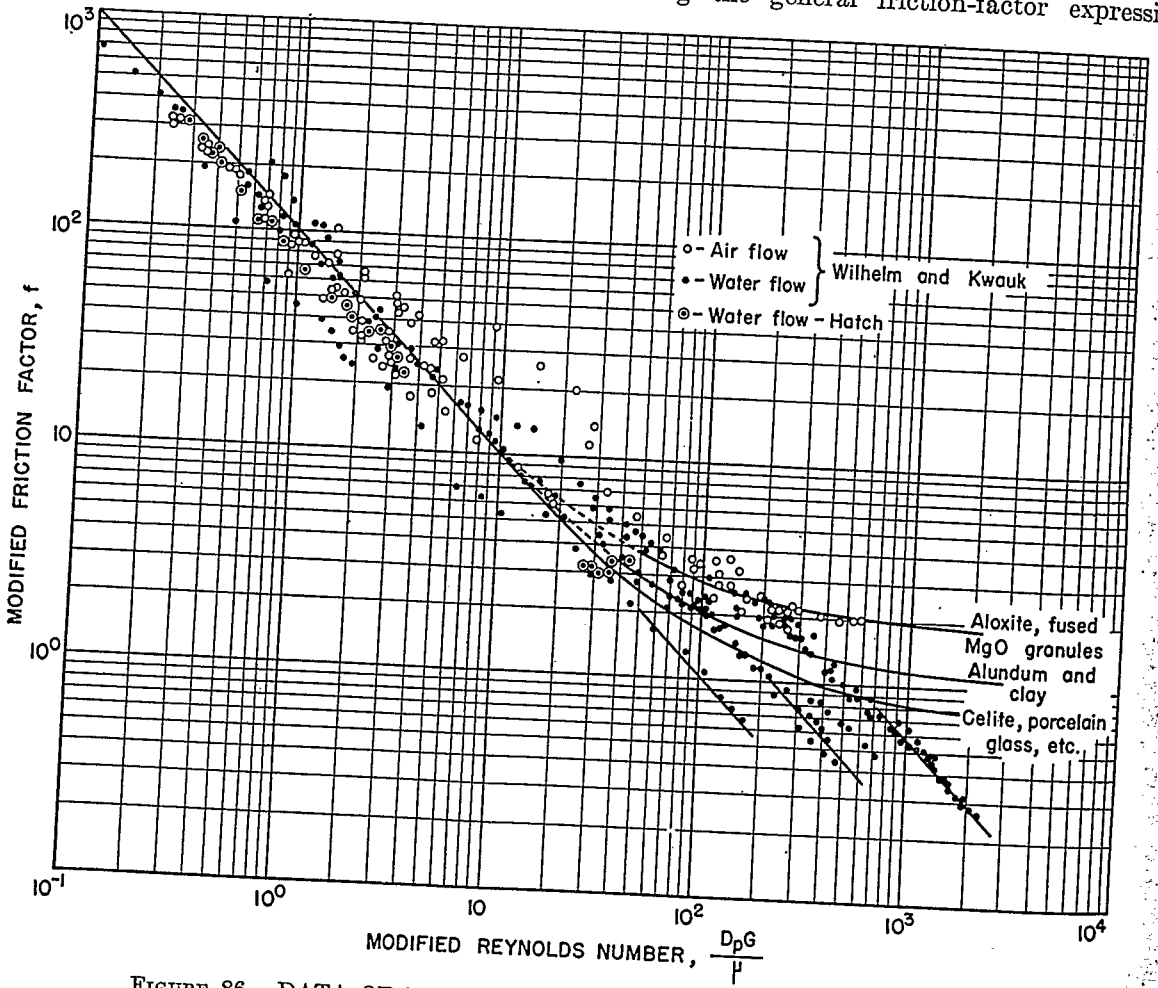

FIGURE 86.—DATA OF WILHELM AND KWAUK AND L. P. HATCH.

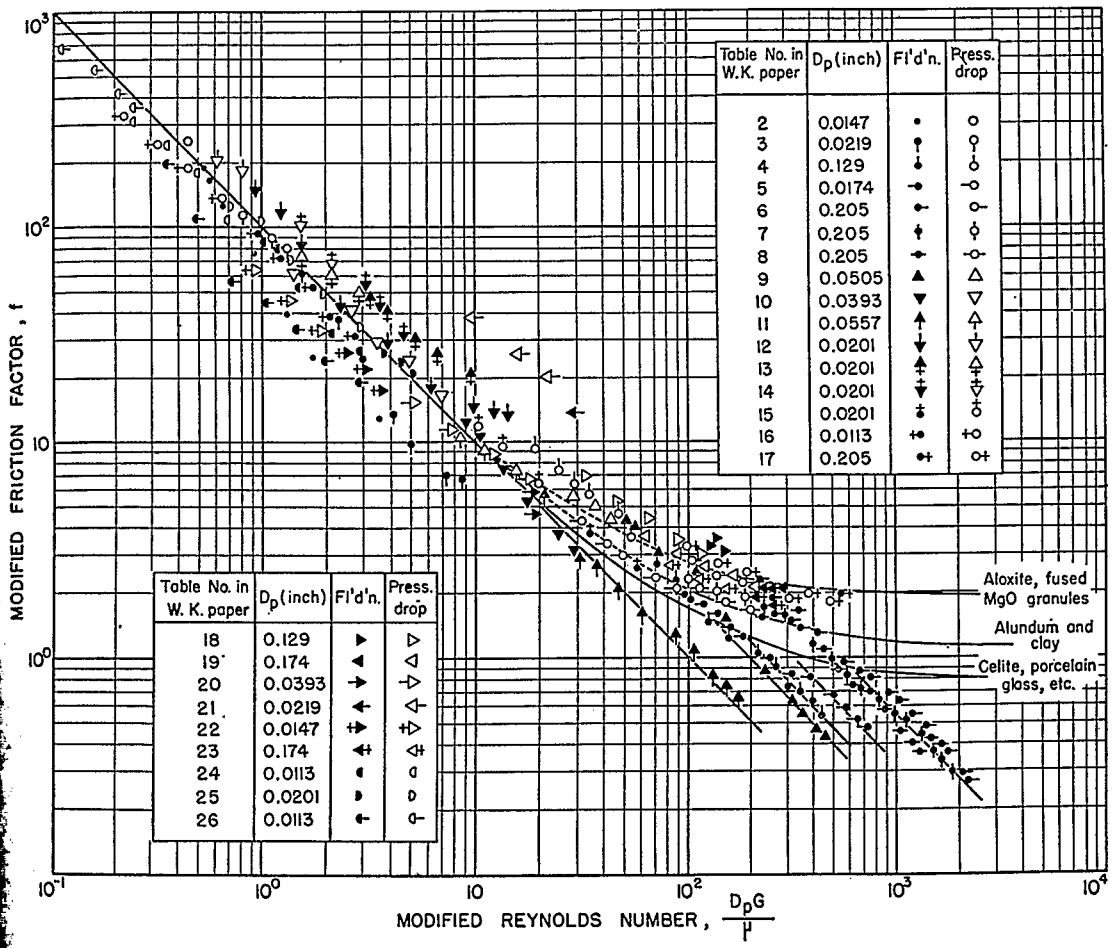

FIGURE 87.—MODIFIED FRICTION FACTOR VERSUS MODIFIED REYNOLDS NUMBER FOR DATA OF WILHELM AND KWAUK.

ation (41), a recalculated voidage of the beds ained from the observed pressure drop at al fluidization, and equation (43), friction- or plots, were calculated and are shown in res 86 and 87. From figure 86, it is appar- that no separation of air and water fluidiza- data exists. Moreover, the data are in d agreement with the friction-factor curve ixed beds proposed earlier. From figure 87 observed that up to Re=200 there is no amental difference between fixed-bed and ized-bed data for the comparatively large icles investigated. The data in the high- olds-number range, however, disagree with fixed-bed correlation. This deviation may plained in the following manner: In the inal derivation of equation (41) it was med that the interstitial pores are of the order of magnitude as the particles them- s. Although this is more or less true for voidages ranging from approximately 40 5 percent, the supposition is violated for y-expanded beds. As the data in the high-Reynolds-number range pertain to highly expanded columns, it is reasonable to expect the deviations indicated in the figure. For the purpose of correcting the data, a larger (effective) particle diameter (as suggested by the increased interstitial channel diameter) should be chosen to bring the data into agreement with fixed-bed behavior.

FLUIDIZATION OF POROUS MATERIAL

GENERAL

From the preceding chapters it appears that for accurate fluidization calculations a knowledge of the percentage voids (effective as far as fluid flow is concerned) is indispensable. With materials of little or no internal porosity, void determinations are readily made by the water-displacement method. However, when dealing with materials such as coal or coke, which have an appreciable internal porosity, the voidage thus obtained will include the

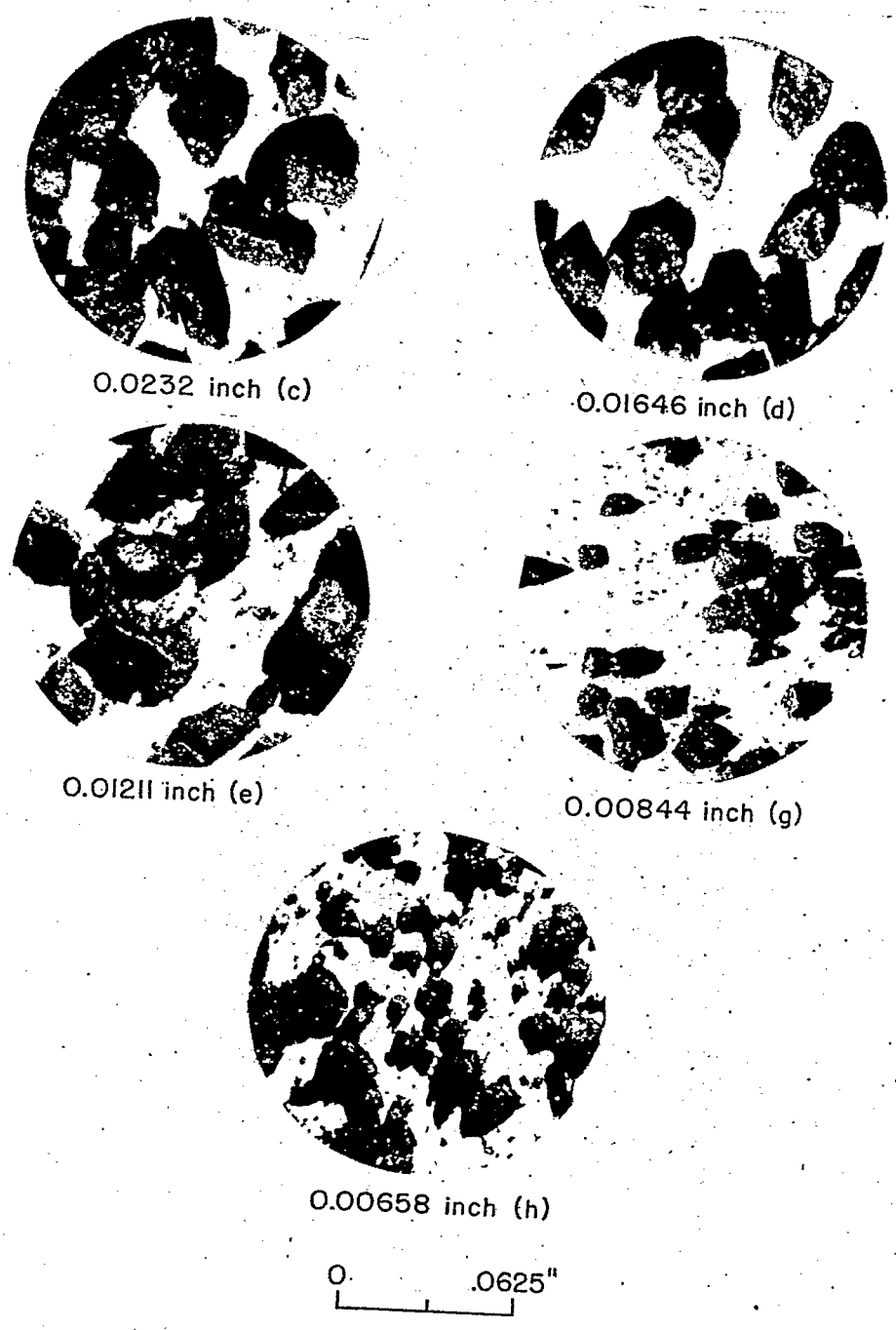

FIGURE 88.—CLOSE CUTS AND MIXTURES OF ANTHRACITE.

$\lambda = 1.6$

crevices inside the particles and therefore does not represent the truly effective voidage as far as fluid flow is concerned. The problem of arriving at a representative voidage for beds of porous materials is vital if it is intended to utilize the fluidization correlations in connection with most commercial materials. In an effort to demonstrate a more general approach than that discussed so far, typical data collected with an anthracite will be discussed, and the steps necessary to permit the use of the correlations previously developed will be outlined.

EXPERIMENTAL DATA

The coal was prepared by crushing egg-size lumps to pieces of approximately 0.25 inch. The fragments were reduced further in a ball mill and passed through standard sieves. Figure 88 shows the various cuts enlarged sufficiently to permit recognition of the characteristic shape of most particles. Densities determined by immersion in water and mercury were 2.37 and 1.97 gm./cc., respectively. Assuming that the water fills all the internal crevices and that the mercury does not penetrate into the particles at all, an average internal porosity of 16.9 percent

$$\left(\frac{2.37-1.97}{2.37}\times 100\right),$$

based on the apparent solid volume of the particles, is calculated.

Cumulative size distributions of the fluidized materials are indicated in figure 89. The uniformity coefficient, a concept frequently used in size classification, is defined as

$$c_u=\frac{d_{60}}{d_{10}},$$

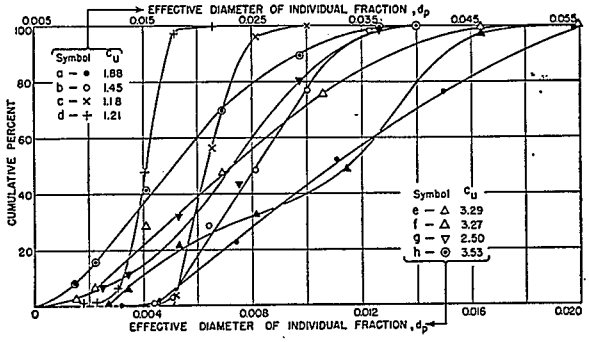

FIGURE 89.—WEIGHT-SIZE DISTRIBUTIONS OF BEDS INVESTIGATED.

d_{60} and d_{10} being sieve openings that permit passage of 60 and 10 percent, respectively, of the weight of sample to be sieved. It is a convenient though approximate index for expressing the degree of homogeneity of a mixture of particles. Figure 89 reveals that all beds were mixtures containing a number of separate components.

The apparatus used was the same as that employed in the study of iron Fischer-Tropsch catalyst. Weighed quantities of the solid were charged into the 4-inch-diameter glass column, and pressure drops were measured across the beds. For definite rates of flow of air or helium, the height of the column was observed as well as the general behavior during fluidization.

Table XV of the appendix gives the original data. A brief orientation of the experimental work is given in table 34. The data, as recorded in figure 90, show the pressure drop in relation to the modified Reynolds number.

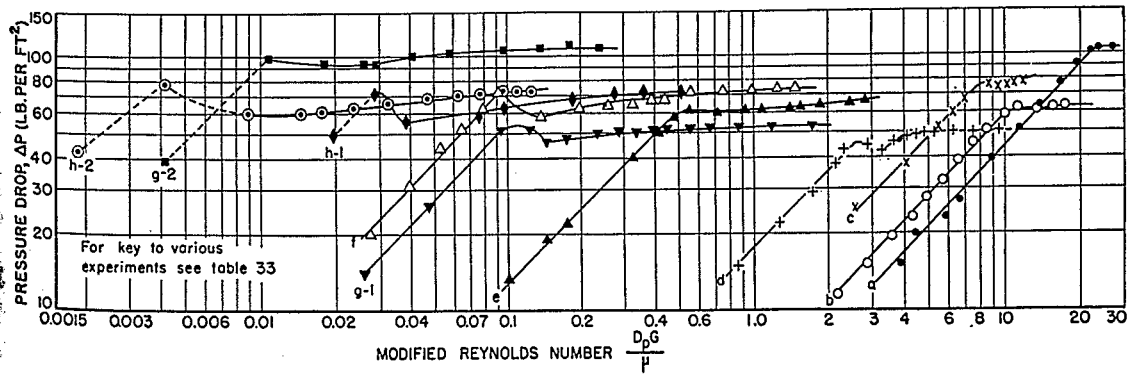

FIGURE 90.—ANTHRACITE-FLUIDIZATION DATA.

TABLE 33.—*Characteristics of anthracite particles and orientation of experimental work*

Run No.	D_p, inches	c_u	Weight, pounds	L_s, feet	Range of l_e	Gas	δ_{mf}
a	0. 03819	1. 85	9. 65	1. 605	1–1. 083	Air	0. 475
b	. 02795	1. 45	5. 56	. 903	1–1. 146	do	. 503
c	. 02321	1. 18	7. 25	1. 259	1–1. 146	do	. 516
d	. 01646	1. 30	4. 44	. 778	1–1. 603	do	. 519
e	. 01211	3. 25	5. 96	1. 002	1–1. 271	do	. 507
f	. 00940	3. 0	6. 80	1. 129	1–1. 277	do	
g–1	. 00844	2. 5	4. 96	. 862	1–1. 408	do	
g–2	. 00844	2. 5	9. 55	1. 613	1–1. 332	Helium	. 47
h–1	. 00658	3. 1	6. 35	1. 106	1–1. 360	Air	. 50
h–2	. 00658	3. 1	6. 35	1. 094	1–1. 340	Helium	

CORRELATION AND COMMENTS

The data may be correlated by plotting

$$\log \frac{G^n \mu^{(2-n)} l_e}{\rho}$$

against

$$\log \frac{(1-\delta)^{3-n}}{\delta^3}.$$

In an analysis of the anthracite data, the state of the flow factor, n, must first be evaluated. Figure 90 shows that the investigations extended over the Reynolds number range 0.002–25, and, therefore, that $n=1$, as evaluated from the inset of figure 41.

Next, it is important to find the effective voidage in the various beds. As the water-immersion method will give high porosity values, and as density measurements by displacement in mercury also are in doubt because of uncertainties in the extent of penetration of the mercury into the pores, it was found more practical to proceed as follows:

1. Procurement of fixed-bed pressure-drop data for definite flows. Measurement of bed height and weight.
2. Estimation of particle-shape factor by comparison with particles of known shape factor.
3. Application of equation (40) for calculation of the effective voidage.

Examination of the plate showing details of the particles indicates that all of them were more or less of the same shape. Further comparison of these photographs with those of sands and iron Fischer catalyst particles (figs. 45–49 and 67) suggested that the shape of the coal fragments was intermediate between that of sharp sand and iron catalyst. Because these particles had shape factors of 1.5 and 1.73, respectively, a value of $\lambda=1.6$ was assigned to the coal particles. This value of λ was then used in combination with pressure drops through the unexpanded beds, as recorded in figure 90, and effective voidages were calculated for all the runs by solving equation (40) for δ. In figure 91, the

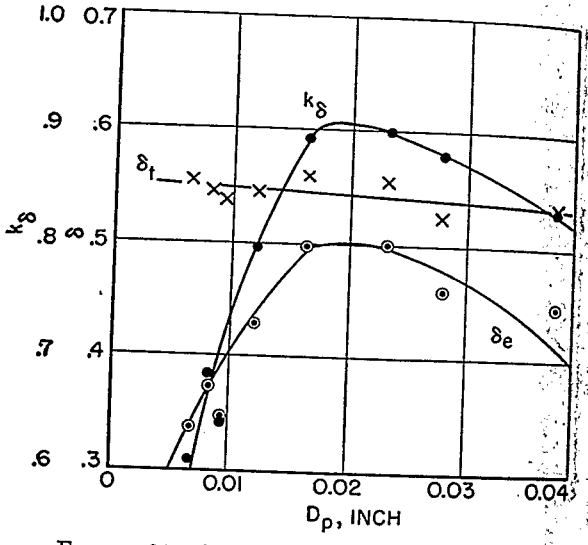

FIGURE 91.—EFFECTIVE VOIDAGE IN ANTHRACITE BEDS

total voidage, δ_t (calculated on the basis of water density), the effective voidage, δ_e, and the proportion of effective voids, k_δ, are shown in relation to the composite particle diameter of the individual cuts. The total voidage is virtually independent of D_p. However, both δ_e and k_δ pass through a maximum near $D_p=0.02$ inch. On the basis of the available data, this is not readily explainable without having to resort to various unsubstantial hypotheses. In view of the considerable variation in sizes as well as the rather wide distribution of sizes, these results should be looked upon as characteristic of the material investigated.

Table 34 lists shape factors that would have resulted from accepting either the water density or the mercury density as a basis for calculation of voids. It is readily seen that most values of λ suggested for the coal particles are considerably higher than would be expected from visual examination.

TABLE 34.—*Shape factors calculated on the basis of water density and mercury density of the coal*

Packing	D_p	λ_{H_2O}	λ_{Hg}
a	0. 03819	2. 23	1. 40
b	. 02795	2. 22	1. 36
c	. 02321	1. 96	1. 26
d	. 01646	2. 15	1. 40
e	. 01211	2. 80	1. 70
f	. 00940	4. 43	2. 71
g	. 00844	3. 64	2. 22
h	. 00658	5. 47	3. 45

With n and δ_e properly evaluated, figure 92 shows the relationship between

$$\log \frac{G\mu l_e}{\rho} \quad \text{and} \quad \frac{(1-\delta)^2}{\delta^3}$$

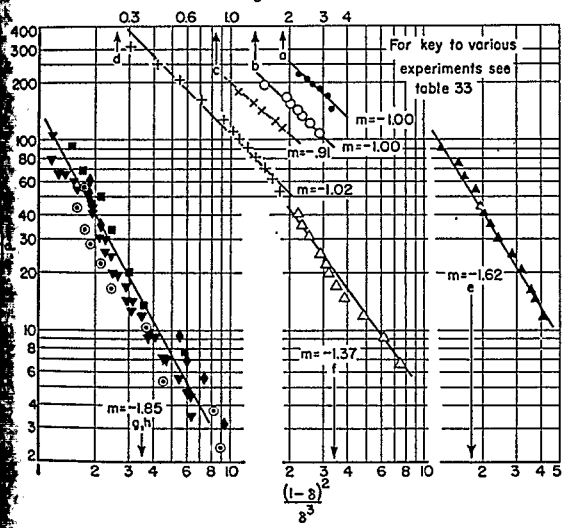

FIGURE 92.—CORRELATION OF ANTHRACITE DATA.

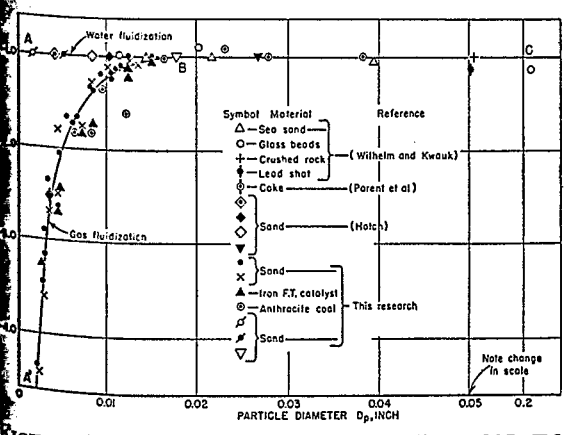

FIGURE 93.—VALUES OF m IN RELATION TO D_p FOR VARIOUS MATERIALS.

for all the data. The correlation is satisfactory, and the slopes, m, of the individual lines, plotted in figure 93 are in substantial agreement with the other data as well as with some of Wilhelm and Kwauk's [48] measurements.

MINIMUM FLUID VOIDAGE

With substances such as sand or iron catalyst particles, determination of δ_{mf} was simple. Attempts to evaluate δ_{mf} for the coal were less successful, however, chiefly because of excessive channeling. This was especially true of the smaller sizes where the beds fluidized only in sections when under the action of low gas flow rates. Reliable data could be collected only with sizes larger than 0.01 inch. For these particles, figure 94 shows the values of δ_{mf} in relation to the particle diameter. From the

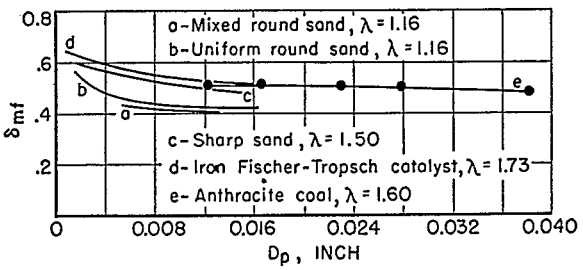

FIGURE 94.—MINIMUM FLUID VOIDAGE, δ_{mf}, FOR VARIOUS MATERIALS IN RELATION TO EFFECTIVE PARTICLE DIAMETER D_p.

other data recorded in the figure, the mutual dependence of δ_{mf} and λ is readily observed. Particles of high shape factor require greater minimum fluid voidages than rounder bodies. The δ_{mf} values for the coal agreed with this requirement and were observed to be intermediate between those of the sharp sand and the iron catalyst, which had, respectively, smaller and larger shape factors than the coal fragments. This agreement may serve as an indirect check for the rather close estimation of λ for coal.

CHANNELING IN FLUIDIZED BEDS

Channeling may be defined as that condition that exists when fluids are flowing through beds of fixed or fluidized solids in such a manner that the rate of flow is not constant over the cross section of the bed. This condition results from the presence in the bed of paths or "channels" that have greater hydraulic radii and that afford a shorter path of travel through

[48] Work cited in footnote 95, p. 7.

the bed than the average winding route between solid particles normally taken by the fluid; as a result, less resistance is offered to the flow of fluid.

The effects of channeling are always undesirable, as they decrease the interfacial area, the existence of which is generally the reason for using the bed. Furthermore, channeling is self-propagating; the high velocity through one path increases the diameter of that path at the expense of the low-velocity paths, which tend to become further choked with fines. This is especially deleterious to fluidized beds, where the velocity in the unchanneled portion of the bed may drop below that necessary to keep the solids fluidized, with the result that a high velocity stream may create a "pipeline" containing very little solids.

In work involving chemical reactions, channeling causes a variation in the effective amount of solids exposed to a given flow of gas. Under these conditions, interpretations based solely on measured values of space velocity may yield entirely spurious conclusions.

Channeling is essentially a function of randomness of particle distribution. It must therefore be analyzed either by complex statistical methods or by comparison with beds of some assumed standard distribution. As most of the relations derived previously have been based upon beds packed with the maximum possible uniformity, these correlations were used as references for pressure-drop flow relations of channeling beds.

Channeling may occur in a fluidized bed in any of the ways indicated in figure 95. A fluidized bed may develop a channel sufficiently greater than the average to cause unequal distribution in gas flow, but not great enough to cause the pressure drop through the rest of the bed to fall below that necessary for fluidization. This situation is represented by figure 95a. The channel may be large enough also to form a "pipe," as described earlier in this section and as represented in figure 95b. In this case, fluidization will stop. A channel of either type may be formed in a limited length of the bed, as in figure 95c. If this channel is of form "b," fluidization may stop in certain zones of the bed but persist in others.

An attempt to analyze situation (a) may be made if it is assumed that equations that have been derived, such as equation (41), hold for any longitudinal section of a bed in which the channels are of constant diameter. For further simplification, one may assume that the flow is laminar and that equation (40) described the flow through the fluidized bed. This equation can be written as

$$\Delta P = k\, L\, G\, \frac{(1-\delta)^2}{\delta^3} \text{ or } \Delta P = k\, \frac{L_{mf} G}{(1-\delta)}\, \frac{(1-\delta)^2}{\delta^3}\, (1-\delta_{mf}). \tag{58}$$

As in case (a), under consideration, the bed is fluidizing, and as ΔP, $(1-\delta_{mf})$ and L_{mf} are constant, equation (58) may be converted to equation (59).

$$G = k' \frac{\delta^3}{(1-\delta)}. \tag{59}$$

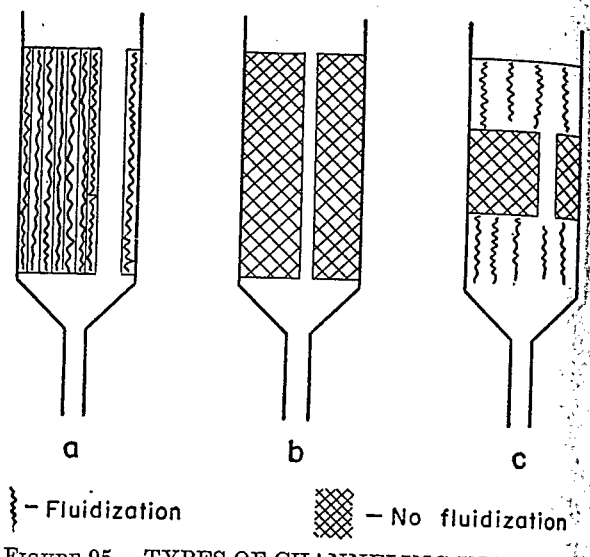

FIGURE 95.—TYPES OF CHANNELING IN FLUIDIZED BEDS.

If channels were created in one part of the bed such that voids increased from 0.50 to 0.55, equation (59) would indicate that the flow for this part of the bed would become 1.48 times the initial flow. If the voidage in another part of the bed decreased from 0.50 to 0.45, the flow in this latter section would become 0.663 times the initial flow. If the section of increased flow represented the same volume as the section of decreased flow, and if the value of the decreased flow was still sufficient to keep the bed fluidized, the total voidage and, hence, the bed expansion would remain essentially constant, but the flow would have increased to 1.14 times its initial value.

This line of reasoning shows that unusual relationships between G and δ for a fluidizing bed may be attributable to channeling, but further quantitative treatment is difficult because of the infinite combinations of channel diameters and number of channels capable of giving the same total voidage.

If the zonal channeling represented by figure 95c is the same type as that of "a", it is even less subject to analysis. If it is of the

"pipe" type, of which "b" is the limiting case, it will make itself evident by the fact that the pressure drop across the bed will be substantially less than that predicted from the weight of the bed, even though fluidization exists. It has, in fact, been noted that observed pressure-drop flow relations deviate most widely from the theoretical for those materials that show the greatest tendency to channel.

Figure 96, curve "a", represents a typical pressure-drop curve of a material of moderate channeling tendencies. The pressure drop will increase in the usual manner until the weight of the bed per unit area is exceeded and then will drop sharply to a minimum value ΔP_d, after which it will rise toward the value $\Delta P = \text{wt.}/A_t$. Observation will generally show that the solids circulation is most erratic and the channeling tendency most severe at the point corresponding to ΔP_d. As the flow is increased beyond this point, agitation in the fluidized portions of the bed increases and tends to destroy the channels in stagnant zones. As a result, the entire bed becomes more uniform, and channeling decreases. Application of this theory to figure 95c explains the rise in pressure to the theoretical. If flow is increased much beyond this point, a new phenomenon—slugging—becomes evident, and

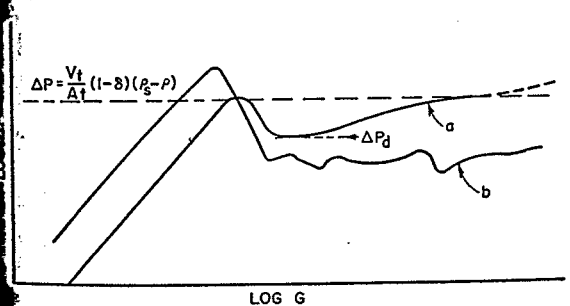

FIGURE 96.—PRESSURE-DROP CURVES FOR CHANNELING BEDS.

the pressure drop exceeds the theoretical because of the increased friction between bed and wall. For very badly channeling materials, the pressure-drop curve will be erratic and never approach the theoretical, as in figure 96b. The pressure deficiency ratio $(\Delta P - \Delta P_d)/\Delta P$, where ΔP represents the value wt./A_t and where ΔP_d is the pressure drop at the dip of the curve, may be used to define a channeling factor, symbolized by χ_d. From the interpretation of figure 95c, a physical significance may be ascribed to χ_d as the equivalent fractional length of bed unfluidized. However, this concept may be used quantitatively only with extreme caution, inasmuch as χ_d cannot include any channeling of the form of figure 95a, which does not affect the pressure drop. χ_d can, however, be used as a means of qualitatively comparing the channeling behavior of various beds. A larger value of χ_d implies a greater tendency to channel.

Figure 97 shows typical pressure-drop mass flow relations for four materials. From data such as these, figure 98 has been constructed

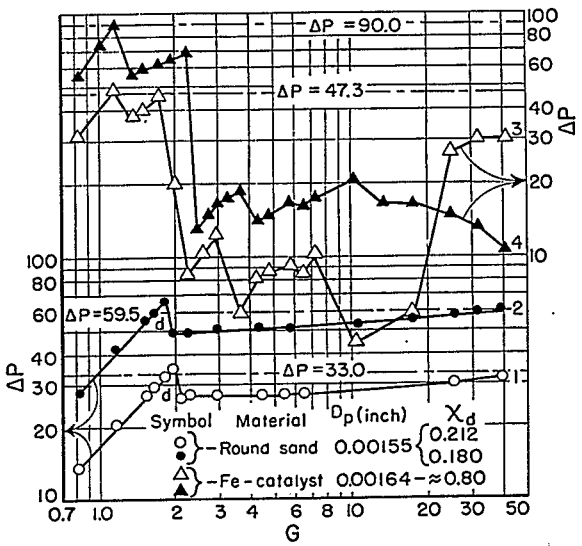

FIGURE 97.—TYPICAL PRESSURE DROP VS. MASS FLOW RELATIONS IN CHANNELING SOLIDS.

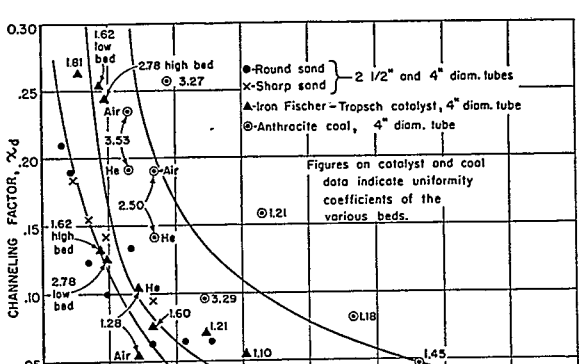

FIGURE 98.—CHANNELING FACTORS IN RELATION TO EFFECTIVE PARTICLE DIAMETER FOR A VARIETY OF MATERIALS.

showing values of χ_d in relation to D_p for round sand, sharp sand, iron Fischer-Tropsch catalyst particles, and also anthracite. In all cases, it is observed that χ_d decreases sharply with increasing values of D_p. This emphasizes, as has been substantiated almost universally, that reduced channeling tendencies are to be expected for operation with large particles.

Comparison of individual channeling data pertaining to round and sharp sand indicates that the rounded particles have greater channeling tendencies. No ready explanation can be given for this behavior. The graphs show further that the iron catalyst particles of $D_p <$ 0.005 inch channel much more severely than the sand. As already mentioned, the coal exhibited by far the worst channeling behavior, and this is significantly reflected by the much higher channeling factor. There was some evidence that the coal differed slightly from the other materials, possessing a certain stickiness as well as a microscopic surface roughness not observed elsewhere. Comparison of the coal with other materials suggested, also, greater irregularities in particle surface. All these observations are factors that might conceivably have a bearing on the channeling intensity of fluidized solids.

Numbers in figure 98 indicate uniformity coefficients of the individual beds. Interpretation of the scatter of the points in the figure should be attempted in the light of the general reproducibility of data of this kind. From an examination of graphs 3 and 4 of figure 97 it appears that one important reason for the scatter found in figure 98 is the experimental difficulty associated with the measurement of basic data. Taking this into consideration, effects of size distribution upon channeling may not be dismissed entirely, although such effects are probably of secondary importance.

Data in figure 99, which is designed to show, within certain limits, the effect of vessel diameter and bed height upon the channeling factor indicate that, for the materials investigated and for the size of apparatus used, no coordinated relation exists.

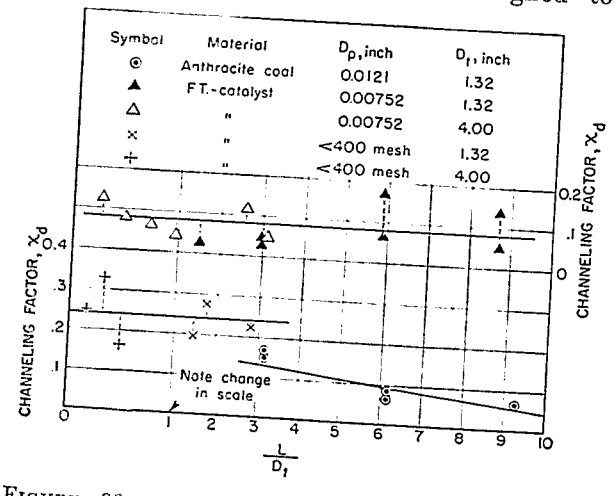

FIGURE 99.—CHANNELING FACTOR χ_d vs. $\frac{L}{D_t}$ FOR VARIOUS MATERIALS.

SUMMARY

Basic fluidization calculations require estimation of the following factors:

1. Flow causing initial bed expansion.
2. Minimum flow required for fluidization.
3. Height of expanded bed and bulk density at operating mass flow rate.
4. Fluidization efficiency and energy.
5. Slugging tendency.
6. Channeling tendency.

For the solution of problems the following data are required:

a. Rate of flow.
b. Density and viscosity of fluid.
c. Effective particle diameter.
d. Shape factor.
e. Minimum fluid voidage.

As factors a to c are usually available from process specifications, solution of problems requires only estimation of the shape factor and the minimum fluid voidage.

In order to estimate the flow necessary for initial bed expansion, the most important quantity is probably the percentage voids in the bed. Knowing the voids, either equation (40) or (21) will give the desired information, depending on whether the flow is laminar or turbulent.

For estimation of the minimum flow required for fluidization, it is necessary to use the minimum fluid voidage in combination with either equation (40) or (21). When working with nonporous materials, the voidage in the bed may be estimated from pycnometric density data of the material. From pressure drops across a fixed bed and by means of equation (40), the shape-factor value may be calculated. From a knowledge of the shape factor and the effective particle diameter, the minimum fluid voidage may be obtained with the aid of such data as those shown in figure 94.

If no facilities are available for obtaining pressure-drop data, estimation of the shape factor will suffice for most engineering work. The estimated value may then be used for obtaining values of the minimum fluid voidage.

When porous particles are used, the pycnometric density cannot be used for void determinations. At present it appears that the only

way to arrive at a representative minimum fluid voidage value is to estimate the shape factor of the particles by comparison with other particles, the shape factors of which have been determined by prior experiment. Use of the estimated shape factors in one of the representative pressure-drop equations will permit solution for the effective bed voidage.

The height of the expanded bed is readily obtained by either using equations (49) to (55) or, preferably, the brief graphical method described in connection with the fluidization of the iron catalyst. The series of calculations for bed density also will permit calculation of efficiency and fluidization energy.

Slugging points may be estimated from the correlation between particle diameter and expansion ratio previously developed. An indication of channeling may be obtained in some cases by comparison of measured pressure drops with those expected from a knowledge of the weight of the bed.

943247°—51——7

SUMMARY OF DESIGN EQUATIONS

The shape factor for any particle is given by

$$\lambda = 0.205 \frac{A}{V_p^{2/3}}. \tag{9}$$

Pressure drop across fixed beds for turbulent flow ($Re > 100$) may be calculated according to:

$$\Delta P = \frac{2fG^2L\lambda^{1.1}(1-\delta)}{D_p g_c \rho \delta^3}, \tag{14}$$

or the slightly more abridged form:

$$\Delta P = \frac{2.12fG^2L\lambda(1-\delta)}{D_p g_c \rho \delta^3}. \tag{21}$$

For smooth particles (glass, porcelain, brass) and turbulent flow (Re $>$ 100)

$$f = 1.75 \left(\frac{D_p G}{\mu}\right)^{-0.1}. \tag{13}$$

For rougher particles (alundum)

$$f = 2.625 \left(\frac{D_p G}{\mu}\right)^{-0.1}. \tag{16}$$

and for still rougher particles (Aloxite, MgO granules)

$$f = 4.0 \left(\frac{D_p G}{\mu}\right)^{-0.1}. \tag{17}$$

With the above values of friction factors substituted into equations (12) or (21), the pressure drop will be obtained as pounds per square foot if all dimensions are expressed in English units.

For a granular charge which is a mixture of sizes, the average particle diameter to be used in equations (12), (21), and (40), given below, may be calculated according to:

$$D_p = (Xd_p)_1 + (Xd_p)_2 + \ldots (Xd_p)_Z. \tag{20}$$

The characteristic volume of a packing was defined as:

$$V_c = \frac{V_P}{\beta}. \tag{23}$$

and the characteristic area as:

$$A_c = \frac{A_P}{\beta}. \tag{24}$$

In the above equations β was termed the bed characterization factor and for turbulent flow ($Re > 100$) was given by

$$\beta = \frac{L\lambda(1-\delta)}{D_p \delta^3}. \tag{22b}$$

The true space velocity through a reactor charged with a granular catalyst is given by:

$$S = \frac{G}{L\rho(1-\delta)}, \tag{30}$$

which expression assumes that the reactor was packed in such a manner as to render the entire charge equally active.

For a cylindrical pellet, the shape factor may be estimated immediately if the ratio of length to diameter of the pellet is known. Thus for,

$$\frac{h}{d_c} = \text{a}, \quad \lambda = 0.757\ \text{a}^{2/3}\left[\frac{1}{2} + \frac{1}{a}\right]. \tag{33a}$$

For viscous flow ($Re < 10$)

$$f = 100 \left(\frac{D_p G}{\mu}\right)^{-1}. \tag{38a}$$

Substituted into (12) yields:

$$\Delta P = \frac{200 G \mu L \lambda^2 (1-\delta)^2}{D_p^2 g_c \rho \delta^3} \tag{40}$$

which will give the pressure drop for the viscous flow range. With English units, the answer will be in pounds per square foot.

For the Reynolds number range 10–100, commonly referred to as the transition range, the general form

$$\Delta P = \frac{2fG^2L\lambda^{3-n}(1-\delta)^{3-n}}{D_p g_c \rho \delta^3} \tag{41}$$

is recommended. The state of flow factor n is a function of the Reynolds number and is readily evaluated from figure 41.

Pressure drop across a fluidizing bed is given by:

$$\Delta P = \frac{V_t}{A_t}(1-\delta)(\rho_s - \rho). \tag{43}$$

For a given bed the minimum fluidization mass velocity may be calculated according to:

$$(G_{mf})^2 = \frac{D_p g_c \rho \delta_{mf}^3}{2f\lambda^{3-n}(1-\delta_{mf})^{2-n}}. \tag{45b}$$

For flow characterized by Re $<$ 10, one obtains:

$$G_{mf} = \frac{0.005 D_p^2 g_c \rho (\rho_s - \rho) \delta_{mf}^3}{\mu \lambda^2 (1-\delta_{mf})}. \tag{45c}$$

For gas-solid systems, equation (45a) may be abridged to read:

$$G_{mf} = C D_p^2 g_c \rho_s \frac{\rho}{\mu}. \tag{57}$$

The constant C is available from figure 79.

NOMENCLATURE

F—Force
L—Length
M—Mass
θ—Time
} If no dimension is stated, the concept is dimensionless.

a—Height/diameter ratio of cylindrical packing element; $a=\frac{h}{d_c}$.

c_u—Uniformity coefficient of a mixture of particles.

d—Differential.

d_c—Diameter of cylindrical pellet (L).

d_p—Diameter of a specific component in a mixture of particles (L).

d_1–d_2–d_3—Adjacent sieve sizes; expressed in fractions of an inch.

d_{10}–d_{60}—Size openings in a sieve, expressed in fractions of an inch, that will pass 10 percent and 60 percent, respectively, of a mixture of particles. By definition: Uniformity coefficient $c_u=\frac{d_{60}}{d_{10}}$.

e—Height of protuberances on packing particles, causing roughness (L).

f—Modified friction factor.

f_m—Modified friction factor (Happel).

g_c—Conversion factor, 4.17 x 10^8 ft./hr.^{2}

h—Height of cylindrical pellet (L).

k, k'—Constant.

k_a—Constant, denoting the proportion of effective surface area in a packed bed.

k_v—Constant, denoting the proportion of effective volume in a packed bed.

k_ϕ—Constant, denoting the proportion of effective voids in a packed bed.

l_e—Expansion ratio or expanded packed bed height on basis of 1 foot of unexpanded section (L).

l_f—Height of fluidized bed, on basis of 1 foot of unexpanded section (L).

l_{mf}—Height of packed bed at onset of fluidization, basis 1 foot of unexpanded section (L).

m—Constant, indicating the deviation of fluidization from fixed bed behavior.

n—State of flow factor.

r_H—Modified hydraulic radius of a packing element in a packed bed (L).

r_p—General denomination of the radius of a particle (L).

r_t—Radius of the vessel (tube) holding the packing (L).

u—Average linear fluid velocity through packed bed ($L\theta^{-1}$).

v—Specific volume of fluid passing through packed bed (L^3M^{-1}).

w—Weight rate of flow ($M\theta^{-1}$).

$wt.$—Weight of bed (M).

z—Compressibility factor of gaseous fluids.

A—Surface area of a particle of arbitrary shape (L^2).

A_c—Characteristic surface area of a packing element in a bed (L^2).

A_p—Surface area of a sphere of equivalent volume (L^2).

A_P—Total surface area of 1 cubic foot of dumped packing (L^2).

A_t—Cross-sectional area of vessel, holding the packed bed (L^2).

C—Constant.

D_m—Diameter of a particle of arbitrary shape (L).

D_p—Diameter of packing particle. For all particles except granular, this denotes the diameter of the equivalent volume sphere. For granules, the particle diameter is obtained from sieve ratings (L).

D_t—Diameter of vessel holding the packed bed (L).

$E\phi$—Efficiency of fluidization.

F—Friction loss of fluid flowing (feet of fluid).

G—Mass velocity of fluid flowing, on basis of open cross-section of tower ($ML^{-2}\theta^{-1}$).

G_e—Mass velocity required for packed bed expansion ($ML^{-2}\theta^{-1}$).

G_f—Mass velocity required for fluidizing a bed of solid particles ($ML^{-2}\theta^{-1}$).

G_{mf}—Minimum fluidization mass velocity for a bed of solid particles ($ML^{-2}\theta^{-1}$).

L—Height of packed bed (L).

L_e—Height of expanded bed (L).

L_o—Height of hypothetical bed compacted to zero voidage (L).

M—Molecular weight.

N—Number of packing elements in a packed section of 1 foot in height.

N_{Rcm}—Modified Reynolds number (Happel).

R—Gas constant.

Re—Modified Reynolds number.

S—Space velocity (θ^{-1}).

T—Absolute fluid temperature, ° K. or ° R.

V_c—Characteristic volume of a packing element in a bed (L^3).

V_p—Solid volume of one individual packing element (L^3).

V_t—Volume of the vessel holding the packed bed (L^3).

V_P—Total solid volume of 1 cubic foot of dumped packing (L^3).

W_e—Energy required for bed expansion (LM).

W_t—Total energy required for fluidization and bed expansion (LM).
W_o—Energy required for fluidization of a bed (LM).
X—Weight percent of any component of particles in a packed bed.
Z—Number of component sizes in a mixed packed bed.
α—Area-shape factor of a particle.
β—Bed characterization factor in turbulent flow.
β_l—Bed characterization factor in laminar flow.
γ—Volume shape factor of a particle.
δ—Gross bed voidage.
δ_e—Effective bed voidage.
δ_{mf}—Minimum fluidization voidage.
δ_t—Total voidage in bed (equal to δ).
Δp—Pressure drop per unit bed height ($FL^{-2}L^{-1}$).
Δp_{40}—Pressure drop per unit bed height, corrected to 40-percent voids reference state. ($FL^{-2}L^{-1}$).
Δp—Pressure drop across entire bed (FL^{-2}).
Δp_d—Pressure drop minimum for channeling solids (FL^{-2}).
λ—Particle shape factor.
μ—Fluid viscosity ($FL^{-1}\theta^{-1}$).
ρ—Fluid density (ML^{-3}).
ρ_s—Solids density (ML^{-3}).
ϕ—Function of
ϕ'—Turbulent flow factor (FL^{-2}).
χ_d—Channeling factor.

APPENDIX

TABLE I.—*Pressure-drop data for flow through smooth particles*

Run	w, lb./hr.	G, lb. ft.$^{-2}$ hr.$^{-1}$	Re	Δp, cm. H_2O	Δp_{40}, p. s. i./ft.	f
	Glass beads, D_p=0.172 in., D_t=2.067 in., air, ρ=0.0886, CH*=33.375 in., CT*=66° F., voids=37.2 percent					
a-1	51.7	2,220	751	252	0.984	0.820
	46.5	1,998	675	200	.781	.802
	41.3	1,773	599	160	.627	.820
	35.8	1,539	520	121	.474	.823
	28.4	1,220	412	80	.313	.860
	23.2	995	336	50	.1954	.808
	19.62	841	285	36	.1407	.812
	13.21	567	192	17	.0665	.850
	Glass beads, D_p=0.172 in., D_t=2.067 in., air, ρ=0.0886, CH=35.0 in., CT=76° F., voids=40.0 percent					
a-1	57.1	2,454	816	261	1.270	0.855
	50.1	2,150	715	200	.975	.855
	45.0	1,933	643	160	.780	.870
	39.3	1,690	561	120	.585	.830
	35.9	1,542	513	100	.487	.831
	31.7	1,362	453	80	.390	.850
	25.2	1,081	360	50	.244	.840
	20.0	858	285	30	.146	.802
	Glass beads, D_p=0.228 in., D_t=2.067 in., air, ρ=0.0884, CH=35.375 in., CT=68° F., voids=41.9 percent					
b-1	70.4	3,015	1,332	236	1.322	0.778
	59.4	2,550	1,125	169	.948	.780
	51.8	2,225	985	127	.713	.773
	38.7	1,662	736	68.5	.384	.745
	26.8	1,152	510	34	.1905	.768
	17.8	764	337	14.8	.0829	.762
	15.85	680	301	12.0	.0674	.780
	Glass beads, D_p=0.228 in., D_t=2.067 in., air, ρ=0.0884, CH=36.0 in., CT=68° F., voids=38.8 percent					
b-1	63.4	2,722	1,203	251	1.056	0.771
	56.3	2,418	1,067	200	.844	.783
	44.5	1,912	846	123	.519	.770
	35.6	1,530	677	78	.329	.762
	26.4	1,134	502	43	.1839	.772
	Glass beads, D_p=0.228 in., D_t=2.067 in., air, ρ=0.0884, CH=36.75 in., CT=70° F., voids=40.0 percent					
b-1	66.1	2,840	1,257	248	1.151	0.770
	59.3	2,550	1,128	200	.930	.772
	53.2	2,285	1,010	160	.744	.768
	46.3	1,988	881	120	.558	.761
	38.0	1,633	724	80	.372	.752
	28.9	1,242	550	46.5	.216	.755
	21.4	918	406	25.5	.1188	.760
	11.7	502	222	8.0	.0372	.795

*CH=column height=L; CT=temperature of gas.

TABLE I.—*Pressure-drop data for flow through smooth particles*—Continued

Run	w, lb./hr.	G, lb. ft.$^{-2}$ hr.$^{-1}$	Re	Δp, cm. H_2O	Δp_{40}, p. s. i./ft.	f
	Glass beads, D_p=0.388 in., D_t=2.067 in., air, ρ=0.0871, CH=35.875 in., CT=70° F., voids=42.5 percent					
c-1	95.8	4,115	3,096	232	1.385	0.740
	88.9	3,820	2,970	200	1.196	.742
	79.4	3,408	2,562	160	.957	.747
	68.8	2,954	2,218	120	.719	.748
	62.7	2,695	2,024	100	.599	.747
	56.3	2,416	1,815	80	.479	.745
	44.4	1,908	1,433	50	.299	.746
	34.7	1,491	1,120	30	.1793	.730
	28.0	1,203	906	20	.1196	.746
	19.48	835	628	10	.0599	.778
	Glass beads, D_p=0.388 in., D_t=2.067 in., air, ρ=0.0871, GII=37.25 in., CT=72° F., voids=44.7 percent					
c-1	104.8	4,495	3,378	225	1.559	0.700
	95.6	4,105	3,082	184	1.278	.684
	89.1	3,830	2,878	160	1.110	.681
	76.4	3,285	2,468	120	.835	.698
	70.2	3,016	2,266	100	.696	.691
	62.8	2,700	2,030	80	.556	.688
	50.3	2,160	1,622	50	.348	.672
	39.4	1,692	1,270	30	.2082	.657
	23.7	1,018	766	11	.0767	.665
	Porcelain balls, D_p=0.5075 in., D_t=2.067 in., air, ρ=0.0860, CH=34.88 in., CT=75° F., voids=41.5 percent					
d-1	110.2	4,730	4,640	221	1.236	0.645
	99.6	4,280	4,195	179	1.050	.670
	91.9	3,950	3,870	152	.910	.682
	78.3	3,365	3,295	111	.624	.642
	74.1	3,182	3,120	99	.555	.653
	65.1	2,800	2,745	76	.426	.634
	53.4	2,292	2,245	51	.286	.638
	31.5	1,354	1,325	17	.0955	.610
	22.8	978	958	10	.0561	.684
	Porcelain balls, D_p=0.5075 in., D_t=2.067 in., air, ρ=0.0680, CH=34.88 in., CT=223° F., voids=41.5 percent					
e-1	85.6	3,675	3,030	176	0.989	0.680
	76.2	3,275	2,700	142	.798	.690
	65.8	2,828	2,328	102	.573	.664
	51.4	2,208	1,820	60	.336	.640
	28.7	1,233	1,023	18	.1010	----
	Porcelain balls, D_p=0.5075 in., D_t=2.067 in., air, ρ=0.0527, CH=34.88 in., CT=340° F., voids=41.5 percent					
f-1	59.4	2,550	1,868	111	0.624	0.704
	53.4	2,292	1,678	86	.482	.675
	46.1	1,980	1,448	60	.336	.629
	38.3	1,646	1,204	40	.224	.606
	27.5	1,182	868	20	.1122	----
	20.2	866	635	10	.0562	----

TABLE I.—*Pressure-drop data for flow through smooth particles*—Continued

Run	w, lb./hr.	G, lb. ft.$^{-2}$ hr.$^{-1}$	Re	Δp, cm. H_2O	Δp_{40}, p. s. i./ft.	f
	Porcelain balls, D_p=0.5075 in., D_t=2.067 in., CO_2 gas, CH=34.88 in., CT=82° F., voids=41.5 percent					
g-1	76.2	3,275	4,090	75	0.421	0.625
	52.6	2,262	2,825	39	.2285	.709
	34.9	1,500	1,870	17	.0956	.695
	26.0	1,118	1,400	10	.0564	.675
	37.4	1,605	2,000	20	.1123	.718
	23.9	1,026	1,280	8.5	.0477	.721
	Mixed glass beads, D_p=0.297 in., D_t=2.067 in., air, ρ=0.0882, CH=38.0 in., CT=72° F., voids=35 percent					
h-1	54.4	2,334	1,333	251	0.695	0.897
	49.0	2,105	1,203	200	.555	.880
	44.1	1,895	1,083	160	.443	.866
	38.1	1,637	938	120	.331	.864
	30.2	1,298	744	80	.2216	.921
	24.3	1,043	598	50	.1448	.935
	18.65	800	458	30	.0832	.920
	10.70	459	263	10	.0278	.926
	Mixed beads, D_p=0.3141 in., D_t=2.067 in., air, ρ=0.0875, CH=36.125 in., CT=71° F., voids=37 percent					
i-1	60.2	2,588	1,572	237	0.841	0.921
	55.5	2,384	1,449	200	.709	.916
	50.0	2,146	1,304	160	.566	.905
	43.0	1,847	1,120	120	.425	.920
	36.1	1,550	942	81	.287	.878
	32.6	1,440	851	70	.248	.930
	26.1	1,120	681	45	.1592	.932
	13.70	587	357	11	.0390	.833
	Mixed beads, D_p=0.393 in., D_t=2.067 in., air, ρ=0.0874, CH=36.75 in., CT=75° F., voids=36.2 percent					
j-1	72.4	3,108	2,338	254	0.820	0.783
	63.6	2,732	2,057	196	.633	.785
	54.7	2,348	1,768	145	.468	.785
	43.2	1,855	1,394	87	.281	.750
	33.3	1,432	1,078	55	.1776	.797
	28.3	1,218	919	40	.1292	.805
	15.84	679	511	12	.0387	.775
	Cylinders, D_p=0.403 in., D_t=2.067 in., air, ρ=0.0864, CH=35.0 in., CT=72° F., voids=45.8 percent					
k-1	83.0	3,565	2,906	215.5	1.745	1.121
	80.0	3,440	2,805	200	1.623	1.123
	71.2	3,060	2,496	160	1.298	1.134
	62.0	2,662	2,174	120	.975	1.132
	51.1	2,195	1,792	80	.650	1.110
	39.2	1,684	1,384	46	.373	1.078
	28.1	1,208	988	25	.2024	1.133
	18.08	775	633	10	.0815	1.114

Run	w, lb./hr.	G, lb. ft.$^{-2}$ hr.$^{-1}$	Re	Δp, cm. CCl_4	Δp_{40}, p. s. i./ft.	f
	Lead spheres, D_p=0.0885 in., D_t=0.824 in., air, ρ=0.0840, CH=11.5 in., CT=77.5° F., voids=43.3 percent					
a-2	11.38	3,170	542	155.8	4.93	0.975
	10.53	2,842	486	126.0	3.99	.979
	9.55	2,580	441	99.6	3.18	.949
	8.11	2,190	374	71.0	2.24	.925
	6.78	1,832	313	55.8	1.767	1.046
	5.10	1,378	236	34.7	1.098	1.145
	4.26	1,152	197	22.6	.716	1.071
	Glass beads, D_p=0.169 in., D_t=0.824 in., air, ρ=0.0840, CH=14.0 in., CT=30° C., voids=43.7 percent					
b-2	15.83	4,276	1,365	165	4.43	0.921
	14.02	3,784	1,209	132	3.55	.939
	11.94	3,222	1,029	98	2.64	.989
	10.18	2,746	879	70	1.88	.950
	8.13	2,198	703	42	1.128	.888

TABLE I.—*Pressure-drop data for flow through smooth particles*—Continued

Run	w, lb./hr.	G, lb. ft.$^{-2}$ hr.$^{-1}$	Re	Δp, cm. CCl_4	Δp_{40}, p. s. i./ft.	f
	Glass beads, D_p=0.169 in., D_t=0.824 in., air, ρ=0.0840 in., CH=14.75 in., CT=25.5° C., voids=40.8 percent					
b-2	14.39	3,885	1,252	158.5	3.13	0.781
	12.38	3,344	1,078	117.7	2.32	.782
	10.23	2,765	892	78.2	1.542	.760
	7.86	2,125	685	52.1	1.027	.857
	5.85	1,583	511	28.0	.554	.830
	4.05	1,095	354	15.0	.296	.926
	Glass beads, D_p=0.169 in., D_t=0.824 in., air, ρ=0.0840, CH=10.875 in., CT=25° C., voids=41.5 percent					
b-2	17.85	4,815	1,564	160.2	4.60	0.755
	15.48	4,175	1,356	116.0	3.322	.728
	12.60	3,400	1,103	83.3	2.382	.786
	Glass beads, D_p=0.204 in., D_t=0.824 in., air, ρ=0.0833, CH=14.0 in., CT=26° C., voids=45.4 percent					
c-2	19.32	5,215	2,037	155.5	4.85	0.810
	16.44	4,445	1,733	115	3.58	.823
	13.80	3,726	1,454	82	2.55	.834
	11.30	3,050	1,188	52.5	1.63	.797
	9.58	2,592	1,010	35	1.088	.735
	5.69	1,538	600	13	.406	.783
	Glass beads, D_p=0.224 in., D_t=0.824 in., air, ρ=0.0843, CH=14.125 in., CT=25.3° C., voids=47 percent					
d-2	21.6	5,840	2,498	161	5.70	0.942
	18.20	4,910	2,104	116.5	4.11	.850
	16.90	4,560	1,952	99	3.50	.845
	15.35	4,145	1,773	81.5	2.88	.845
	12.05	3,254	1,392	48	1.698	.808
	9.10	2,460	1,053	25	.885	.740
	Glass beads, D_p=0.391 in., D_t=0.824 in., air, ρ=0.0826, CH=14.0 in., CT=25.5° C., voids=52.3 percent					
e-2	35.8	9,670	7,235	145.5	7.92	0.720
	30.58	8,250	6,165	114	6.20	.785
	27.75	7,495	5,600	89	4.84	.741
	26.62	7,200	5,385	87.5	4.76	.792
	22.96	6,200	4,640	66	3.59	.804
	18.96	5,120	3,825	46	2.504	.825
	15.35	4,145	3,095	31.5	1.714	.860
	12.18	3,286	2,454	20	1.086	.868
	9.02	2,440	1,822	9.5	.516	.753
	Porcelain balls, D_p=0.5075 in., D_t=0.824 in., air, ρ=0.0810, CH=11.625 in., CT=76° F., voids=65.1 percent					
f-2	67.0	18,125	17,635	117.6	20.3	0.673
	60.4	16,330	15,900	97.8	16.84	.689
	55.3	14,950	14,560	83.5	14.39	.699
	47.6	12,875	12,530	61.6	10.62	.700
	42.0	11,350	11,030	48.2	8.29	.704
	30.7	8,280	8,165	27.8	4.80	.765
	25.9	6,975	6,795	20.5	3.53	.792
	22.4	6,040	5,880	15.2	2.62	.784
	15.03	4,058	3,957	7.1	1.222	.806
	9.58	2,590	2,522	2.6	.448	.729
	Copper pellets, D_p=0.274 in., D_t=0.824 in., air, ρ=0.0830, CH=14.75 in., CT=25° C., voids=54.7 percent					
g-2	27.14	7,310	3,935	154.5	9.60	0.775
	24.50	6,610	3,550	128.2	7.96	.783
	21.80	5,885	3,160	103.0	6.40	.797
	19.38	5,235	2,805	82.3	5.11	.803
	16.21	4,378	2,350	60.0	3.73	.900
	13.41	3,620	1,944	43.0	2.67	.972
	10.03	2,708	1,453	23.9	1.49	.943
	7.51	2,032	1,090	12.4	.771	.870
	4.97	1,343	722	5.4	.336	.859

TABLE I.—*Pressure-drop data for flow through smooth particles*—Continued

Run	w, lb./hr.	G, lb. ft.$^{-2}$ hr.$^{-1}$	Re	Δp, cm. CCl_4	Δp_{40}, p. s. i./ft.	f
	Copper pellets, D_p=0.274 in., D_t=0.824 in., air, ρ=0.0830, CH=14.0 in., CT=25° C., voids=52.5 percent					
g-2	25.86	6,985	3,750	156.8	8.68	0.768
	23.22	6,265	3,370	127.0	7.03	.828
	20.03	5,405	2,905	96.9	5.36	.843
	17.28	4,660	2,508	74.3	4.11	.870
	14.59	3,940	2,116	54.9	3.03	.901
	11.28	3,040	1,632	31.9	1.767	.881
	8.77	2,370	1,272	17.4	.966	.797
	5.06	1,368	735	7.0	.387	.955
	Aluminum pellets, D_p=0.254 in., D_t=0.824 in., air, ρ=0.0825, CH=8.625 in., CT=77° F., voids=49.3 percent					
h-2	27.0	7,290	3,420	158.8	11.08	0.781
	24.86	6,710	3,155	137.7	9.63	.800
	22.26	6,005	2,820	112.2	7.86	.821
	19.18	5,175	2,332	85.6	5.99	.903
	16.30	4,400	2,064	64.0	4.52	.865
	13.69	3,690	1,733	46.2	3.22	.889
	11.66	3,145	1,475	34.0	2.374	.891
	9.62	2,600	1,220	22.3	1.562	.857
	6.26	1,694	796	11.6	.812	-------
	Cylinders, D_p=0.403 in., D_t=0.824 in., air, ρ=0.0810, CH=12.25 in., CT=80° F., voids=65.9 percent					
i-2	60.5	16,350	10,800	116.2	19.60	0.560
	54.1	14,650	9,700	94.8	15.95	.568
	46.3	12,500	8,250	70.0	11.80	.575
	39.7	10,720	7,090	51.4	8.66	.574
	30.0	8,090	5,350	31.4	5.30	.616
	25.8	6,955	4,600	23.5	3.97	.626
	21.67	5,850	3,870	16.4	2.77	.617
	18.27	4,925	3,260	11.7	1.976	.620
	15.25	4,110	2,720	8.3	1.398	.626
	11.70	3,155	2,090	4.6	.775	.594
	8.95	2,420	1,600	2.3	.388	.494
	Glass beads, D_p=0.228 in., D_t=3.068 in., air, ρ=0.0762, CH=17.375 in., CT=24° C., voids=37.5 percent					
a-3	82.8	1,616	711	38.1	0.469	0.835
	74.1	1,447	636	31.6	.390	.865
	65.4	1,276	561	25.0	.308	.880
	56.6	1,105	486	19.4	.239	.905
	45.6	888	391	13.1	.1612	.950
	Glass beads, D_p=0.388 in., D_t=3.068 in., air, ρ=0.0750, CH=14.0 in., CT=24° C., voids=40.9 percent					
b-3	89.2	1,742	1,302	13.4	0.282	0.719
	78.3	1,528	1,141	11.3	.2376	.788
	71.8	1,401	1,048	8.9	.1872	.740
	52.9	1,031	772	5.6	.1176	.860
	Porcelain balls, D_p=0.5075 in., D_t=3.068 in., air, ρ=0.0751, CH=14.5 in., CT=23° C., voids=38.1 percent					
c-3	88.9	1,734	1,697	11.8	0.1842	0.623
	84.5	1,650	1,613	10.7	.1672	.626
	74.8	1,460	1,428	8.8	.1378	.657
	64.8	1,263	1,235	6.5	.1017	.650
	56.0	1,092	1,068	5.2	.0814	.696
	45.0	876	858	3.3	.0501	.664
	39.1	761	745	2.6	.0407	.715
	29.4	573	561	1.5	.0234	.703
	21.8	425	416	0.90	.0140	.787
	Porcelain balls, D_p=0.73 in., D_t=3.068 in., air, ρ=0.0745, CH=21.5 in., CT=24° C., voids=47.5 percent					
d-3	92.5	1,806	2,554	6.5	0.1562	0.696
	80.6	1,572	2,220	5.1	.1227	.723
	71.2	1,390	1,965	4.2	.1010	.758
	59.8	1,167	1,649	3.0	.0722	.771
	48.6	947	1,335	1.9	.0459	.743

TABLE I.—*Pressure-drop data for flow through smooth particles*—Continued

Run	w, lb./hr.	G, lb. ft.$^{-2}$ hr.$^{-1}$	Re	Δp, cm. CCl_4	Δp_{40}, p. s. i./ft.	f
	Cylinders, D_p=0.403 in., D_t=3.068 in., air, ρ=0.0755, CH=15.875 in., CT=22.5° C., voids=38.2 percent					
e-3	88.9	1,735	1,150	17.7	0.292	0.665
	75.7	1,478	975	13.2	.218	.683
	66.1	1,290	850	10.5	.1728	.711
	55.6	1,084	715	7.5	.1234	.723
	45.6	888	587	5.2	.0859	.746
	37.3	726	480	3.5	.0578	.752
	28.6	557	367	2.3	.0384	.840
	16.42	320	210	.8	.0132	.919
	Cylinders, D_p=0.188 in., D_t=1.049 in., air, ρ=0.0870, CH=12.25 in., CT=80° F., voids=42.5 percent					
a-4	19.38	3,230	1,159	119.2	3.34	0.835
	17.48	2,910	1,043	97.6	2.74	.843
	16.21	2,700	970	81.1	2,258	.813
	13.87	2,312	830	63.7	1.788	.892
	12.25	2,042	733	50.3	1.412	.884
	10.80	1,804	648	38.6	1.080	.870
	9.87	1,650	592	33.6	.944	.825
	Brass rings, D_p=0.350 in., D_t=1.049 in., air, ρ=0.0830, CH=10.5 in., CT=75° F., voids=74.4 percent					
b-4	83.8	14,000	9,350	121	46.6	0.814
	74.0	12,350	8,250	95.5	36.9	.825
	66.6	11,100	7,410	78	30.1	.834
	58.8	9,820	6,550	61.5	23.8	.839
	48.8	8,150	5,450	42.0	16.2	.833
	36.8	6,150	4,110	23.5	9.05	.818
	24.1	4,025	2,690	10.0	3.85	.806
	Copper cylinders, D_p=0.420 in., D_t=1.049 in., air, ρ=0.0830, CH=11.125 in., CT=75° F., voids=56.25 percent					
c-4	64.2	10,800	8,640	132	12.25	0.815
	52.1	8,800	7,050	90	8.34	.835
	43.6	7,350	5,900	62	5.75	.826
	36.8	6,200	4,970	44	4.075	.821
	28.0	4,720	3,780	25.5	2.360	.819
	22.1	3,730	2,990	16.0	1.482	.822
	15.2	2,560	2,050	7.0	.647	.764
	Glass spheres, D_p=0.393 in., D_t=1.049 in., air, ρ=0.0830, CH=12.0 in., CT=78.5° F., voids=51.3 percent					
d-4	65.1	10,875	8,175	132	7.79	0.566
	56.9	9,460	7,100	104.6	6.155	.592
	46.6	7,760	5,825	70.4	4.045	.576
	35.85	5,970	4,480	41.0	2.41	.580
	28.55	4,755	3,565	28.2	1.66	.627
	26.32	4,385	3,285	23.3	1.372	.613
	21.60	3,600	2,695	15.1	.890	.589
	13.92	2,320	1,736	5.7	.335	.535
	Porcelain balls, D_p=0.505 in., D_t=1.049 in., air, ρ=0.0830, CH=11.875 in., CT=78.5° F., voids=52.0 percent					
e-4	66.95	11,170	10,750	129.7	8.11	0.718
	56.9	9,460	9,140	95.8	6.00	.735
	47.2	7,860	7,590	66.8	4.17	.742
	37.8	6,300	6,085	43.4	2.71	.752
	31.0	5,160	4,980	28.0	1.753	.723
	25.35	4,220	4,070	20.1	1.256	.773
	18.98	3,165	3,050	10.6	.662	.728
	14.00	2,330	2,250	5.3	.330	.671
	Cylinders, D_p=0.403 in., D_t=1.049 in., air, ρ=0.0820, CH=12.25 in., CT=75° F., voids=56.6 percent					
f-4	64.05	10,700	8,350	131.6	11.37	0.738
	56.0	9,340	7,255	101.2	8.77	.746
	47.4	7,890	6,125	70.9	6.14	.734
	38.65	6,445	5,005	47.5	4.10	.732
	31.82	5,305	4,130	30.4	2.63	.693
	25.9	4,315	3,355	21.5	1.865	.741
	20.53	3,420	2,655	12.2	1.055	.673

TABLE I.—*Pressure-drop data for flow through smooth particles*—Continued

Run	w, lb./hr.	G, lb. ft.$^{-2}$ hr.$^{-1}$	Re	Δp, cm. CCl_4	Δp_{10}, p. s. i./ft.	f
	Glass beads, D_p=0.228 in., D_t=1.049 in., N_2 gas, ρ=0.0785, CH=11.75 in., CT=71.5° F., voids=40.4 percent					
a-5	5.92	987	447	7.6	0.1838	0.912
	6.06	1,010	458	8.0	.1932	.904
	9.14	1,524	692	16.0	.387	.795
	9.75	1,627	737	18.6	.450	.812
	10.88	1,811	822	22.0	.531	.771
	12.98	2,162	981	30.2	.731	.746
	13.77	2,292	1,037	33.6	.814	.743
	15.82	2,638	1,192	39.8	.964	.664
	17.14	2,852	1,291	48.8	1.180	.691
	Glass beads, D_p=0.228 in., D_t=1.049 in., N_2 gas, ρ=0.1040, CH=11.75 in., CT=72° F., voids=40.4 percent					
b-5	6.14	1,022	463	6.6	0.159	0.962
	9.24	1,540	698	12.8	.309	.824
	10.57	1,758	796	16.2	.392	.804
	12.40	2,066	937	21.0	.507	.754
	14.52	2,420	1,096	28.6	.691	.748
	15.38	2,560	1,160	31.4	.759	.734
	16.02	2,663	1,207	33.0	.809	.721
	17.02	2,836	1,285	37.2	.900	.713
	18.38	3,060	1,387	42.4	1.022	.694
	18.68	3,110	1,410	44.0	1.060	.695
	19.46	3,242	1,470	46.4	1.119	.676
	22.30	3,710	1,682	59.0	1.422	.656
	Glass beads, D_p=0.228 in., D_t=1.049 in., N_2 gas, ρ=0.1355, CH=11.75 in., CT=70.5° F., voids=40.4 percent					
c-5	4.74	789	359	3.4	0.0820	1.089
	6.61	1,103	502	5.8	.1398	.945
	7.64	1,273	579	7.2	.1733	.879
	7.75	1,292	588	7.6	.1832	.899
	9.92	1,655	753	11.2	.270	.811
	10.53	1,756	799	12.4	.299	.798
	15.01	2,500	1,138	23.2	.559	.736
	17.02	2,836	1,289	27.2	.656	.674
	17.27	2,874	1,306	30.0	.724	.723
	18.22	3,035	1,381	32.8	.791	.710
	20.22	3,370	1,533	39.4	.951	.690
	22.12	3,682	1,676	45.0	1.082	.658
	22.68	3,780	1,720	47.4	1.140	.658
	Glass beads, D_p=0.228 in., D_t=1.049 in., N_2 gas, ρ=0.1670, CH=11.75 in., CT=73.5° F., voids=40.4 percent					
d-5	5.41	903	406	3.5	0.0918	1.148
	7.74	1,291	581	6.0	.1442	.979
	8.46	1,412	636	7.2	.1732	.884
	9.74	1,625	731	9.0	.2164	.832
	11.18	1,863	839	11.2	.270	.794
	12.02	2,003	902	13.0	.313	.792
	12.92	2,153	969	14.6	.352	.774
	15.82	2,638	1,184	20.8	.501	.735
	Glass beads, D_p=0.228 in., D_t=1.049 in., N_2 gas, ρ=0.1840, CH=11.75 in., CT=77.5° F., voids=40.4 percent					
e-5	5.44	906	406	3.2	0.0772	1.055
	8.07	1,348	604	6.3	.1516	.936
	9.22	1,540	690	7.8	.1880	.890
	12.45	2,075	930	12.6	.304	.791
	14.40	2,400	1,072	16.4	.396	.770

TABLE II.—*Pressure-drop data for flow through beds composed of rough particles*

Run	w, lb./hr.	G, lb. ft.$^{-2}$ hr.$^{-1}$	Re	Δp, cm. CCl_4	Δp_{10}, p. s. i./ft.	f
	Clay balls, D_p=0.368 in., D_t=3.068 in., air, ρ=0.0785 CH*=25.5 in., CT*=23° C., voids=43.8 percent					
1	87.1	1,700	1.203	21.5	0.322	0.865
	76.4	1,490	1.056	17.5	.261	.884
	67.0	1,308	928	13.7	.2044	.889
	55.6	1,085	770	9.9	.1478	.931
	46.1	898	637	7.8	.1165	1.080
	37.3	726	515	4.8	.0717	1.011
	28.5	555	394	3.2	.0478	1.150
	21.4	416	295	1.9	.0283	1.219
	Clay balls, D_p=0.310 in., D_t=0.824 in., air, ρ=0.0815, CH=10.875 in., CT=77° F., voids=51.5 percent					
2	31.3	8,450	5,054	130.3	8.91	0.844
	28.46	7,685	4,594	113.7	7.79	.891
	26.2	7,085	4,238	96.7	6.61	.891
	23.8	6,435	3,844	81.6	5.58	.911
	21.3	5,755	3,440	65.7	4.49	.913
	17.98	4,850	2,900	49.0	3.35	.960
	15.15	4,092	2,445	35.9	2.46	.990
	12.34	3,330	1,990	23.8	1.627	.985
	9.59	2,590	1,547	13.8	.946	.955
	6.57	1,775	1,059	8.2	.561	1.209
	4.53	1,224	735	3.6	.246	1.107
	Clay balls, D_p=0.298 in., D_t=0.824 in., air, ρ=0.0815, CH=14.0 in., CT=25.5° C., voids=56.1 percent					
3	27.4	7,400	4,200	129.0	9.45	1.12
	24.7	6,670	3,790	106.5	7.80	1.139
	21.46	5,800	3,294	82	6.00	1.161
	18.46	4,985	2,826	61.5	4.50	1.181
	15.25	4,115	2,335	43	3.15	1.202
	12.52	3,380	1,920	28	2.055	1.164
	9.07	2,452	1,392	13	.953	1.030
	5.86	1,584	901	6.5	.475	1.231
	Clay balls, D_p=0.325 in., D_t=1.049 in., air, ρ=0.0824, CH=12.625 in., CT=72° F., voids=51.7 percent					
4	49.8	8,300	5,240	128.4	10.24	1.065
	44.1	7,360	4,640	101.6	8.25	1.086
	38.6	6,440	4,055	76	6.16	1.060
	30.9	5,150	3,245	48.8	3.95	1.059
	25.5	4,250	2,675	35.5	2.87	1.131
	20.95	3,490	2,195	22.2	1.79	1.044
	17.12	2,855	1,798	13.8	1.12	.981
	12.72	2,120	1,334	7.3	.592	.942
	Raschig rings, D_p=0.252 in., D_t=3.068 in., air, ρ=0.0761, CH=16.25 in., CT=23° C., voids=54.7 percent					
5	85.3	1,665	809	25.6	1.175	1.39
	78.3	1,529	743	22.3	1.023	1.44
	68.7	1,340	651	17.6	.810	1.43
	59.8	1,168	567	13.7	.630	1.51
	52.1	1,015	493	10.6	.488	1.55
	43.6	849	412	7.4	.340	1.53
	34.0	663	321	4.8	.221	1.63
	27.9	544	264	3.6	.1658	1.80
	21.3	415	201	2.2	.1040	----

*CH=column height=L; CT=temperature of gas.

TABLE II.—*Pressure-drop data for flow through beds composed of rough particles*—Continued

Run	w, lb./hr.	G, lb. ft.$^{-2}$ hr.$^{-1}$	Re	Δp, cm. CCl_4	Δp_{40}, p. s. i./ft.	f
	Raschig rings, D_p=0.252 in., D_t=0.824 in., air, ρ=0.0823, CH=11.75 in., CT=80° F., voids=62.2 percent					
6	29.1	7,855	3,790	152.8	21.06	1.21
	26.4	7,125	3,432	128.2	17.72	1.245
	23.9	6,450	3,005	106.1	14.65	1.256
	21.2	5,720	2,755	84.7	11.68	1.270
	18.20	4,910	2,370	63.8	8.80	1.30
	14.20	3,830	1,845	41.0	5.67	1.37
	11.42	3,085	1,485	26.1	3.60	1.24
	8.65	2,340	1,128	13.5	1.928	1.25
	6.00	1,622	781	7.6	1.048	1.42
	3.93	1,062	512	3.2	.442	1.39
	Raschig rings, D_p=0.252 in., D_t=1.049 in., air, ρ=0.0830, CH=12.75 in., CT=72° F., voids=61.2 percent					
7	46.1	7,690	3,750	134.2	15.72	0.948
	37.85	6,305	3,130	87.7	10.29	.917
	31.8	5,300	2,585	61.7	7.24	.915
	26.1	4,350	2,120	44.5	5.21	.978
	19.93	3,320	1,620	23.4	2.745	.888
	14.42	2,400	1,170	11.4	1.330	.824
	Raschig rings, D_p=0.252 in., D_t=1.049 in., air, ρ=0.0830, CH=11.5 in., CT=72° F., voids=57.0 percent					
7	41.0	6,840	3,340	135	12.80	0.975
	35.2	5,860	2,865	98.5	9.37	.969
	31.0	5,170	2,525	75	7.13	.946
	25.15	4,190	2,142	53.4	5.07	1.030
	19.77	3,290	1,605	30.5	2.90	.950
	14.42	2,400	1,170	15.2	1.44	.892
	10.93	1,825	892	8.2	.780	.835
	Aloxite (round), D_p=0.170 in., D_t=0.824 in., air, ρ=0.0834, CH=14.625 in., CT=29.5° C., voids=54.2 percent					
8	15.32	4,140	1,342	160.5	9.86	2.30
	13.42	3,620	1,175	119.5	7.34	2.12
	11.48	3,100	1,007	90.5	5.56	2.19
	9.48	2,562	834	58	3.56	2.06
	7.24	1,958	637	40	2.46	2.44
	5.31	1,435	467	21.4	1.312	2.42
	Aloxite (round), D_p=0.170 in., D_t=0.824 in., air, ρ=0.0834, CH=14.75 in., CT=25.5° C., voids=55.6 percent					
8	17.03	4,596	1,490	158.7	10.57	1.910
	14.82	4,000	1,299	123.8	8.25	1.957
	12.88	3,474	1,128	95.1	6.35	2.000
	10.75	2,900	944	64.0	4.27	1.925
	8.44	2,280	742	37.4	2.50	1.852
	6.31	1,708	555	28.1	1.872	2.47
	4.25	1,148	373	11.8	.787	2.27
	Aloxite (rough), D_p=0.165 in., D_t=3.068 in., air, ρ=0.0760, CH=12.625 in., CT=23° C., voids=54.0 percent					
9	87.1	1,700	541	21.4	1.554	1.800
	75.7	1,478	470	17.1	1.240	1.904
	66.1	1,290	410	13.3	.965	1.954
	55.6	1,084	345	9.8	.679	2.118
	44.3	863	274	6.4	.444	2.000
	39.1	762	242	4.4	.319	1.840
	28.2	548	174	3.2	.232	2.596
	21.6	421	134	2.0	.1450	2.742

TABLE II.—*Pressure-drop data for flow through beds composed of rough particles*—Continued

Run	w, lb./hr.	G, lb. ft.$^{-2}$ hr.$^{-1}$	Re	Δp, cm. CCl_4	Δp_{40}, p. s. i./ft.	f
	Aloxite (rough), D_p=0.170 in., D_t=0.824 in., air, ρ=0.0830, CH=14.5 in., CT=29.5° C., voids=57.3 percent					
10	17.17	4,640	1,502	153.7	11.83	2.06
	14.94	4,140	1,341	117.5	9.06	1.985
	13.40	3,620	1,173	94.2	7.27	2.08
	11.59	3,130	1,015	68.6	5.29	2.02
	10.01	2,702	877	49.0	3.78	1.936
	7.39	2,000	649	31.7	2.444	2.28
	5.06	1,370	444	15.1	1.165	2.33
	Aloxite (rough), D_p=0.170 in., D_t=0.824 in., air, ρ=0.0830, CH=14.5 in., CT=25.5° C., voids=58.0 percent					
10	18.08	4,875	1,582	156.7	12.72	2.04
	15.62	4,210	1,368	124.8	10.12	2.16
	13.45	3,628	1,178	93	7.55	2.28
	11.36	3,063	997	66	5.36	2.16
	9.05	2,466	803	40.1	3.26	2.02
	6.67	1,803	586	30	2.44	2.85
	4.34	1,172	381	11.6	.943	2.60
	Aloxite, D_p=0.159 in., D_t=2.067 in., air, ρ=0.0837, CH=36.5 in., CT=87° F., voids=54.4 percent					
11	59.3	2,542	744	148	3.596	1.974
	52.3	2,244	656	115	2.800	1.982
	44.6	1,915	559	82.5	2.010	1.960
	35.2	1,511	442	52.0	1.265	1.965
	27.7	1,190	348	33.0	.770	1.934
	16.24	696	204	13.5	.329	2.42
	12.97	556	163	9.0	.219	2.52
	Alundum, D_p=0.180 in., D_t=0.824 in., air, ρ=0.0845, CH=14.5 in., CT=23.5° C., voids=48.5 percent					
12	16.86	4,550	1,582	165.5	6.40	1.09
	14.00	3,780	1,317	116.5	4.51	1.11
	11.73	3,168	1,102	81.0	3.22	1.13
	9.84	2,658	926	55.5	2.14	1.07
	6.36	1,720	599	28.5	1.10	1.31
	4.46	1,206	419	12.9	.499	1.21
	Alundum, D_p=0.180 in., D_t=0.824 in., air, ρ=0.0845, CH=14.5 in., CT=23.5° C., voids=44.7 percent					
12	14.83	4,000	1,392	166.3	5.02	1.10
	11.73	3,168	1,102	106.5	3.244	1.130
	9.84	2,658	926	71.5	2.175	1.08
	6.36	1,720	599	35.9	1.091	1.29
	4.16	1,125	393	14.1	.430	1.19
	Alundum, D_p=0.180 in., D_t=0.824 in., air, ρ=0.0845, CH=12.0 in., CT=77° F., voids=44.2 percent					
12	15.33	4,145	1,434	159.8	5.23	1.09
	13.33	3,600	1,276	124.0	4.06	1.11
	11.05	2,980	1,057	86.9	2.84	1.14
	9.42	2,546	905	60.0	1.964	1.08
	7.03	1,900	675	35.7	1.168	1.15